Prioritizing Characterization of Potentially Habitable Worlds

by

Austin Ware

A Dissertation Presented in Partial Fulfillment
of the Requirements for the Degree
Doctor of Philosophy

Approved October 2024 by the
Graduate Supervisory Committee:

Patrick Young, Chair
Jennifer Patience
Michael Line
Evgenya Shkolnik
Steven Desch

ARIZONA STATE UNIVERSITY

December 2024

ABSTRACT

Through the combined efforts of the *Kepler* space telescope, *Transiting Exoplanet Survey Satellite*, and various other ground- and space-based observations, thousands of exoplanets have been discovered, some Earth-sized and in the habitable zones of their host stars. With this, the exoplanet community begins the transition from exoplanet detection to exoplanet characterization. Detailed atmospheric characterization brings the hope of detecting the signatures of life on other worlds and constraining the prevalence of life in our galaxy. Probing the atmospheres of terrestrial exoplanets in the habitable zones of their host stars will require significant time and resources, particularly for those orbiting stars most similar to our Sun. To increase the likelihood of success for future missions dedicated to finding habitable exoplanets and detecting life, we should prioritize targets where life will have had sufficient time to make a detectable impact on the atmosphere. This work expands upon and applies a method for prioritizing targets based on the likelihood of remaining continuously within the habitable zone for 2 billion years (Gyr), similar to the amount of time life on Earth took to make a significant impact on our atmosphere. Chapter 1 provides a broad background detailing how exoplanets are determined to be potentially habitable and their estimated occurrence rate, current and future missions that will search for the signatures of life and what they will search for, and the importance of target prioritization and how continuous habitable zone estimates can aid in this effort. Chapter 2 updates and expands upon a Bayesian method for calculating the likelihood an exoplanet is within the 2 Gyr continuous habitable zone (CHZ_2), using a combination of stellar evolution tracks and habitable zone models, and applies this method to a sample of known potentially habitable exoplanets. Chapter 3 explores an alternative to the commonly used method of defining habitable zone boundaries,

pairing results from a perturbed parameter ensemble of planetary atmosphere general circulation models with the Bayesian CHZ_2 framework. Chapter 4 presents an updated grid of stellar evolution tracks and applies the Bayesian CHZ_2 method to the current highest priority targets for the future NASA Habitable Worlds Observatory. This method is also generalized such that it can be easily incorporated into an open-source stellar model grid interpolation code and used with any stellar model grid or habitable zone prescription.

DEDICATION

To all those devastated by the COVID-19 pandemic and the wars in Ukraine and Palestine. Your loss will stay with me forever.

ACKNOWLEDGMENTS

My journey to receive a doctorate in Astrophysics would not have been possible without the support of numerous people and animals over the past two decades. Here I would like to thank as many of them as possible:

To my advisor, Prof. Patrick Young: Thank you for all of your support and guidance for the past 6+ years. I could not think of a better human being and scientist to guide me through this process. I'll be honored to have you as a mentor, collaborator, and friend for life.

To my dissertation committee – Prof. Jennifer Patience, Prof. Michael Line, Prof. Evgenya Shkolnik, and Prof. Steve Desch: Thank you for your support and perspectives that have helped me see how my niche subject matter can have a more significant impact on the exoplanet community as a whole. Further, the opportunities to conduct research with you have provided me the broad knowledge base needed to exceed in the inherently interdisciplinary field of exoplanets.

To my collaborators – Dr. Amanda Truitt, Dr. Alexander Spacek, and Dr. Nancy Kiang: Thank you Amanda and Alex for your critical help and support at the beginning of my graduate career. Your advice was critical to me publishing my first paper when I was struggling during the pandemic. Thank you Nancy for the opportunity to work with you on exciting research outside my direct expertise that has significantly helped progress my understanding of both atmospheric and biological sciences.

To DEXTERS Lab and all my fellow exoplanet researchers at ASU: Thank you for welcoming me into the exoplanet group here even though I didn't know a retrieval from a retriever when I first started. Simply listening to the extensive yap sessions

held in the offices has broadened my knowledge and exposed me to research I wouldn't have been otherwise. Also, I guess you all are cool for a bunch of nerds.

To my family: Thank you to my parents, Lisa and Bob Ware, for your support through my whole life and for dealing with my obsessive watching of science and history shows as a kid. Thank you to my siblings, Ryan, Shane, Chad, and Alyson, for your support and always keeping things interesting growing up. Thank you to my grandparents, Mary Staub, Elmer Staub, Nancy Ware, and Donald Ware, for your support growing up.

To my friends: Thank you to Seth, Ryan, and Olivia for supporting me in my journey through high school and/or college and giving me memories I'll keep with me forever.

To my comrades: You know who you are. Thank you.

To my animal friends: Thank you to Brandy, Rocky, Katy, Riley, Abby, Mr. Whiskers, Tiki, Morgan, Luna, Roo, Kepler, Momo, Trucy, Tess, and Umbra for your companionship and deepening my love for life on this planet.

To Marah Brinjikji: Thank you for being the one constant I could always rely on during one of the most difficult times of my life. Here's to hoping any future kids of ours aren't as insufferable as I expect the kids of two doctors to be.

To everyone else I did not include here, thank you.

TABLE OF CONTENTS

LIST OF TABLES

LIST OF FIGURES

Chapter 1

OVERTURE

We currently stand at the precipice of answering - or at least constraining - one of the fundamental questions of humanity: are we alone? With the discovery of thousands of exoplanets, primarily through dedicated space telescope surveys like *Kepler* (Borucki et al. 2010) and the *Transiting Exoplanet Survey Satellite* (*TESS*) (Ricker et al. 2014), $>$ 30 Earth-sized planets orbiting in the habitable zone (HZ) of their host stars have been identified (Hill et al. 2023). With an ever increasing number of known terrestrial HZ exoplanets, the exoplanet community has begun the transition from exoplanet detection to exoplanet characterization. The *James Webb Space Telescope* (*JWST*) has enabled astronomers to start searching for atmospheres around terrestrial HZ exoplanets transiting the nearest, lowest mass M dwarf stars (Cadieux et al. 2024; Damiano et al. 2024). Future high-contrast direct imaging missions, such as the planned NASA Habitable Worlds Observatory (HWO), will deliver the needed sensitivity to probe the atmospheres of Earth-sized planets in the HZ of Sun-like (F-, G-, K-type) stars (Fujii et al. 2018; The LUVOIR Team 2019; Gaudi et al. 2020). With detailed atmospheric characterization comes significantly greater observational cost, emphasizing the need for proper target prioritization in order to maximize the chance of detecting Earth-like life or demonstrate the rarity of Earth.

1.1 Defining Potentially Habitable Exoplanets

With only one data point for a habitable world, Earth, an exoplanet's potential habitability is currently defined only by whether the exoplanet has a rocky composition and if the exoplanet presently resides in the HZ of its host star. Determining if an exoplanet has a nominally rocky composition requires modeling the interior structure using the mass, radius, and bulk composition as inputs (Unterborn et al. 2023). However, the large number of exoplanets discovered by the *Kepler* mission provided a constraint on the upper radius limit for rocky planets through population statistics. A dearth was found in the number of exoplanets discovered between $\sim 1.5 - 2$ $R_\oplus$ (Fulton et al. 2017), now known as the small planet "radius valley" (Figure 1.1). This radius valley separates rocky super-Earths from gaseous sub-Neptunes.

The proposed mechanism that causes the distinction between these two regimes is thermally-driven atmospheric escape of the primordial H-He envelopes planets form with. Small, short period planets below the radius valley lose their primordial atmospheres to space soon after formation through XUV-driven photoevaporation (e.g., Owen and Wu 2017) and/or core-powered mass loss (e.g., Gupta and Schlichting 2019), whereby the atmosphere is heated sufficiently by the cooling core to drive escape. Above the radius valley, the mass of the planet is sufficient to retain the primordial atmosphere. The trough of the radius valley occurs at $\sim 1.7 - 1.8$ $R_\oplus$, which is typically taken to be the upper radius limit for rocky planets. This corresponds to an upper mass limit of $\sim 8 - 9$ $M_\oplus$, assuming an Earth-like composition and interior structure (Zeng, Sasselov, and Jacobsen 2016). To a first order approximation, these radius and mass limits can be used to determine if a discovered exoplanet is potentially rocky.

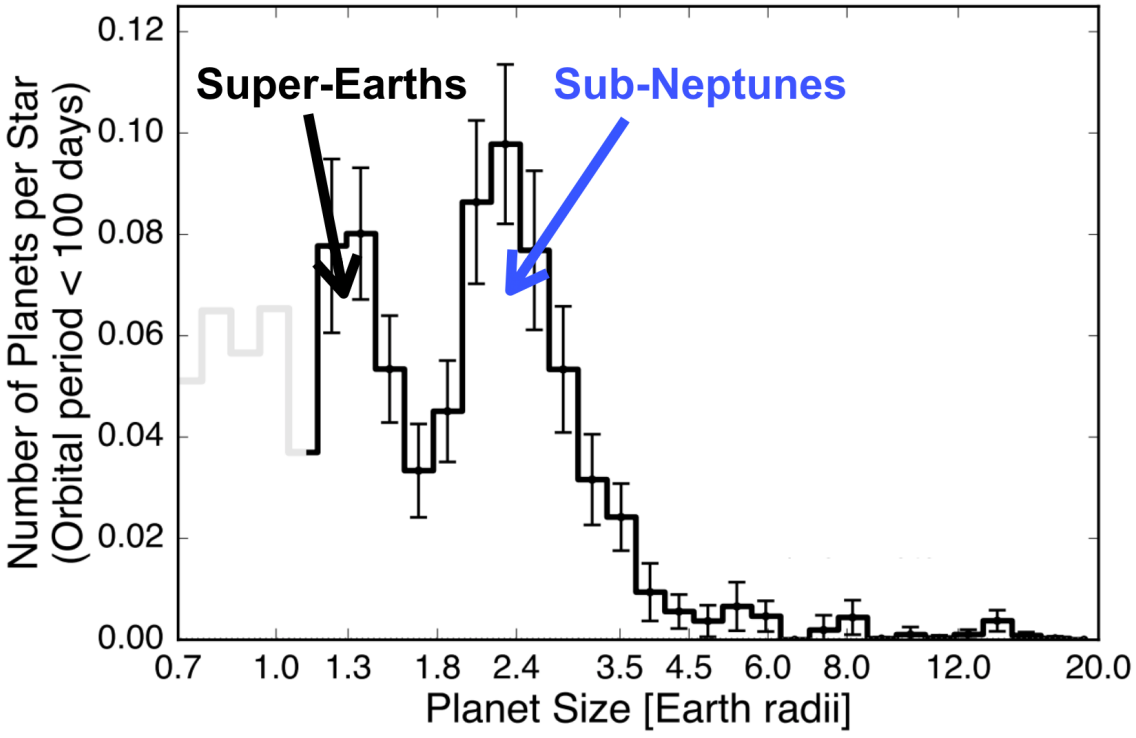

Figure 1.1. Modified figure from Cloutier 2024 showing the distribution of planet radii for discovered short period exoplanets. The radius valley between $\sim 1.5 - 2$ $R_\oplus$ separates small, rocky super-Earths from gaseous sub-Neptunes.

For a rocky exoplanet to be considered potentially habitable, it must reside within the host star's HZ. This is typically defined by the orbital area around a star where the flux received by a planet allows the presence of liquid water on the surface, assuming an Earth-like atmosphere. In the simplest case, the HZ boundaries are calculated by scaling the current HZ boundaries for our solar system with respect to the host star's luminosity:

$$d = d_\oplus \times \left(\frac{L}{L_\odot}\right)^{0.5} \tag{1.1}$$

where $d_\oplus$ is the inner HZ (IHZ) or outer HZ (OHZ) boundary for Earth, L is the host star luminosity, and $L_\odot$ is the Sun's luminosity. In reality, the HZ distance also depends on the stellar effective temperature ($T_{\rm eff}$) (e.g., Kasting, Whitmire, and Reynolds 1993), which determines the wavelength of peak energy emission according to Wien's Law. The total stellar flux absorbed by a planet is dependent on the wavelength, with reflection due to Rayleigh scattering increasing and absorption due to the dominant greenhouse gases, H_2O and CO_2, decreasing with increasing wavelength. The limiting effective stellar flux is typically expressed relative to Earth, with $S_{\rm eff} = S/S_\oplus$, and is determined via climate models for an Earth-like planet.

At the IHZ, the limiting $S_{\rm eff}$ usually corresponds to two possible scenarios: a moist or runaway greenhouse. Once a planet is close enough to the star that the mean surface temperature reaches ~ 340 K (for 1D models), a moist greenhouse may occur where the stratosphere becomes sufficiently wet for photolysis to cause the volume of Earth's oceans to escape in ~ 4.5 Gyr (Kasting, Whitmire, and Reynolds 1993). At closer distances, a runaway greenhouse may ensue where a thermal runaway, caused by water vapor rendering the atmosphere opaque to outgoing long-wave radiation, pushes surface temperatures past the critical point of water (~ 647 K at 220 bars,) and the oceans fully evaporate. At the OHZ, the limiting $S_{\rm eff}$ corresponds to the maximum greenhouse or complete freezing point. By increasing the partial pressure of CO_2 and moving the planet outward, the maximum greenhouse boundary is found when the cooling effects of Rayleigh scattering and CO_2 condensation dominate over the CO_2 greenhouse (Kasting, Whitmire, and Reynolds 1993). Similarly, the complete freezing point, assuming a constant amount of CO_2, denotes the point where the planet becomes permanently covered in snow or ice (Abe et al. 2011).

A commonly used set of HZ constraints are from the 1D, cloud-free, radiative

convective models of Kopparapu et al. 2013; Kopparapu et al. 2014, which furthered the pioneering work of Kasting, Whitmire, and Reynolds 1993. The authors report predictive equations for the limiting S_{eff} at the IHZ and OHZ with respect to T_{eff} for an idealized Earth model. These take the form

$$S_{\text{eff}} = a_1 T_{\text{eff}} + a_2 T_{\text{eff}}^2 + a_3 T_{\text{eff}}^3 + a_4 \tag{1.2}$$

where a_i are the coefficients from the regression on the S_{eff} limits for each value of T_{eff}. Taking the effect of T_{eff} into account, Eq. 1.1 becomes

$$d = \left(\frac{L/L_{\odot}}{S_{\text{eff}}} \right)^{0.5} \text{AU}. \tag{1.3}$$

The resulting HZ range for Earth is $\sim 0.95 - 1.68$ AU for the runaway and maximum greenhouse case. However, the Kopparapu et al. 2014 HZ limits take into account results from 3D general circulation models (GCM) (Leconte, Forget, Charnay, Wordsworth, Selsis, et al. 2013). Without accounting for the GCM results, the runaway greenhouse limit would be ~ 1 AU, placing Earth right on the boundary and highlighting the limitations of 1D models. While 1D models benefit from their relative simplicity and fast equilibration times, they are unable to self-consistently account for clouds, surface variations, atmospheric and oceanic heat transport, and orbital variables that would lead to uncertainty in HZ estimates. GCMs are able to account for these multidimensional effects, enabling more realistic simulations of planetary climates at the cost of added complexity. Using 1D and 3D models, numerous HZ constraints have been reported over the past two decades and convey the multitude of planetary properties that may effect the climate, such as atmospheric composition (e.g., Kopparapu et al. 2013; Wolf and Toon 2013; Del Genio et al. 2019), mass (Kopparapu et al. 2014), rotation rate (e.g., Yang, Cowan, and Abbot 2013;

Kopparapu et al. 2017; Jansen et al. 2019; Chen et al. 2019), water inventories and surface water distributions (e.g., Abe et al. 2011; Kodama et al. 2018; Kodama et al. 2019), and the initial conditions following formation (Turbet et al. 2021; Turbet et al. 2023). Figure 1.2 provides a summary of some recent HZ constraints from the literature. These studies show the potential diversity of habitable and uninhabitable terrestrial exoplanet atmospheres, but prove the difficulty of estimating an exoplanet's potential habitability when focusing on a small set of possible planetary and system configurations. We may need a more concerted effort to determine a generalized and flexible HZ that takes into account as many stellar and planetary parameters as possible.

1.2 The Importance of Target Prioritization

A key goal of the *Kepler* mission was to determine $\eta_\oplus$, the occurrence rate of terrestrial HZ exoplanets orbiting Sun-like stars. Using constraints on rocky planet sizes and the HZ, various studies sought to determine $\eta_\oplus$ (e.g., Silburt, Gaidos, and Wu 2015; Kopparapu et al. 2018; Bryson et al. 2021). These give a range of $\sim 0.064 - 0.88$ planets per star, depending on the definition of Sun-like stars, rocky planet sizes, HZ range, the exoplanet sample and properties used, and how survey selection effects and biases are handled. The Astro2020 Decadal Survey recommended NASA design a direct imaging mission with a 6-m aperture to search for and obtain atmospheric spectra of ~ 25 potentially habitable exoplanets in an effort to constrain the prevalence of habitable planets. This number is based off an adopted occurrence rate of $\eta_\oplus = 0.24$ (Kopparapu et al. 2018), approximately in the middle of estimates assuming more

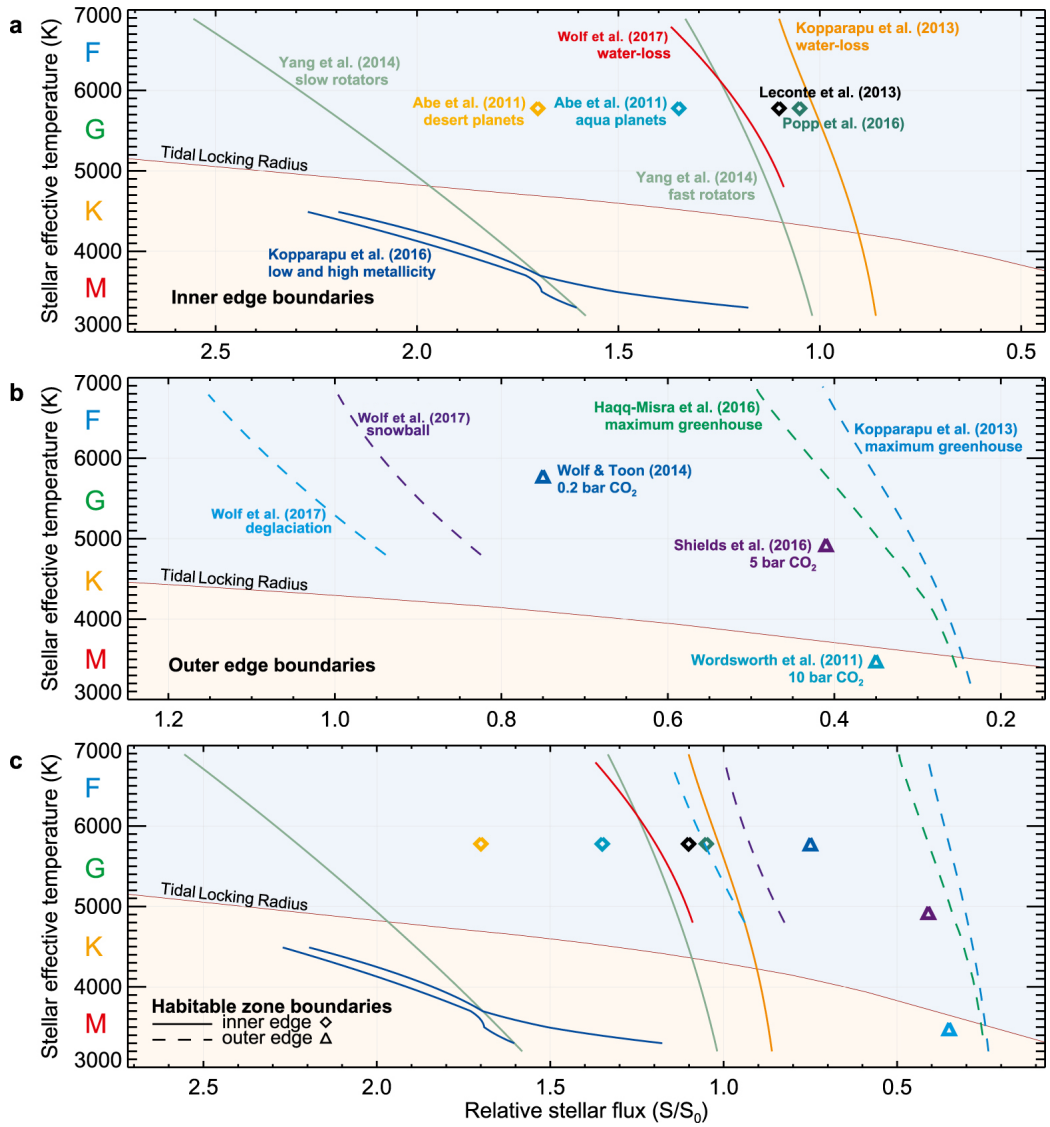

Figure 1.2. Modified figure from Wolf et al. 2017 showing various constraints from the literature for the (a) IHZ, (b) OHZ (b), and (c) the full HZ range. Tidally locked planets fall below the light yellow shaded region. Diamonds and solid lines denote IHZ constraints. Triangles and dashed lines denote OHZ constraints.

conservative HZ limits. Achieving this goal will require surveying the HZs of ~ 100 nearby stars and makes it clear why a dedicated direct imaging mission is needed.

While *JWST* may be capable of detecting atmospheric biosignatures (Stevenson et al. 2016), markers indicating the presence of life, these observations rely on the

transit method. Transmission spectroscopy requires that the exoplanet pass in front of the host star relative to Earth, enabling an absorption spectrum of the exoplanet's atmosphere to be obtained as the star's light passes through (e.g., Sing 2018). This first limits the available targets to those with edge-on orbital planes relative to the line-of-sight to Earth. Assuming a random distribution for orbital plane inclinations, the probability of observing a transit can be estimated from the ratio of the stellar radius to the orbital radius. For Earth orbiting the Sun, this corresponds to a $\sim 0.47\%$ chance of observing a single transit. Additionally, the depth of the transit signal is proportional to the planetary radius over the stellar radius squared, giving a ratio of $\sim 8 \times 10^{-5}$ for the Earth and Sun. Therefore, *JWST* will be limited to terrestrial HZ exoplanets transiting the smallest, nearby M dwarfs where the orbital periods are short and the planet-star radius ratio is larger (e.g., Greene et al. 2016; Morley et al. 2017).

The method of directly imaging exoplanets, where an image or spectrum is taken directly of reflected or emitted light from the planet with the aid of a coronagraph blocking the star, provides several benefits compared to transits in the search for habitable exoplanets around Sun-like stars (e.g., Kaltenegger and Traub 2009; Snellen et al. 2015). Direct imaging is not limited by the orbital plane inclination, enabling observations of both transiting and non-transiting exoplanets. Also, the spectrum of the planet does not need to be disentangled from the spectrum of the star, which can cause significant degeneracies for exoplanets orbiting active stars (e.g., Apai et al. 2018; Rackham, Apai, and Giampapa 2018). As accurately determining the potential habitability of a planet will require probing the near-surface conditions and biosignatures that aren't present at higher altitudes, reflected light observations provide a shorter line-of-sight through the atmosphere down to the surface (e.g., The

LUVOIR Team 2019; Gaudi et al. 2020). The main problem with direct imaging is the needed sensitivity to detect Earth-sized exoplanets, where the planet-star contrast ratio is $\sim 10^{-10}$ for the Earth and Sun. This is why only next-generation, direct imaging space telescopes will be capable of achieving the goals set by the Decadal Survey, as current technologies need further development (Fujii et al. 2018).

With a planned aperture of ~ 6 meters, a coronagraph to suppress starlight, and the need to both image and spectrally characterize terrestrial HZ exoplanets in a reasonable amount of time, the number of stars accessible to HWO will be limited (Mamajek and Stapelfeldt 2024). Exoplanets in the HZ must be bright enough to observe and sufficiently separated from the host star such that the exoplanet will not be covered by the coronagraph. The minimum separation will be determined by the inner working angle (IWA) of the coronagraph, which is the on-sky angle blocked by the coronagraph, and the distance to star. All combined, this will largely limit targets to the nearest Sun-like stars, with the majority of M dwarfs being too faint and having too small and close-in HZs to be observable. The NASA Exoplanet Exploration Program mission star list (EMSL) for HWO (Mamajek and Stapelfeldt 2024) compiled the currently most accessible targets for this survey. Taking into account the conservative moist and maximum greenhouse HZ limits for Earth ((0.95-1.67 AU,) Kasting, Whitmire, and Reynolds 1993; Kopparapu et al. 2013) scaled by Eq. 1.1 for other stars, exoplanet brightness, planet-star contrast ratio, the presence of dust disks and/or close-in binaries, and hypothetical IWAs for HWO, the EMSL reports a total of 164 potential targets. These targets are prioritized according to Tiers A, B, and C based on the constraints used, with Tier A stars meeting the strictest constraints (Table 1.1).

As a driving force behind the goal of atmospheric characterization is the detection

Table 1.1. EMSL tier constraints

Parameter	Tier A	Tier B	Tier C
IWA (mas)	83	72	65
Exoplanet brightness (R_c mag)	≤ 30.5	≤ 31	≤ 31
Contrast ratio	$\geq 4 \times 10^{-11}$	$\geq 4 \times 10^{-11}$	$\geq 2.5 \times 10^{-11}$
Disk criterion	No disk	$\leq 10^{-4}$ contrast	All disks allowed
Binary separation	> 10"	$5 - 10$"	$3 - 5$"
F stars	14	15	37
G stars	15	23	17
K stars	17	11	12
M stars	1	2	0
Total stars	47	51	66

of biosignatures, further prioritization will be essential to maximize the chance of detecting life on another world. Commonly cited atmospheric biosignatures, and signatures of a potentially habitable planet, which may have been detectable at various points in Earth's history are O_2, O_3, CH_4, and H_2O (e.g., Schwieterman et al. 2018). Ruling out abiotic false positives will likely require the detection of multiple biosignatures, such as O_2 and CH_4, which makes obtaining as complete a spectrum as possible critical. Obtaining a full spectrum of modern Earth from $0.2 - 2$ μm with a sufficient signal-to-noise ratio (SNR) could take $\sim 10^2$-10^5 hours of exposure time (Figure 1.3) (The LUVOIR Team 2019), not including the initial time required to survey the HZs of each target for terrestrial exoplanets. The EMSL assumed an upper limit of 60 days of total integration when selecting suitable targets, indicating targets may be observed for months to achieve the desired goals. Without proper prioritization, significant time and resources may be dedicated to targets with lower likelihoods of hosting detectable life.

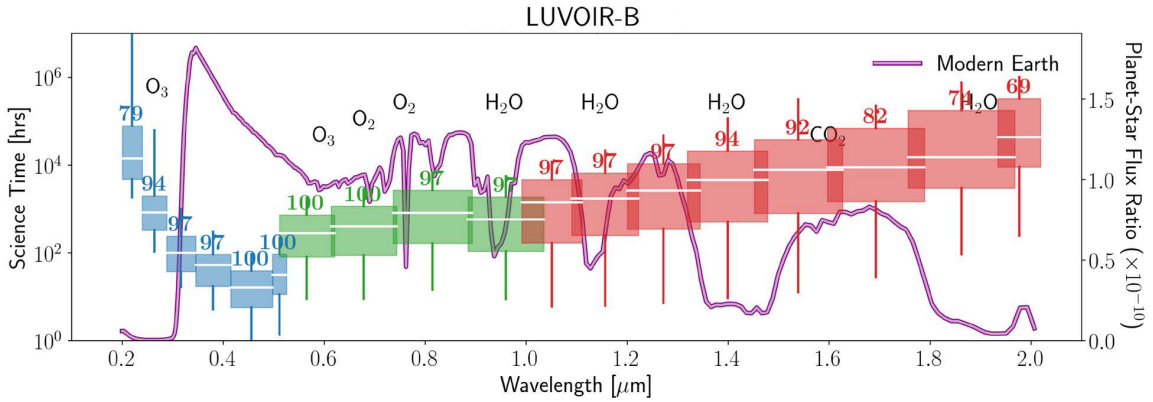

Figure 1.3. Figure from the LUVOIR Final Report (The LUVOIR Team 2019) showing the required exposure time per bandpass (left axis) to achieve SNR=8.5 for LUVOIR-B (similar to concepts for HWO). The box and whisker plots show the median, 50%, and 95% confidence intervals for the exposure time required to observe each bandpass of the spectrum for modern Earth plotted underneath. The values above each box and whisker are the percentage of targets for which a full spectrum can be obtained over the mission lifetime.

1.3 Continuous Habitable Zones

For defining potentially habitable exoplanets, we used the current HZ boundaries and assumed that the HZ is static. However, the HZ is not static and is inherently tied to the host star's evolution as L and $T_{\rm eff}$ evolve with time. Calculating the evolution of the HZ requires combining stellar evolution models, or functions describing the luminosity evolution of the star (e.g., Gallet et al. 2017), with HZ models. Figure 1.4 shows the evolution of the HZ for a 1 $M_\odot$, solar metallicity star from the pre-main sequence to the red giant branch. The continuous habitable zone (CHZ) can be defined as the orbital area remaining continuously with the HZ for some length of time. For determining the CHZ, one usually starts from the beginning of the main sequence (MS), which is referred to as the zero-age main sequence (ZAMS), and ends at the terminal-age main sequence (TAMS). Prior to the ZAMS, planets are still undergoing formation and significant evolution occurs as the star contracts until conditions in

the core are sufficient for the fusion of hydrogen. At the ZAMS, the approximate minimum in L is reached and increases from then on. Following the TAMS, the star once again rapidly evolves, expands, and the HZ moves quickly outward. We must consider the stellar evolutionary history to properly assess whether an exoplanet or system is suitable for detailed characterization. It should be noted that a robust analysis of an exoplanet's potential for habitability and the presence of life requires an interdisciplinary effort, taking into account additional factors like stellar activity and planetary geophysical and chemical evolution (e.g., Lammer et al. 2009; Güdel et al. 2014). However, we must start by considering the L and $T_{\rm eff}$ evolution of the host star, for which we will have the most complete information and understanding.

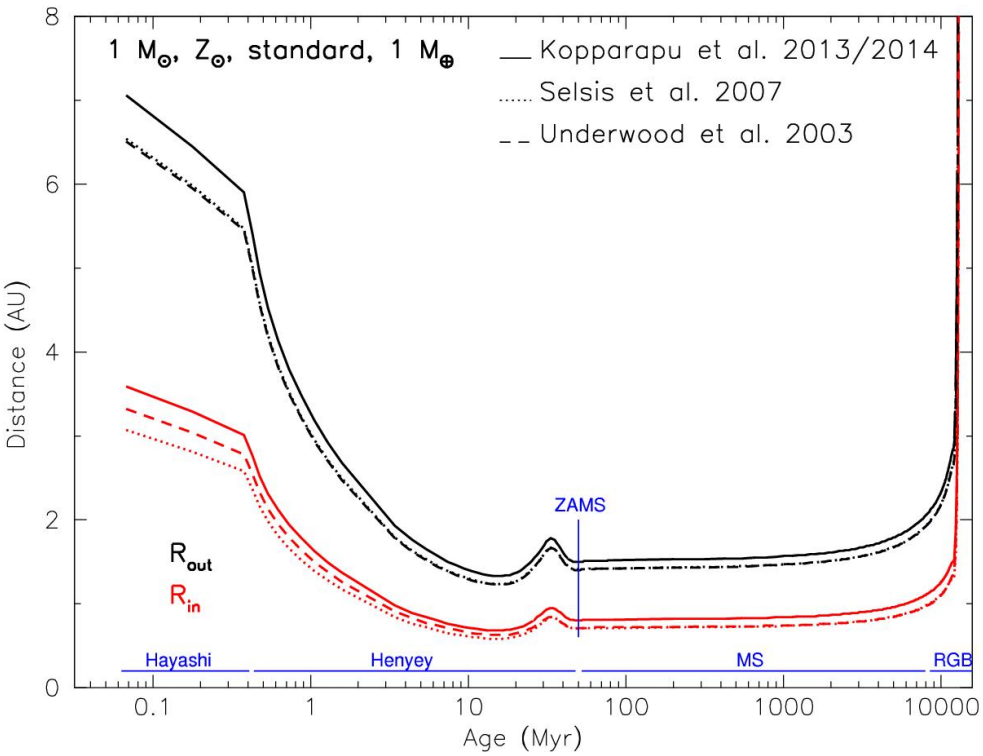

Figure 1.4. Figure from Gallet et al. 2017 showing the evolution of the HZ for a 1 $M_{\odot}$, solar metallicity star. The IHZ (red) and OHZ (black) are shown for various HZ prescriptions. The blue lines at the bottom mark various evolutionary phases.

This work focuses on expanding upon a catalog of stellar evolution tracks and a method for estimating the likelihood of exoplanet continuous habitability (Truitt et al. 2015; Truitt and Young 2017; Truitt et al. 2020), as well as applying this method to known terrestrial HZ exoplanets and systems. We use a definition for the CHZ describing the orbital area around a star that has remained continuously within the HZ for at least 2 Gyr, here referred to as the CHZ_2. This constraint corresponds to when the Great Oxidation Event occurred on Earth, about 2 Gyr after formation, and denotes the approximate time life on Earth took to make a detectable impact on the atmosphere (e.g., Holland 2006). At this point, modern Earth's canonical biosignatures, O_2 and O_3, became potentially observable (Figure 1.5). How long a given orbital radius will remain in the CHZ and whether a CHZ_2 will even exist is governed by the stellar lifetime. The MS lifetime of a star is primarily determined by the initial stellar mass, as more massive stars consume their hydrogen fuel quicker, with $t_{\rm MS} \sim M^{-2.5}$ for Sun-like stars. The secondary determinant is the initial stellar metallicity (Z), the fraction of elements heavier than helium, which impacts the efficiency of energy transport within the stellar interior. Increasing metallicity will increase the atmospheric opacity, reducing the efficiency of energy transport and increasing outward pressure. This causes less energy production to be needed to resist gravitational collapse and maintain hydrostatic equilibrium.

Knowledge of the initial mass and metallicity are sufficient to determine the likelihood a given orbital radius is within the CHZ_2 over the full MS lifetime. By taking the output L and $T_{\rm eff}$ from stellar evolution models, initialized for a given mass and metallicity, the HZ boundaries are calculated over time (Figure 1.6). Summing the total time spent in the HZ for a given orbital radius and comparing to the total length of the evolution track determines the likelihood of continuous habitability. However,

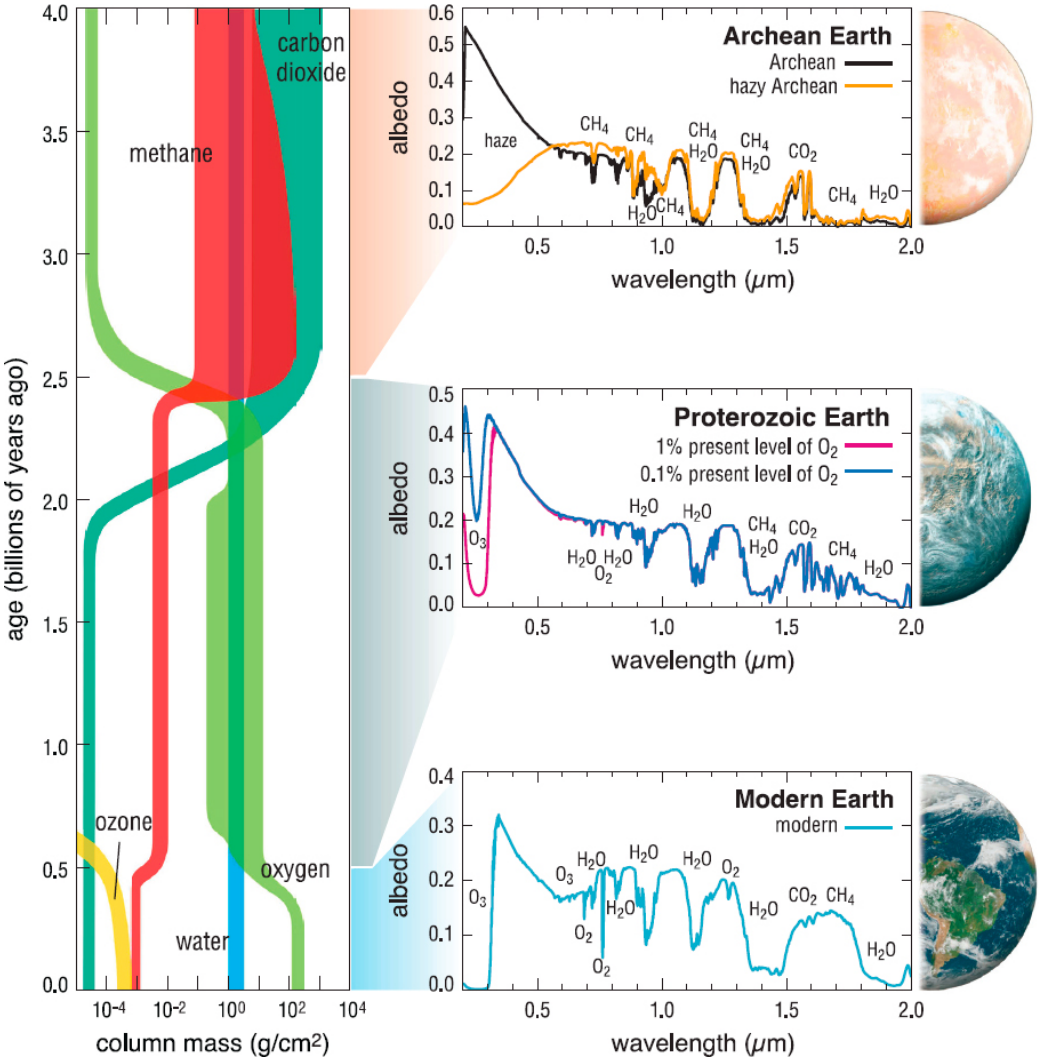

Figure 1.5. Figure from the LUVOIR Final Report (The LUVOIR Team 2019) showing the atmospheric composition (left) and simulated spectra (right) throughout Earth's history. Modern Earth's canonical biosignatures, O_2 and O_3, become potentially observable ~ 2 Gyr after formation during the Proterozoic eon.

an observer will want to know the probability of continuous habitability at the time of observation, not the full MS. This requires constraining the current evolutionary stage via measurement of the stellar age. We will discuss the difficulties of measuring stellar ages for field stars in this work, but we must often rely on comparisons to stellar evolution tracks.

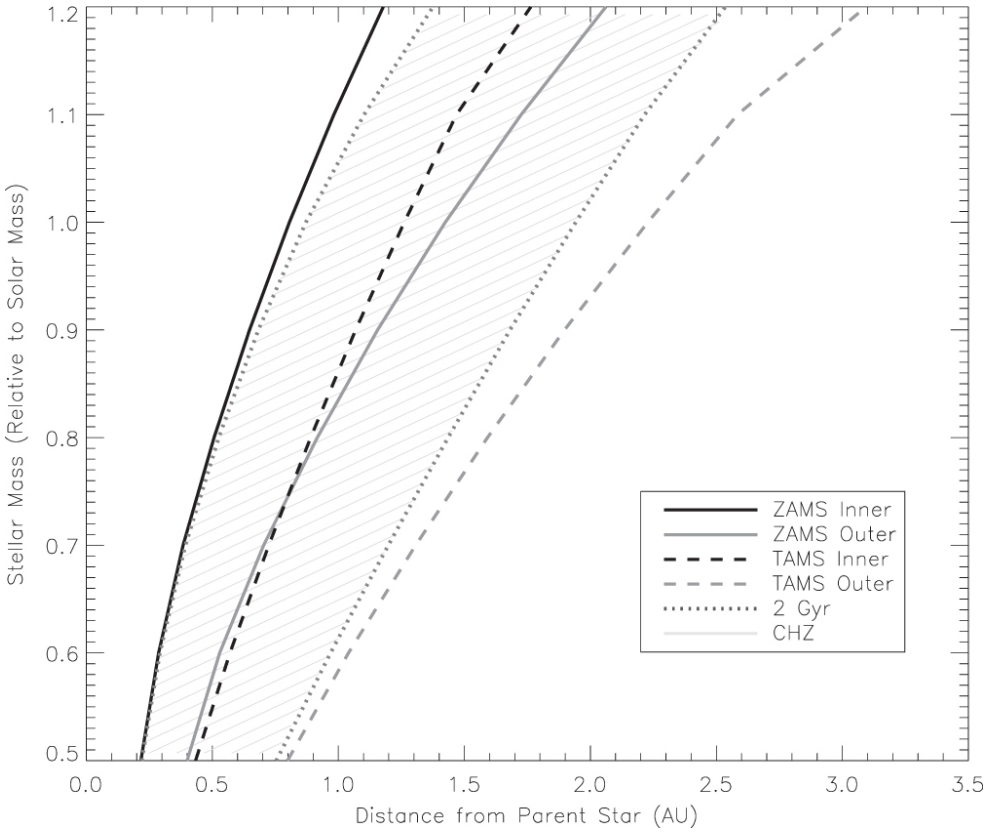

Figure 1.6. Figure from Truitt et al. 2015 showing the IHZ (black) and OHZ (dark grey) at the ZAMS (solid) and TAMS (dashed) with respect to stellar mass. The range of orbital radii that would at some point, over the full MS lifetime, be in the HZ for 2 Gyr or longer are indicated by the dotted lines and shaded region.

1.4 Thesis Overview

Chapter 2 presents an updated version of the Bayesian method used in Truitt et al. 2020 to estimate the likelihood that specific exoplanets are currently in the CHZ_2. The authors considered the orbital radius of a potentially habitable planet and, by comparing measured host star properties to those from stellar evolution models, fit a HZ evolution model. They used only the measured stellar mass and metallicity to constrain the fit to HZ models over the full MS lifetime. We incorporated stellar age in the Bayesian calculation, allowing us to determine the current probability that a

specific radius is in the CHZ_2. We then applied this method to Venus, Earth, Mars, and a sample of 9 terrestrial HZ exoplanets, combining an updated grid of stellar evolution models with the widely used HZ prescriptions from Kopparapu et al. 2013; Kopparapu et al. 2014. We demonstrate the importance of having precise stellar ages when calculating the likelihood an exoplanet is in the CHZ_2, which is most exemplified by the results for our own solar system.

Chapter 3 explores an alternative to how HZ prescriptions are typically derived, where the instellation is increased or decreased, for a limited set of planetary configurations, until the planet's climate reaches a limiting stellar flux and transitions to an uninhabitable state. We incorporate a new HZ model using results from Kiang et al. (2024, in prep). The authors use the ROCKE-3D GCM to model a perturbed parameter ensemble (PPE) of terrestrial planetary atmospheres. They sample 11 variables, including $T_{\rm eff}$, instellation (S_{0X}), CO_2 pressure, and additional planetary orbital, atmospheric, and surface parameters, for Earth-size planets in circular orbits. By performing a multivariate regression on the output model atmosphere diagnostics, we determine predictive equations for the HZ with uncertainty estimates, a novel feature for HZ prescriptions. This enables us to propagate an error through the Bayesian HZ model and place confidence bounds on the probability of any given orbital radius being in the CHZ_2. Although our results were impacted by sampling errors in the land planets ensemble, we still demonstrate the benefit of determining HZs with large GCM PPEs and pairing these within a Bayesian framework for predicting continuous habitability.

Chapter 4 applies our Bayesian HZ evolution method to the set of stars in the EMSL (Mamajek and Stapelfeldt 2024). The EMSL represents the sample of nearby stars with HZs most accessible to a future direct imaging survey with a 6-m-class

telescope. The current system of prioritization for these targets uses the HZ boundaries for our solar system from Kopparapu et al. 2013 scaled by the relation given in Eq. 1.1. There is no consideration of $T_{\rm eff}$ and HZ evolution, presenting a perfect opportunity to demonstrate our Bayesian HZ evolution method on a large set of high-priority targets. In order to encompass the diversity of stars in the EMSL, we generate an updated grid of stellar evolution tracks with the Tycho stellar evolution code (Young and Arnett 2005), which includes a new set of opacities, nuclear reaction rates, and initial abundances. The updated grid spans masses of $0.2 - 1.6$ $M_{\odot}$, metallicities ([M/H]) of -1.75 to 0.5 dex, and evolutionary phases from the pre-MS to the end of the subgiant branch. We will make the grid of stellar evolution tracks publicly available through GitHub. We use the HZ prescriptions from Kopparapu et al. 2014, but incorporating the recent water condensation limit proposed in Turbet et al. 2023. Finally, we demonstrate an easy method for calculating CHZ_2 likelihoods with any model grid using the open source stellar model grid interpolation tool `kiauhoku` (Claytor et al. 2020).

Chapter 2

CONTINUOUS HABITABLE ZONES: USING BAYESIAN METHODS TO PRIORITIZE CHARACTERIZATION OF POTENTIALLY HABITABLE WORLDS

Austin Ware[1], Patrick Young[1], Amanda Truitt[2], and Alexander Spacek[2]

1. School of Earth and Space Exploration, Arizona State University, Tempe, AZ 85287, USA
2. Los Alamos National Laboratory, Los Alamos, NM 87545, USA

Citation: Ware, A., Young, P., Truitt, A., & Spacek, A. 2022, *ApJ*, 929, 143, doi: 10.3847/1538-4357/ac5c4e

Abstract

The number of potentially habitable planets continues to increase, but we lack the time and resources to characterize all of them. With ~ 30 known potentially habitable planets and an ever-growing number of candidate and confirmed planets, a robust statistical framework for prioritizing characterization of these planets is desirable. Using the ~ 2 Gyr it took life on Earth to make a detectable impact on the atmosphere as a benchmark, we use a Bayesian statistical method to determine the probability that a given radius around a star has been continuously habitable for 2 Gyr. We perform this analysis on 9 potentially habitable exoplanets with planetary radii < 1.8 $R_\oplus$ and/or planetary masses < 10 $M_\oplus$ around 9 low-mass host stars ($\sim 0.5 - 1.1$ $M_\odot$) with measured stellar mass and metallicity, as well as Venus, Earth, and Mars. Ages for the host stars are generated by the analysis. The technique is also used to provide age estimates for 2768 low-mass stars ($0.5 - 1.3$ $M_\odot$) in the *TESS* Continuous Viewing Zones.

2.1 Introduction

The search for habitable worlds is at the forefront of astronomy and astrobiology. Over 4000 currently confirmed exoplanets and over 5000 *Transiting Exoplanet Survey Satellite* (*TESS*) candidates (Ricker et al. 2014) are currently cataloged. It is now known that exoplanets are fairly common in the habitable zones (HZ) of Sun-like and M-type stars (e.g., Tarter et al. 2007; Batalha et al. 2011; Petigura, Howard, and Marcy 2013; Dressing and Charbonneau 2015; Bryson et al. 2020), and rocky planets have been found inside HZs (e.g., Dittmann et al. 2017; Gillon et al. 2017; Bryson et al. 2021). Preliminary target lists have been mooted for NASA direct imaging

missions: HabEx (Gaudi et al. 2020), LUVOIR A/B (The LUVOIR Team 2019), and Starshade Rendezvous (Seager et al. 2019). Therefore, it is now important to quantitatively characterize these known and potential planetary systems in terms of potential for habitability. The large number of theoretical and observational uncertainties mean that any given planet can only be assigned a probability that it is within the HZ and has been for some amount of time. With many known HZ planets, and additional HZ planets likely to be discovered by current and future missions, a robust statistical framework with estimates of as many contributing probability distributions is desirable.

Each system with planets inside the HZ is of interest due to the potential for the emergence of life. However, we assume that life's ability to establish itself relies largely on the stability of the planet's environment (e.g., McKay 2014; Dong et al. 2018). We therefore need to know how long a planet has resided within the HZ to accurately predict the likelihood of life emerging and making a detectable impact on the planet's environment. Determining the length of time a planet spends in the HZ is difficult due to the various uncertainties in the actual definition of the HZ and in the characterization of the planetary system. Using the time it took for life on Earth to significantly alter the atmosphere as a benchmark, we can use a Bayesian method to determine the likelihood that a planet in a given system will spend a similar amount of time in the continuous habitable zone (CHZ).

Previous work has shown that life on Earth made a detectable impact on the atmosphere after $\sim 1-2$ Gyr following the Earth's formation (Kasting, Whitmire, and Reynolds 1993; Brocks et al. 1999; Kopp et al. 2005; Anbar et al. 2007; Crowe et al. 2013), with the Great Oxidation Event (GOE) occurring around 2 Gyr following formation (Summons et al. 1999; Kasting and Catling 2003; Holland 2006). Following

the work of Truitt et al. 2015, Truitt and Young 2017, and Truitt et al. 2020, we therefore define the orbital area around a host star that will remain habitable for at least 2 Gyr, here called the 2 Gyr continuous habitable zone (CHZ_2), as a conservative estimate of the potential habitability of planets in the system across the entire main sequence. More importantly, for specific planets, it is necessary to determine whether they have already spent 2 Gyr in the HZ. We acknowledge that different timescales could be adopted considering the HZ lifetimes of planets around various stellar types (Rushby et al. 2013), but using Earth's evolutionary history is a useful starting point in order to narrow down the list of potentially habitable planets. Different timescales can also be adopted considering the history of disequilibrium chemistry in the Earth's atmosphere. As far back as the Archean eon ($4.0 - 2.5$ Gyr ago), likely levels of biogenic CH_4 spurred detectable disequilibrium chemistry (Krissansen-Totton, Olson, and Catling 2018). However, the magnitude of the Earth's atmospheric disequilibrium increased with time in correlation with increased biomass and the evolution of oxygenic photosynthesis. Therefore, we find 2 Gyr to be a sufficiently conservative amount of time to allow life to make a large, detectable impact on a planet's atmosphere. Our framework is flexible and allows this limit to easily be adjusted in the future.

Placing a likelihood on the current potential habitability of a detected planet will require knowing the age of the system, but difficulties in directly measuring stellar ages (Soderblom 2010) means field stars typically lack age measurements. By fitting measurements of stellar properties to stellar evolutionary tracks, we can calculate approximate ages for field stars. Uncertainties on estimates of stellar ages for Sun-like stars are often on the order of 1 Gyr (Soderblom 2010; Torres, Andersen, and Giménez 2010). However, even a poorly known age can influence the prioritization of planets by considering the necessary time for life to produce detectable biosignatures in their

atmospheres. Stellar age estimates then prove critical for stars without proper age measurements.

Along with our age estimates from fits to stellar evolution tracks, we incorporate age measurements from the literature. A common observational measurement method for field stars is gyrochronology, an approach to estimating the age of a low-mass star via its rotation period. Over the course of a typical solar-type star's life (F7 - K2 type, Mamajek and Hillenbrand 2008), magnetic braking leads to the loss of angular momentum through mass loss (Weber and Davis 1967), which in turns causes a slowdown in the rotation rate (Skumanich 1972). By comparing field star rotation periods to stars with known ages and periods, the age of the star can be roughly constrained. Barnes 2007 presents a color-dependent law for the rotational period of solar-type stars, which can be used to create *gyrochrones* or plots of stars with the same age, but differing periods and colors. If a star's rotational period and color is known, they can be matched to the nearest gyrochrone and give an estimate of the age.

Samples of potentially habitable exoplanets can vary greatly depending on the HZ and terrestrial planet limits. Determining which planets around a star lie within the HZ requires using a model to determine where liquid surface water could potentially exist. These models can vary from a simple consideration of the stellar flux to more complex models considering a range planet masses and atmospheric compositions. Depending on the size of the estimated HZ, contrasting models can predict a significantly different sample of potentially habitable planets. Using optimistic constraints for the HZ (Kopparapu et al. 2013) and rocky-planet boundaries (Zeng, Sasselov, and Jacobsen 2016; Fulton et al. 2017; Thompson et al. 2018), we estimate there to be ~ 30 currently known potentially habitable exoplanets.

With these goals in mind, we use a Bayesian statistical method to determine the likelihood that a given radius from each star has been continuously habitable for 2 Gyr (Truitt et al. 2020) for 9 potentially habitable exoplanets around 9 $0.5 - 1.1$ $M_{\odot}$ host stars with planetary radii < 1.8 $R_{\oplus}$ and/or masses < 10 $M_{\oplus}$ (see Section 2.2.1), as well as Venus, Earth, and Mars. The results are intended to inform target prioritization for future NASA missions, such as LUVOIR and HabEx, and ground-based follow-up aimed at characterizing potentially habitable worlds. For planets that are not viable candidates for follow-up with these missions due to distance or other factors, this procedure provides characterization that can be validated by the observable planets, providing a statistical estimate of the habitability potential of the local region of the Galaxy. The method also enables rapid characterization of future discoveries in the working angles of HabEx and LUVOIR target stars.

We use stellar mass, metallicity, and age, with their associated uncertainties, to be our observational priors. Because stellar ages are not known for many systems, we also develop an algorithm to determine best-fit model ages, generated using the Tycho database of stellar evolution models, for potentially habitable systems. We compare best-fit model ages for the sample of 9 potentially habitable exoplanet host stars to known ages and perform the CHZ_2 analysis. As an addition to this work, we determine best-fit ages for a sample of 2768 *TESS* Continuous Viewing Zone (CVZ) F, G, K, and early-M stars between $0.5 - 1.3$ $M_{\odot}$. Future work includes expanding this Bayesian method to include additional stellar and planetary properties and testing various HZ model prescriptions.

2.2 Methods

2.2.1 Sample Selection

We chose a sample of 9 potentially habitable exoplanets around host stars approximately $0.5 - 1.1$ $M_\odot$ with the lower limit determined by the current lower mass limit on the Tycho Stellar Evolution Catalog. Parameters for the sample of exoplanets are listed in Table 2.1 and the associated host star parameters are listed in Table 2.2. The planets have radii < 1.8 $R_\oplus$ and/or masses < 10 $M_\oplus$, putting them within the optimistic range for rocky planets. The upper radius limit for rocky planets is adopted from Fulton et al. 2017; Thompson et al. 2018. 1.8 $R_\oplus$ is the approximate center of the $1.5 - 2.0$ $R_\oplus$ gap between rocky ("super-Earth") and gaseous ("mini-Neptune") planets, indicating an optimistic threshold. For candidates with mass measurements, we adopt the upper mass limit derived from the planetary mass-radius relation for rocky cores from Zeng, Sasselov, and Jacobsen 2016, $M = R^{3.7}$. Assuming the above upper radius limit of 1.8 $R_\oplus$, we determine a value of ~ 9 $M_\oplus$ and round up to 10 $M_\oplus$.

All 9 planets have instellation values within the optimistic Recent Venus (RV) inner habitable zone (IHZ) and Early Mars (EM) outer habitable zone (OHZ) boundaries for their system, calculated using the equations defined in Kopparapu et al. 2013 and discussed in Section 2.2.3. From a HZ perspective, these are high-priority candidates for spectral characterization.

Table 2.1. Selected potentially habitable planets

Planets	$M_\oplus$	$R_\oplus$	Period [d]	Ref.	NexSci Conf.?[a]
Kepler-1455 b	-	1.75	49.27684	1	Y
Kepler-438 b	-	1.12	35.23319	2	Y
KIC-7340288 b	-	1.51	142.5324	3	N
Kepler-441 b	-	1.462	207.2482	4(R),1(P)	Y
Kepler-442 b	-	1.34	112.3053	2	Y
HD 40307 g	7.1	-	197.8	5	Y
Kepler-62 f	-	1.531	267.291	4(R),6(P)	Y
Kepler-1544 b	-	1.685	168.8116	4(R),7(P)	Y
Kepler-452 b	-	1.511	384.843	4(R),8(P)	Y

References: 1. Thompson et al. 2018 2. Torres et al. 2015 3. Kunimoto, Matthews, and Ngo 2020 4. Berger et al. 2018 5. Tuomi et al. 2013 6. Borucki et al. 2013 7. Torres et al. 2017 8. Jenkins et al. 2015

[a]NexSci confirmed exoplanet via two different detection methods

2.2.2 Tycho Stellar Evolution Catalog

We use the stellar evolution code Tycho (Young and Arnett 2005) to expand the catalog of evolutionary tracks in Truitt et al. 2015 and Truitt and Young 2017. Tycho is a 1D stellar evolution code that utilizes a hydrodynamic formulation of the stellar evolution equations. Tycho contains OPAL opacities (Alexander and Ferguson 1994; Iglesias and Rogers 1996; Rogers and Nayfonov 2002), utilizes a combined OPAL and Timmes equation of state (Timmes and Arnett 1999; Rogers and Nayfonov 2002), gravitationally induced diffusion (Thoul, Bahcall, and Loeb 1994), general relativistic gravity, automatic rezoning, and an adaptable nuclear reaction network paired with a sparse solver. Low-temperature ($\sim$ 2400 K) opacities, which include dust grain opacities, were added in Truitt and Young 2017 and are based on Ferguson et al. 2005 and Serenelli et al. 2009. Tycho uses an adaptable 177 element network up to ^{74}Ge

Table 2.2. Stellar parameters for potentially habitable systems

Stars	$M/M_\odot$	$T_{\rm eff}$ [K]	$log(L/L_\odot)^a$	[M/H]
Kepler-1455	$0.528^{+0.036}_{-0.030}$ (1)	3899 ± 78 (2)	$-1.233^{+0.056}_{-0.081}$ (2[R,T])	-0.21 ± 0.11 (3)
Kepler-438	$0.544^{+0.028}_{-0.043}$ (1)	3748 ± 112 (4)	$-1.357^{+0.142}_{-0.138}$ (4)	0.16 ± 0.14 (4)
KIC-7340288	$0.57^{+0.02}_{-0.01}$ (5)	3949^{+79}_{-52} (5)	$-1.190^{+0.088}_{-0.111}$ (6)	-0.31 ± 0.14 (7)
Kepler-441	0.573 ± 0.026 (1)	4340 ± 87 (8)	$-1.067^{+0.048}_{-0.053}$ (8[R,T])	-0.58 ± 0.15 (1)
Kepler-442	0.613 ± 0.03 (1)	4402 ± 88 (8)	$-0.862^{+0.048}_{-0.053}$ (8[R,T])	-0.37 ± 0.1 (4)
HD 40307	0.71 ± 0.02 (9)	4827 ± 44 (10)	$-0.642^{+0.011}_{-0.012}$ (11)	-0.25 ± 0.03 (10)
Kepler-62	$0.727^{+0.029}_{-0.059}$ (1)	4859 ± 97 (8)	$-0.595^{+0.048}_{-0.052}$ (8[R,T])	-0.37 ± 0.04 (12)
Kepler-1544	$0.743^{+0.034}_{-0.030}$ (3)	4852 ± 97 (8)	$-0.604^{+0.048}_{-0.052}$ (8[R,T])	-0.08 ± 0.1 (3)
Kepler-452	$1.07^{+0.06}_{-0.04}$ (13)	5772^{+63}_{-65} (13)	$0.089^{+0.062}_{-0.067}$ (8[R],13[T])	0.23 ± 0.04 (13)

References: 1. Mathur et al. 2017 2. Thompson et al. 2018 3. Torres et al. 2017 4. Torres et al. 2015 5. Kunimoto, Matthews, and Ngo 2020 6. Stassun et al. 2019 7. Gaidos et al. 2016 8. Berger et al. 2018 9. Bonfanti, Ortolani, and Nascimbeni 2016 10. Valenti and Fischer 2005 11. Sousa et al. 2008 12. Borucki et al. 2013 13. Johnson et al. 2017

[a][R,T] indicates value calculated using referenced radius and effective temperature.

that is utilized throughout the evolution. The network uses REACLIB rates (Angulo et al. 1999; Rauscher and Thielemann 2000; Iliadis et al. 2001; Wiescher et al. 2006), weak rates from Langanke and Martínez-Pinedo 2000, and screening from Graboske et al. 1973. Mass loss is included, but is trivial for the mass range considered in this work. Neutrino cooling due to the Urca process and plasma processes is included. Turbulent convection is defined via a hydrodynamic formulation (Meakin and Arnett 2007; Arnett, Meakin, and Young 2009, 2010; Arnett and Meakin 2011) based on 3D, well-resolved simulations of convection between stable layers. Unlike most stellar evolution codes relying on mixing-length theory, Tycho has no free convective overshoot parameter.

The catalog currently contains models between $0.5 - 1.3$ $M_\odot$, with metallicities that fall between $0.1 - 3.0$ of $Z_\odot$. The metallicity models are in steps of 0.1 $Z_\odot$ between

$0.1 - 1.5$ $Z_\odot$ and steps of 0.25 $Z_\odot$ between $1.5 - 3.0$ $Z_\odot$. We added a finer grid of mass models, in steps of 0.05 $M_\odot$, between $0.5 - 1.0$ $M_\odot$. The mass models are in steps of 0.1 $M_\odot$ between $1.0 - 1.3$ $M_\odot$. We use these models in Section 2.2.3 to determine the HZ boundaries over the evolution of the star. The catalog also varies in [O/Fe] between 0.44×, 1.0×, and 2.28× $(O/Fe)_\odot$ for the full metallicity range. These models are included in Section 2.2.5 when fitting the ages for stars.

While future direct detection mission such as HabEx and LUVOIR will concentrate on Sun-like stars, virtually all of the simulated HZ planet detections for *TESS* are around M-type and late K-type stars (Sullivan et al. 2015; Barclay, Pepper, and Quintana 2018). There is then significant value in including host stars below 0.5 $M_\odot$. We will expand this catalog further and include stars down to 0.1 $M_\odot$ in a future paper.

2.2.3 Habitable Zone Models

Tycho outputs information on stellar surface quantities for each time-step of the evolution. For this work, we use the stellar effective temperature and luminosity to define the inner and outer boundaries of the HZ, as a function of stellar age, utilizing equations from Kopparapu et al. 2013; Kopparapu et al. 2014. This method can be used substituting other HZ prescriptions, but Kopparapu et al. are a commonly used point of reference. These HZ prescriptions parameterize the location of the HZ as a function of the host star luminosity and effective temperature, from which we can calculate the associated time-dependent HZ distance for each stellar evolution track. For a given orbital distance from any star we can predict how long and at what stellar age a planet would remain habitable. Thus, for a perfectly characterized star (mass,

metallicity, and age known exactly), we can say with high confidence whether a planet has been continuously within the circumstellar HZ for 2 Gyr for a given HZ model.

Kopparapu et al. 2013; Kopparapu et al. 2014 give several possible definitions for the HZ boundaries. The most optimistic HZ definition follows from Kopparapu et al. 2013, where they empirically determine the inner and outer HZ edge assuming that Venus and Mars once hosted habitable conditions. For the inner habitable zone (IHZ) edge, the "recent Venus" (RV) case, they determined the effective solar flux on Venus 1 Gyr ago, under the assumption that there may have been liquid water on the surface prior to this time. Similarly, for the outer habitable zone (OHZ) edge, the "early Mars" (EM) case, they determined the effective solar flux on Mars ~ 3.8 Gyr ago, when liquid water likely existed on the surface.

The conservative HZ definitions follow from Kopparapu et al. 2014, where they define an IHZ edge by the "runaway greenhouse" case. Here, the effective solar flux incident on the planet becomes sufficient to completely vaporize the oceans. The OHZ edge is defined by the "maximum greenhouse" case. This outer edge is the point where Rayleigh scattering becomes dominant over the greenhouse effect of CO_2. The conservative cases were calculated for masses of 0.1, 1, and 5 $M_\oplus$ to account for gravitational effects on the atmosphere.

2.2.4 Bayesian Habitable Zone Probabilities

Bayesian statistics have been previously used to better understand the emergence of life on planets (Spiegel and Turner 2012) and statistical analysis has been used in Bean, Abbot, and Kempton 2017 to develop a method for surveying key terrestrial exoplanet atmosphere composition characteristics, like H_2O and CO_2 abundances, in

order to broadly assess many exoplanet habitability potentials, rather than spending time gathering extensive data about individual exoplanets. However, these methods focus on the characteristics of the exoplanet, but do not take into account the star and the stellar environment. Truitt et al. 2015; Truitt and Young 2017 discuss how the initial mass and composition will affect the surface properties, and therefore the HZ evolution (e.g., Rushby et al. 2013; Waltham 2017).

This Bayesian approach to HZs aims to determine the probability that a given orbital distance from the host star has spent 2 Gyr in the HZ, following the methods of Truitt et al. 2020. Depending on the known properties of the star, this approach could follow several different cases. The simplest example would involve knowing the mass and metallicity of the star arbitrarily well, but not knowing the age. The probability in this case would depend solely on how long the orbit remains in the HZ of the star as predicted by the models. In other cases, there is an additional or multiple uncertainties. If the metallicity and/or mass is unknown, then all metallicity and/or mass models must be integrated over. If the metallicity or mass is known to within some uncertainty, assumed to be Gaussian, then we must weight the contribution of each model by the fit of the model mass and model metallicity to the Gaussian of each measured value. Introducing the age for the star adds an additional Gaussian prior distribution to the calculation. Here, we focus on the cases where the metallicity and mass are known to within some uncertainty, but the age is unknown, as well as the case where the metallicity, mass, and age are known to within some uncertainty. The other cases are described in detail in Truitt et al. 2020. Although this work is limited to considering metallicity, mass, and age, it can in principle be extended to include other properties, such as planetary composition and stellar activity.

2.2.4.1 Case 1: Metallicity and Mass Measurement but No Age Measurement

We first describe the case where the stellar metallicity and mass are known to within some uncertainty, but the age is unknown. In this case, the age is limited to 12 Gyr to account for the age of the Universe. Our method relies on the expansion of Bayes' Theorem:

$$P(A|B) = \frac{P(B|A)P(A)}{P(B|A)P(A) + P(B|\neg A)P(\neg A)} \tag{2.1}$$

where $P(A|B)$ is the posterior likelihood, or the likelihood of outcome A occurring given B, $P(B|A)$ is the likelihood of B given that A is true, and $P(A)$ is the prior probability that the outcome A is true.

We apply Equation (2.1) to the Tycho models and measured distributions for the stellar metallicity (Z) and mass (M) to calculate the Bayesian posterior probability. In Equation (2.1), $B = Z, M$ and $A = CHZ_2$, or the outcome where a given radius is in the CHZ_2. Equation (2.1) therefore becomes

$$P(CHZ_2|Z,M) = \frac{P(Z,M|CHZ_2)P(CHZ_2)}{P(Z,M|CHZ_2)P(CHZ_2) + P(Z,M|\neg CHZ_2)P(\neg CHZ_2)}. \tag{2.2}$$

We now describe how we compute each component of Equation (2.2) for a chosen model metallicity Z_k and mass M_k, for any given radius from the star. The index k refers to the specific model used, interpolated if necessary. We calculate $P(CHZ_2)$, the initial probability that a given radius is within the CHZ_2, by

$$P(CHZ_2) = \frac{\sum_{i,j}(t_{CHZ_2,ij}\Delta Z_j)\Delta M_i}{\sum_{i,j}(t_{tot,ij}\Delta Z_j)\Delta M_i} \tag{2.3}$$

where the index i runs through the Tycho model masses $M = 0.5 - 1.3\ M_\odot$ and the index j runs through the model metallicities from $Z = 0.1 - 3.0\ Z_\odot$, $t_{CHZ_2,ij}$ is the

total time the radius is in the CHZ_2 for a given Tycho model (M_i,Z_j), $t_{tot,ij}$ is the total lifetime for the given Tycho model (with a maximum of 12 Gyr), ΔM_i ($M_{i+1} - M_i$) is the distance between M values, and ΔZ_j ($Z_{j+1} - Z_j$) is the distance between Z values. Note that we first sum over all model metallicities and then over all model masses. The initial probability that a radius is not in the CHZ_2, $P(\neg CHZ_2)$, is given by

$$P(\neg CHZ_2) = 1 - P(CHZ_2). \tag{2.4}$$

The likelihood that a star has a model metallicity Z_k and mass M_k if a given radius is in the CHZ_2 is given by

$$P(Z_k, M_k|CHZ_2) = \frac{t_{CHZ_2,k}P(Z_k)P(M_k)}{\sum_{i,j}(t_{CHZ_2,ij}P(Z_j))P(M_i)} \tag{2.5}$$

where $P(Z)$ and $P(M)$ are probabilities given by the Gaussian distributions for each measured value ($Z' \pm \sigma_Z$, $M' \pm \sigma_M$). For example, the measured metallicity distribution is given by

$$P(Z) = \frac{1}{\sqrt{2\pi}} e^{\frac{1}{2}\frac{\Delta' Z^2}{\sigma_Z^2}} \tag{2.6}$$

where $\Delta' Z$ is defined as $Z' - Z$, the difference between the measured mean and model values. The likelihood that a star has metallicity Z_k and mass M_k if a given radius is not in the CHZ_2 is given by

$$P(Z_k, M_k|\neg CHZ_2) = \frac{(t_{tot,k} - t_{CHZ_2,k})P(Z_k)P(M_k)}{\sum_{i,j}((t_{tot,ij} - t_{CHZ_2,ij})P(Z_j))P(M_i)}. \tag{2.7}$$

We combine Equations (2.3)-(2.5) and (2.7) to calculate the Bayesian posterior probability in Equation (2.2), $P(CHZ_2|Z_k, M_k)$. With a factor of $P(Z_k)$ and $P(M_k)$ cancelling out, we get

$$P(CHZ_2|Z_k, M_k) = \frac{\frac{t_{CHZ_2,k}\sum_{i,j} t_{CHZ_2,ij}}{\sum_{i,j}(t_{CHZ_2,ij}P(Z_j))P(M_i)\sum_{i,j} t_{tot,ij}}}{\frac{t_{CHZ_2,k}\sum_{i,j} t_{CHZ_2,ij}}{\sum_{i,j}(t_{CHZ_2,ij}P(Z_j))P(M_i)\sum_{i,j} t_{tot,ij}} + \frac{(t_{tot,k}-t_{CHZ_2,k})(1-\frac{\sum_{i,j} t_{CHZ_2,ij}}{\sum_{i,j} t_{tot,ij}})}{\sum_{i,j}((t_{tot,ij}-t_{CHZ_2,ij})P(Z_j))P(M_i)}}. \tag{2.8}$$

We can now calculate the Bayesian posterior probability at each radius, for a given Z and M, that it is in the CHZ_2 at any time during the main sequence lifetime, limited to 12 Gyr. Therefore, probabilities cannot exceed 10/12 because each radii from the star must be habitable for at least 2 Gyr, limiting the maximum CHZ_2 time to 10 Gyr.

2.2.4.2 Case 2: Metallicity, Mass, and Age Measurement

Without knowledge of the age, we previously summed the total CHZ_2 time and main sequence lifetime. If we know the age measurement in the form of Gaussian errors, $A \pm \sigma_A$, we can similarly use this as the probability term $P(A)$ using the Gaussian probability

$$P(A) = \frac{1}{\sqrt{2\pi}} e^{\frac{1}{2}\frac{\Delta' A^2}{\sigma_A^2}} \tag{2.9}$$

where $\Delta' A$ is defined as $A' - A$. $P(A)$ is used to place a prior probability on the total and CHZ_2 times, t_{tot} and t_{CHZ_2}, thereby prioritizing model timesteps closer to the mean age of the star in a similar way to how $P(Z)$ and $P(M)$ prioritize model metallicities and masses closer to the mean stellar metallicity and mass. t_{tot} is now given by

$$t_{tot} = \sum_m (t_{tot,m} - t_{tot,m-1})P(A) \tag{2.10}$$

where the index m runs through each model step and $A = t_{tot,m}$. By combining Equations (2.10) and (2.8), we can now calculate the Bayesian posterior probability that each radius is currently within the CHZ_2. We apply this method to our sample of potentially habitable planets, with results summarized in Table 2.5 for each planet and the Bayesian posterior distributions for each star shown in Figure 2.4. For all 9 sample stars, we applied a $4\times$ linear and cubic interpolation to the mass models.

We use the methods for Case 1 and Case 2, as well as the 1 $M_\oplus$ HZ model from Kopparapu et al. 2014, to calculate the the CHZ_2 posterior likelihood for the Sun with and without the age prior. The age of the Sun, determined via helioseismology and solar models, is taken to be 4.57 ± 0.11 Gyr (Bonanno, Schlattl, and Paternò 2002). The results are shown in Figure 2.1, which includes the orbits of Venus, Earth, and Mars. This comparison exemplifies the extent to which a precise age measurement can have on the CHZ_2 probability distribution. Without an age measurement, Earth is given only a $\sim 20\%$ probability of being in the CHZ_2, while Mars has a $\sim 80\%$ probability. Earth's closer proximity to the Sun means it will leave the HZ sooner than Mars, significantly reducing the probability that it would currently be within the CHZ_2 without knowing the age. With knowledge of the Sun's age, we see that both Earth and Mars have a 100% probability of being currently in the CHZ_2, which matches our current understanding of the Sun's HZ.

2.2.5 Stellar Ages

Although most stars in this sample have measured ages, the vast majority of *TESS* targets and some known potentially habitable systems lack age measurements. Without measurements of the ages, we cannot determine how long planets have

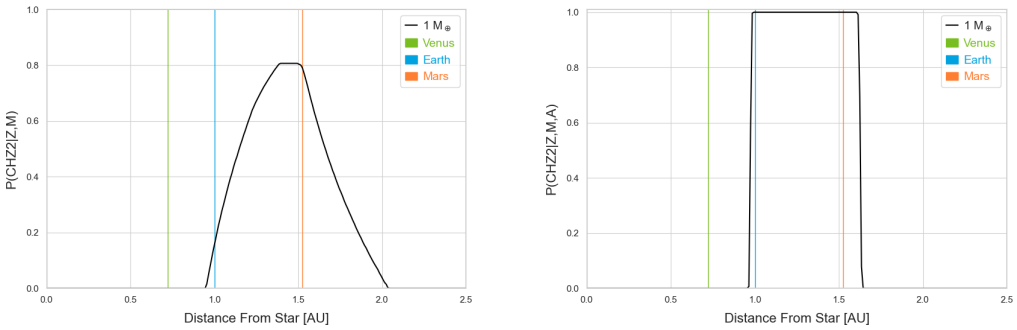

Figure 2.1. P(CHZ_2 | Z,M) (left) and P(CHZ_2 | Z,M,A) (right) for the Sun assuming a 1 $M_\oplus$ planet with a runaway greenhouse conservative IHZ and maximum greenhouse conservative OHZ.

resided in the HZ. Therefore, it is essential to estimate the stellar age in order to more accurately predict the potential for life not only existing, but having made a detectable impact. Measurement of stellar ages is relatively straightforward if the star resides in a cluster (e.g., Sandage 1970; Lastennet and Valls-Gabaud 2002), but is very difficult for field stars (Soderblom 2010). This often relies on estimates given by fits to stellar evolution models like Tycho. By using luminosity (L) and effective temperature ($T_{\rm eff}$) measurements, we can perform χ^2 fits to models from the Tycho stellar evolution catalog (Truitt et al. 2015; Truitt and Young 2017) to determine the best-fit model ages:

$$\chi^2 = \frac{(L_{\rm mod} - L_{\rm obs})^2}{\sigma_L^2} + \frac{(T_{\rm mod} - T_{\rm obs})^2}{\sigma_T^2} \tag{2.11}$$

where $L_{\rm mod}$ and $L_{\rm obs}$ are the model and observed luminosities, $T_{\rm mod}$ and $T_{\rm obs}$ are the model and observed stellar effective temperatures, and σ_L and σ_T are the errors in the observations (Young et al. 2001; Pagano et al. 2015). If mass and compositional measurements are available, the search is constrained to models bracketing the measured values of mass and metallicity. Model points were averaged and weighted by their

associated χ^2 value. Upper and lower uncertainties were derived from the weighted standard deviation of the sample.

Uncertainties on estimates of stellar age for Sun-like stars are rarely less than 1 Gyr, often times even significantly larger (Soderblom 2010; Torres, Andersen, and Giménez 2010). By operating within a Bayesian statistical framework, we can still extract useful information from a roughly constrained age. Assuming a Gaussian distribution for the best-fit age and uncertainty, we introduce the age as a prior probability distribution in the calculation. Even a poorly known age can then influence the prioritization of planets by taking into account that some planets may not have had enough time for life to produce detectable biosignatures in their atmospheres. The best-fit ages will then prove useful to determining the current habitability of the planets in these systems.

Ages for 8 stars, except KIC-7340288, were available in the literature. We also generated best-fit ages for all of the stars in the sample. The ages for all 9 host stars along with source references are provided in Table 2.3. We prefer stellar ages determined via gyrochronology for use as the age prior in Section 2.3 to determine the $P(CHZ_2)$ profiles for each system. Ages determined via gyrochronology tend to have tighter constraints on the age and the method is observationally calibrated, rather than relying on fits to isochrones or evolutionary tracks. For those stars with only isochrone ages, we take the average of the literature age and our fits to evolutionary tracks. For Kepler-442, which has a large upper error of ~ 8 Gyr, we also average the literature age with our age. Figure 2.2 shows an over-plot of the measured literature ages and the best-fit model ages. Aside from Kepler-1455 and Kepler-441, the observed values fall within the predicted range of values determined by the models. Kepler-1455 and Kepler-441 are near the lower mass tail of the model space (~ 0.5 $M_\odot$) and will

likely benefit from further increasing the mass and metallicity resolution and range of the model space.

Table 2.3. Stellar ages for potentially habitable systems

Stars	Age_{Tycho} [Gyr]	Age_{lit} [Gyr]	Ref.	Tech.[a]
Kepler-1455	$5.84^{+3.55}_{-3.49}$	$1.4^{+0.6}_{-0.2}$	1	1,2
Kepler-438	$6.03^{+3.45}_{-3.49}$	$4.4^{+0.8}_{-0.7}$	2	1,2
KIC-7340288	$5.77^{+3.50}_{-3.31}$	-	-	-
Kepler-441	$4.99^{+2.04}_{-1.13}$	$1.9^{+0.5}_{-0.4}$	2	1,2
Kepler-442	$6.09^{+3.41}_{-3.47}$	$2.9^{+8.1}_{-0.2}$	2	1,2
HD 40307	$4.65^{+3.63}_{-2.79}$	6.9 ± 4.0	3	1
Kepler-62	$5.82^{+3.55}_{-3.48}$	4.0 ± 0.6	2	1,2
Kepler-1544	$3.50^{+2.30}_{-1.12}$	$3.90^{+7.30}_{-0.80}$	1	2
Kepler-452	$4.62^{+2.67}_{-1.36}$	6 ± 2	4	2

References: 1. Torres et al. 2017 2. Torres et al. 2015 3. Bonfanti, Ortolani, and Nascimbeni 2016 4. Jenkins et al. 2015

[a]Measurement Techniques: 1. Gyrochronology 2. Isochrone

Since the age determination is easily automated, we have determined ages for a sample of *TESS* continuous viewing zone (CVZ) targets from the *TESS* Input Catalog (TIC). The sample of 2768 stars was retrieved from the TIC version 8.1 via the Mikulski Archive for Space Telescopes (MAST) at the Space Telescope Science Institute. The sample spans masses of $0.5 - 1.3$ $M_{\odot}$, ecliptic latitudes of $\theta < -78^{\circ}$ and $\theta > 78^{\circ}$, *TESS* apparent magnitudes $T_{mag} < 10$, and all stars have luminosities consistent with dwarf stars. Potential planets in these systems will receive the most observation time from *TESS* and likely from both ground- and space-based follow-up missions. Stellar ages will be essential for placing probabilistic constraints on the habitability potential of each for future target prioritization. A sample of estimated

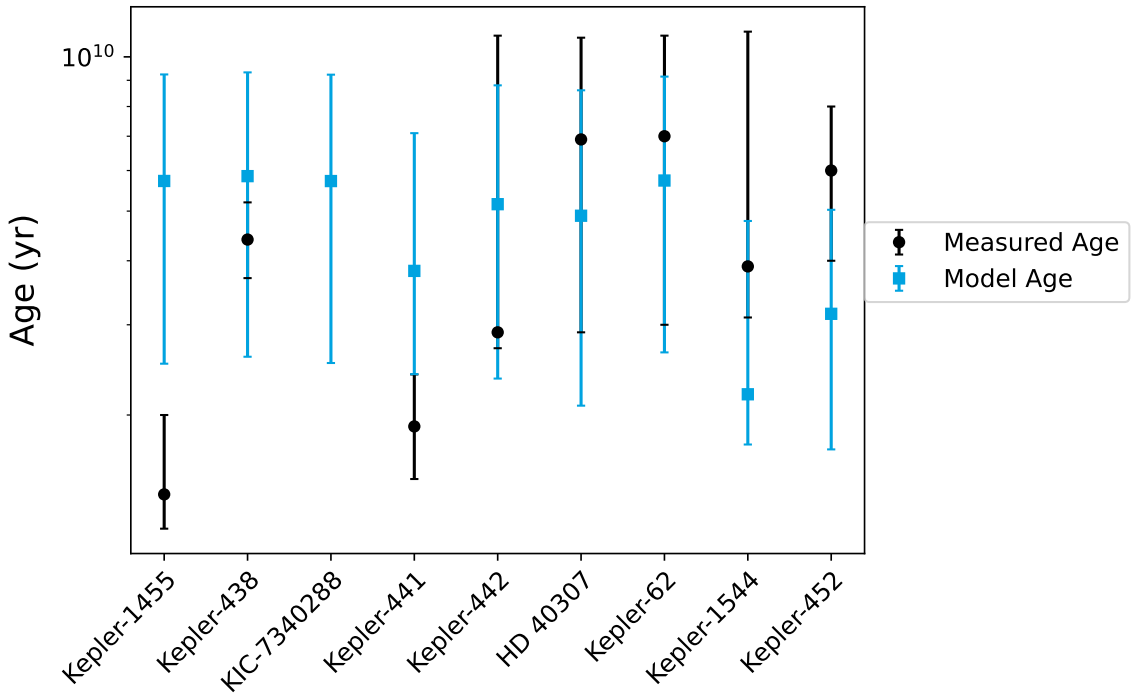

Figure 2.2. Comparison of measured literature ages and Tycho stellar evolution catalog best-fit model ages for sample of potentially habitable systems.

ages is included in Table 2.4, which includes the stellar parameters taken from the TIC.

An overview of the results of this age analysis is shown in Figure 2.3. Notably, we see a concentrated band of stars at higher ages and a more dispersed group of stars at lower ages. This feature is present in both the Northern and Southern CVZ samples, indicating no directional correlation. In addition, only one star in the sample, TIC 30270183, is known to be a member of a cluster or moving group. Hayden et al. 2015 observed two distinct populations in compositional ([α/Fe] versus [Fe/H]) space at $R > 5$ kpc in the Milky Way's disk. One population is roughly solar-α and spans a large range of [Fe/H], which merges with a lower-α population at super-solar [Fe/H]. This could be indicative of a lower metallicity, older stellar population and a higher

Table 2.4. *TESS* CVZ stellar ages

TIC	Age_{Tycho} [Gyr]	$M/M_\odot$	T_{eff} [K]	$L/L_\odot$	[M/H]
55454149	$6.62^{+1.59}_{-2.32}$	1.03 ± 0.13	5754 ± 132	2.45 ± 0.08	-
141912469	$2.79^{+1.83}_{-1.45}$	1.20 ± 0.18	6232 ± 138	2.68 ± 0.12	-0.59 ± 0.09
38844604	$5.67^{+2.29}_{-2.48}$	1.05 ± 0.13	5813 ± 131	3.27 ± 0.12	-
350824257	$6.16^{+1.65}_{-1.71}$	1.05 ± 0.13	5830 ± 117	2.76 ± 0.10	-0.10 ± 0.10
233080190	$3.05^{+0.92}_{-0.51}$	1.23 ± 0.18	6290 ± 128	4.45 ± 0.16	-
33879314	$5.06^{+1.95}_{-3.17}$	1.04 ± 0.12	5782 ± 104	1.26 ± 0.05	-0.12 ± 0.05
280162266	$2.85^{+1.50}_{-1.05}$	1.24 ± 0.19	6304 ± 129	2.85 ± 0.12	-
289540757	$2.04^{+3.80}_{-0.95}$	1.12 ± 0.15	6034 ± 119	1.22 ± 0.04	-
441724181	$5.72^{+2.29}_{-2.59}$	1.06 ± 0.13	5865 ± 124	1.52 ± 0.05	-
232629681	$4.80^{+2.64}_{-1.70}$	1.10 ± 0.14	5987 ± 108	4.81 ± 0.17	-0.04 ± 0.03
55295030	$6.24^{+1.76}_{-3.09}$	1.11 ± 0.14	6005 ± 119	2.55 ± 0.10	-0.53 ± 0.05
220411843	$4.18^{+4.23}_{-2.91}$	0.94 ± 0.12	5398 ± 140	0.58 ± 0.02	0.06 ± 0.05
219898046	$6.41^{+1.95}_{-2.35}$	1.01 ± 0.13	5697 ± 131	2.52 ± 0.07	-
149625812	$8.12^{+1.35}_{-2.35}$	1.03 ± 0.13	5751 ± 128	1.87 ± 0.07	-
287140180	$5.62^{+2.32}_{-2.44}$	1.04 ± 0.12	5778 ± 112	3.31 ± 0.09	-
198161860	$2.41^{+2.42}_{-1.37}$	1.25 ± 0.19	6330 ± 127	2.00 ± 0.07	-
441812317	$3.52^{+2.20}_{-1.25}$	1.16 ± 0.16	6124 ± 124	2.93 ± 0.10	-
256299260	$3.14^{+1.22}_{-0.32}$	1.20 ± 0.17	6219 ± 119	4.33 ± 0.18	-
289572073	$4.80^{+0.70}_{-1.12}$	1.12 ± 0.14	6024 ± 120	3.75 ± 0.14	-

Note: Table 2.4 is published in its entirety in the machine-readable format. A portion is shown here for guidance regarding its form and content.

metallicity, younger population. Determining the exact nature of these age bands is beyond the scope of this work, but we will further investigate this in the future.

2.3 CHZ_2 Planet Profiles

CHZ_2 posterior probabilities for the sample of 9 potentially habitable exoplanets, as well as Venus, Earth, and Mars, are included in Table 2.5, with the full CHZ_2

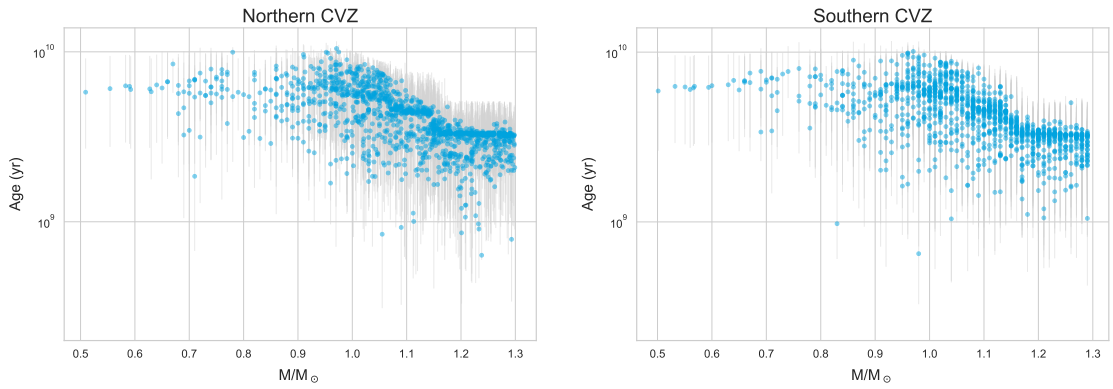

Figure 2.3. Tycho best-fit model ages for *TESS* Northern and Southern CVZ sample of F, G, K, and early-M stars, using stellar properties from the TIC version 8.

distributions for each star, including the Sun, displayed in Figure 2.4. $< P_{0.1} >$, $< P_1 >$, $< P_5 >$, and $< P_{RV/EM} >$ are the posterior probabilities averaged over the orbital range of the planet for each HZ model from Section 2.2.3 (0.1 $M_\oplus$, 1 $M_\oplus$, 5 $M_\oplus$, and Recent Venus/Early Mars).

Although all 9 exoplanets fall within the current HZ around their host star, we determine Kepler-1455 b and Kepler-438 b to have approximately P(CHZ_2) ≈ 0 for all cases, or essentially little to no chance of having been continuously in the HZ for 2 Gyr. This indicates that they are situated too close to the inner edge to spend a significant amount of time in the HZ and will likely soon leave the HZ.

KIC-7340288 b, an unconfirmed super-Earth planet candidate (Kunimoto, Matthews, and Ngo 2020), is consistently a high probability target in our sample. The planet candidate's orbital range puts it at the peak CHZ_2 probability ($P \approx 0.9$) for all HZ cases considered. Given KIC-7340288 b's relatively large size ($R = 1.511$ $\mathrm{R}_\oplus$), the planet candidate is more likely to have retained its atmosphere and would be better able to regulate the surface temperature and retain water. Therefore, our prediction

Table 2.5. Planetary CHZ_2 posterior likelihoods

Planets	$M_\oplus$	$R_\oplus$	Orbit [au]	$< P_{0.1} >$	$< P_1 >$	$< P_5 >$	$< P_{RV/EM} >$
Kepler-1455 b	-	1.75	$0.20 - 0.23$	0.0	0.0	0.0	0.048
Kepler-438 b	-	1.12	$0.16 - 0.18$	0.001	0.005	0.007	0.068
KIC-7340288 b	-	1.51	$0.44 - 0.45$	0.900	0.905	0.905	0.906
Kepler-441 b	-	1.462	$0.55 - 0.58$	0.345	0.345	0.34	0.362
Kepler-442 b	-	1.34	$0.37 - 0.40$	0.340	0.458	0.584	0.903
HD 40307 g	7.1	-	$0.57 - 0.61$	0.797	0.865	0.885	0.906
Kepler-62 f	-	1.531	$0.70 - 0.75$	0.801	0.838	0.850	0.894
Kepler-1544 b	-	1.685	$0.53 - 0.56$	0.523	0.661	0.743	0.959
Venus	0.815	0.950	0.72	0.0	0.0	0.0	0.0
Earth	1.00	1.00	1.00	0.0	1	1	1
Mars	0.107	0.531	1.52	1	1	1	1
Kepler-452 b	-	1.511	$1.04 - 1.09$	0.402	0.499	0.533	0.833

Note: The orbital radius ranges indicated here are representative of $\pm 1\sigma$ semimajor axis orbits and these are calculated using the periods in Table 2.1 and stellar masses in Table 2.2.

that KIC-7340288 b has remained in a stable HZ environment for 2 Gyr should be seen as a substantial indicator of the planet candidates potential habitability.

Notably, Earth resides at the inner edge of the CHZ_2 for the 1 $M_\oplus$ HZ model and is outside the inner edge for the 0.1 $M_\oplus$ model. Being that Earth is the only habitable planet we know of in the Universe, this shows that too conservative of HZ models are likely to exclude planets that have a high potential of being habitable. Although Mars has a 100% probability of being in the CHZ_2 across all models and would generally be considered uninhabitable, it is better to include a potential Mars-like planet rather than excluding an Earth-like planet.

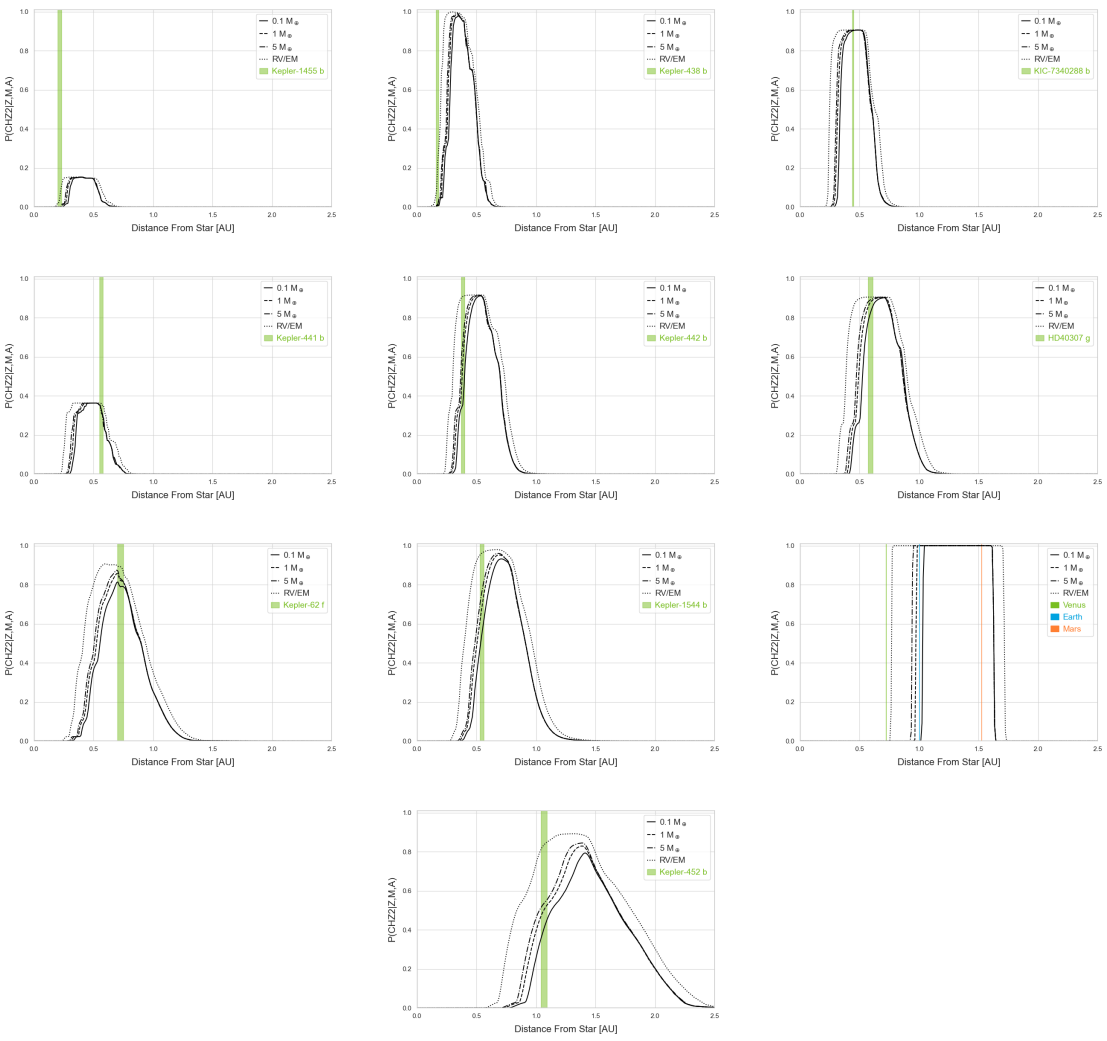

Figure 2.4. P(CHZ_2 |Z,M,A) for Kepler-1455 b, Kepler-438 b, KIC-7340288 b, Kepler-441 b, Kepler-442 b, HD 40307 g, Kepler-62 f, Kepler-1544 b, the Sun (Venus, Earth, Mars), and Kepler-452 b assuming a 0.1, 1, and 5 $M_\oplus$ runaway greenhouse conservative inner habitable zone (IHZ) and maximum greenhouse conservative outer habitable zone (OHZ), as well as an optimistic case assuming a Recent Venus (RV) IHZ and Early Mars (EM) OHZ. The orbital range of planets are indicated by filled rectangles.

2.4 Conclusions

This work builds upon Truitt et al. 2020 by further expanding the Tycho model space and adding a stellar age prior. The additions improve the framework's ability to estimate the time-dependent habitability of a planet given only limited knowledge of stellar properties and planetary orbital radius. We further applied this Bayesian method to analyzing the long-term habitability of 9 likely-rocky exoplanets with a high probability of being in the HZ (Table 2.5). The posterior probability distributions used priors of measured stellar metallicity, mass, and age fitted to Tycho stellar evolution models and HZ definitions from Kopparapu et al. 2013; Kopparapu et al. 2014. Two such exoplanets, Kepler-1455 b and Kepler-438 b, are shown to be unlikely to have spent 2 Gyr in the HZ for this model. KIC-7340288 b, a recently discovered super-Earth planet candidate included in our sample, is consistently found to have the highest probability of having been in the HZ for 2 Gyr.

The addition of an age prior and a method for estimating stellar ages from Tycho models will prove invaluable in future work estimating the continuous habitability of unstudied *TESS* candidates. By attaining fits to stellar ages comparable to published gyrochronology measurements and other isochrone ages, we demonstrate the ability to estimate ages for future potentially habitable systems with existing observations. We applied this method for age estimation to a sample of F, G, K, and early-M *TESS* CVZ stars from the TIC and produced ages for 2768 stars. Stars in the *TESS* CVZs will receive the most observing time from *TESS* and are the only *TESS* targets likely to yield detections of potentially habitable planets around Sun-like stars. The inner 5° of the *TESS* CVZs are also coincident with that of JWST, so many candidates found

here are the most likely for JWST follow-up. The techniques presented here can be rapidly applied to candidates detected around HabEx and LUVOIR target stars.

In the near-term, we will include stellar evolution models down to 0.1 $M_{\odot}$, as this will enable the analysis of the remainder of potentially habitable systems, as well as the majority of the systems likely to be found with *TESS*. Increasing the resolution of the models in the lower-mass regime will provide better fits to K and M dwarfs as well.

Our finding that Mars is given an equal probability to Earth of being in the CHZ_2 by our model is a prime example of the need for additional observational and model constraints in order to more accurately predict potential habitability. To explore the effects of introducing additional priors to the Bayesian method, we will include stellar and planetary properties important to stellar and planetary evolution, such as stellar [O/Fe] ratios, planetary composition, and stellar activity, an increasingly important factor in the study of M-dwarf systems. Expanding the suite of HZ models will provide additional confidence constraints on individual systems. Planetary mass, atmospheric composition, stellar multiplicity, and various other factors will impact the ability of liquid water to remain present on a planet for long enough for the presence of life to be remotely detectable. These properties can be added individually as priors as measurements and theoretical predictions become available.

Acknowledgements

The results reported herein benefitted from collaborations and/or information exchange within NASA's Nexus for Exoplanet System Science (NExSS) research coordination network sponsored by NASA's Science Mission Directorate. We would like to thank Eric Mamajek for information regarding spectral classification and

current habitable zone exoplanets. We would also like to thank the reviewers for comments that lead to significant improvements in the quality of this work.

Chapter 3

PAIRING A GENERAL CIRCULATION MODEL ENSEMBLE AND BAYESIAN FRAMEWORK TO PREDICT HABITABLE ZONE EVOLUTION

3.1 Introduction

With the launch of *JWST*, we have entered a new era for exoplanet science as atmospheric detection and characterization of terrestrial exoplanets in the circumstellar habitable zone (HZ) becomes possible. This will initially be limited to transiting exoplanets orbiting nearby M dwarfs, those most amenable to transmission and emission spectroscopy with *JWST* (e.g., Greene et al. 2016; Morley et al. 2017). In the near- and medium-future, potential ground-based extreme precision radial velocity (EPRV) surveys (Laliotis et al. 2023; Newman et al. 2023) and next-generation space telescopes, such as the NASA Habitable Worlds Observatory direct-imaging mission, will aim to detect, measure masses, and characterize the atmospheres of terrestrial exoplanets in the HZs of nearby Sun-like (F-, G-, K-type) host stars (Astro2020 Decadal Survey). A driving force behind attempts to characterize the atmospheres of terrestrial HZ exoplanets is the detection of biosignatures, the markers left by life, which will enable us to determine if we are not alone in the universe (e.g., Seager and Deming 2010). While biosignatures may be detectable in the atmospheres of Earth-sized transiting exoplanets orbiting M dwarfs with *JWST* (Stevenson et al. 2016) and extremely large telescopes (Hawker and Parry 2019), only a next-generation direct imaging mission will be capable of doing so for both transiting and non-transiting exoplanets in the HZs of Sun-like stars (Fujii et al. 2018).

For both M dwarf and Sun-like hosts, detailed characterization of terrestrial exoplanet atmospheres will require a significant amount of time and resources for even a single planet. This makes it essential to prioritize observations by those most likely to host detectable life. A critical first step is determining if liquid water could remain stable on the surface of a given exoplanet by using planetary climate models. These models typically determine the HZ boundaries by the limiting stellar flux that results in a moist or runaway greenhouse at the inner HZ (IHZ) edge and maximum greenhouse or complete freezing point at the outer HZ (OHZ) edge. A common point of reference in the exoplanet community are the 1D, cloud-free, radiative convective models of Kopparapu et al. 2013; Kopparapu et al. 2014, which built upon the work of Kasting, Whitmire, and Reynolds 1993. The authors provide predictive equations for the HZ boundaries with respect to the stellar effective temperature for an idealized Earth model. Numerous studies use these HZ definitions to determine the potential habitability of discovered exoplanets (e.g., Borucki et al. 2013; Wright et al. 2016; Luque et al. 2019; Gilbert et al. 2023), the occurrence rate of terrestrial exoplanets in the HZs of Sun-like stars ($\eta_{\oplus}$) (e.g., Silburt, Gaidos, and Wu 2015; Kopparapu et al. 2018; Bryson et al. 2021), or for prioritizing target stars with HZs most accessible to potential missions (The LUVOIR Team 2019; Gaudi et al. 2020; Mamajek and Stapelfeldt 2024).

Although 1D models benefit from their relative simplicity and fast equilibration times, they are unable to self-consistently account for clouds, surface variations, atmospheric and oceanic heat transport, and orbital variables that would lead to uncertainty in habitability estimates. 3D general circulation models (GCMs) are needed to simulate these multidimensional effects. While uncertainties in GCMs arise from needing to account for a large number of boundary conditions and pa-

rameterizations for scale-dependent physical processes, multi-model intercomparison projects (MIPs) are organized to quantify model mean predictions (e.g., the Coupled Model Intercomparison Project, Eyring et al. 2016), and such MIPs are emerging now for exoplanet models (e.g., Fauchez et al. 2021; Haqq-Misra et al. 2022; Christie et al. 2022). Including the effects of atmospheric and ocean dynamics can extend the HZ compared to estimates from 1D models (Leconte, Forget, Charnay, Wordsworth, and Pottier 2013; Way et al. 2017). The complexity of 3D models leads to long computational times to reach climatological equilibrium, but present a means to more rigorously constrain the variability of habitable atmospheres.

Both 1D and 3D models aimed at determining the limits of habitability have focused on specific planetary configurations or scenarios and vary a single or narrow set of parameters. Kasting, Whitmire, and Reynolds 1993 and Kopparapu et al. 2013 focused on Earth-like planets with H_2O and CO_2 dominated atmospheres, with Kopparapu et al. 2014 expanding to planets with different masses. Others have explored the importance of rotation rate or tidal locking (e.g., Yang, Cowan, and Abbot 2013; Kopparapu et al. 2017; Jansen et al. 2019; Chen et al. 2019), water inventories and surface water distributions (e.g., Abe et al. 2011; Kodama et al. 2018; Kodama et al. 2019), the ability for atmospheric water to condense following formation (Turbet et al. 2021; Turbet et al. 2023), atmospheric composition (e.g., Wolf and Toon 2013; Del Genio et al. 2019), and various other factors. These studies have shown the diversity of potentially habitable, and uninhabitable, climates with respect to potential stellar and planetary properties and initial conditions, but also prove the difficulty in trying to define the HZ based on correlations to a limited sampling of possible variables or specific scenarios.

Beyond determining whether an exoplanet currently resides within the HZ, the

continuous habitability until the time of observation should also be considered when prioritizing exoplanets by those most likely to host detectable life. Earth likely required $\sim 1-2$ Gyr of continuous habitability in order for life to make detectable impacts on the atmosphere through disequilibrium chemistry or high O_2 and O_3 abundances (Krissansen-Totton, Olson, and Catling 2018). If Earth is a typical example of a habitable planet and life on Earth is typical of life in the universe, then exoplanets must maintain habitable conditions for billions of years before life would be remotely detectable. This leads to the concept of the continuous habitable zone (CHZ), the orbital area around a star remaining continuously within the HZ for a given length of time.

The CHZ is generally studied with respect to the stellar luminosity evolution, by pairing HZ definitions with a parameterization of the stellar luminosity evolution or stellar evolution models. The length of time required for a planet to be in CHZ typically ranges from $2-4$ Gyr (Valle et al. 2014; Truitt et al. 2015), but can also be defined by the maximum amount of time a planet or orbital radius resides in the HZ (Gallet et al. 2017). Recently, Mello and Friaça 2023 used a minimal mantle and atmospheric model to simulate the evolution of the HZ, showing that the stellar luminosity evolution moves the IHZ outward and the cooling of the planetary interior, and subsequent decrease in CO_2 outgassing, contracts the OHZ with time. While low-dimensional models are computationally efficient and can be run over geologic timescales to explore continuous habitability, 3D models are restricted to short timescales. In order to determine the habitability lifetime for a GCM planet model, equilibrated model runs at different incident stellar fluxes are stages in the planet's atmospheric evolution. By then considering the stellar luminosity evolution

of the host star, the limiting incident stellar fluxes for the IHZ and OHZ determine the habitability lifetime for that planet (Wolf et al. 2017).

Truitt et al. 2020 developed a Bayesian method to determine the probability that a planet is within the 2 Gyr continuous habitable zone, referred to as the CHZ_2. By pairing HZ models from Kopparapu et al. 2013 and Kopparapu et al. 2014 with Tycho (Young and Arnett 2005) stellar evolution models, they evolve the HZ over the full main sequence evolution, up to 12 Gyr. For a given star, the measured mass and metallicity, with assumed Gaussian uncertainties, place a likelihood on each HZ evolution model. Integrating over all models determines the posterior likelihood distribution, where each orbital radius is assigned a probability of being within the CHZ_2. Ware et al. 2022 expanded upon this Bayesian framework by including the stellar age as a prior on the stellar evolution models. This enables the calculation of the current CHZ_2 probability, the time at which a telescope would observe the planet. This method was applied to several known HZ exoplanets (as well as Venus, Earth, and Mars for validation), providing a demonstration of how these probabilities of continuous habitability can be used to prioritize follow-up observations of potentially habitable exoplanets.

In this work, we introduce the use of statistics of the 3D planetary general circulation model (GCM) perturbed parameter ensemble from Kiang, N. Y. et al. (2024, in preparation) (referred to as K24 from here on) to define HZ boundaries and estimate CHZ_2 probabilities. We compare to results using the Kopparapu et al. 2014 HZ models. K24 use the ROCKE-3D GCM (Way et al. 2017) to model an ensemble of land planet atmospheres, with the goal of exploring the influence of a large subset of parameters on the fractional habitability of land planets within the HZ. While most studies focus on aqua planets similar to Earth, which can include planets completely

covered by a global ocean or planets with exposed land surrounded by circulating oceans, land planets with small water inventories and dominated by exposed land are shown to have wider HZs (Abe et al. 2011; Leconte, Forget, Charnay, Wordsworth, Selsis, et al. 2013). This is a result of drier tropics, which allow increased radiative cooling at the IHZ and lower cloud fractions (lower albedo) at the OHZ.

By performing multivariate regressions on the output climate diagnostics from K24, we determine predictive equations and uncertainty estimates for the HZ boundaries with respect to the stellar effective temperature (T_{eff}) and planet instellation, with other perturbed parameters imposing uncertainties in those predictions. Using outputs from Tycho stellar evolution models, we use these equations to model the HZ as the star evolves and calculate the CHZ_2 posterior distributions for a sample of known potentially habitable systems. Excluding the planetary parameters, such as CO_2 partial pressure and surface albedo, in the regressions quantifies their role as unknowns for exoplanets observed with near-term missions. The variance in model climate diagnostics from these excluded parameters is included in the associated standard error for each regression coefficient, which leads to uncertainty in the HZ boundaries. This enables us to propagate HZ uncertainties through the Bayesian model and place confidence bounds on the probability of any given orbital radius being in the CHZ_2.

The goal of this work is to provide a demonstration of concept for defining HZ boundaries through the statistics of GCM PPEs, where each planet model provides a time slice equilibrium of the climate for the sampled parameters, and combining this with a Bayesian framework to predict the potential continuous habitability of exoplanets. While the results of this analysis are ultimately limited by the ensemble size, choice of sampled parameters, and sampling ranges, we provide a starting point for combining theoretical planetary system science models with stellar evolution

models for the purpose of informing future studies and observations. This work can be expanded upon through more comprehensive GCM model ensembles and stellar evolution catalogs, coupled models for planetary interior evolution and surface life, and future observations of terrestrial exoplanets.

In Section 3.2, we describe our methodology and sample of known potentially habitable exoplanets and host stars. In Section 3.3, we present our results for the HZ definitions using the ROCKE-3D land planets ensemble and calculated CHZ_2 posterior distributions compared against the Kopparapu et al. 2014 HZ models. Finally, Section 3.4 presents the discussion of results.

3.2 Methods

3.2.1 Sample Selection

Our methods frame continuous habitability from the perspective of the luminosity and T_{eff} evolution of the host star. Although the majority of known HZ exoplanets orbit M dwarfs (Hill et al. 2023), exoplanets in the HZs of M dwarfs pose problems for our current methods. Very low-mass stars evolve slowly and the luminosity and T_{eff} of these stars change little over time, rendering our framing less informative over the lifetime of the universe. The continuous habitability of these exoplanets will depend more on the evolution of the X-ray/UV environment and the planetary rotation rate. M dwarf stars retain active chromospheres far longer than Sun-like stars (e.g., Miles and Shkolnik 2017; Loyd et al. 2018), potentially causing photo-evaporation of short period exoplanet atmospheres (e.g., Cloutier and Menou 2020) and harm to life. Further, exoplanets in their HZs tend to be in synchronous rotation (e.g., Barnes

2017), leading to a reliance on a stable sub-stellar cloud deck to maintain habitable surface conditions (e.g., Kopparapu et al. 2016). Additionally, the future NASA direct imaging mission will aim to characterize Earth-like exoplanets around nearby Sun-like stars (Astro2020 Decadal Survey). For these reasons, we choose to focus our analysis on rocky exoplanets in the HZs of Sun-like stars.

We selected a sample of 7 confirmed exoplanets in the HZ around K- and G-type host stars, including 6 exoplanets from Ware et al. 2022. We exclude 3 exoplanets from that sample that orbit M dwarfs. Planetary and stellar parameters from the literature for the sample of exoplanets are listed in Table 3.1 and Table 3.2, respectively. The exoplanets fall within the optimistic range for rocky planets, with radii < 1.8 $R_\oplus$ and masses < 10 $M_\oplus$. The upper radius limit for rocky planets is adopted from Fulton et al. 2017; Thompson et al. 2018, where 1.8 $R_\oplus$ is the approximate center of the $1.5 - 2.0$ $R_\oplus$ gap between rocky super-Earth and gaseous sub-Neptune planets. The upper mass limit is adopted from the planetary mass-radius relation for rocky cores from Zeng, Sasselov, and Jacobsen 2016, $M = R^{1.37}$. Assuming a radius of 1.8 $R_\oplus$, we determine an upper mass limit of ~ 9 $M_\oplus$ and round up to 10 $M_\oplus$. This optimistic upper mass limit is influenced by known, large exoplanets with densities consistent with a rocky composition (e.g., Kepler-20 b, Bonomo et al. 2023).

All 7 exoplanets have instellations within the optimistic Recent Venus (RV) and Early Mars (EM) HZ boundaries, determined using the equations defined in Kopparapu et al. 2014. We did not include exoplanets from Hill et al. 2023 that only spend a portion of their orbit in the HZ due to eccentricity. The HZ boundaries for each star were calculated using the luminosities and $T_{\rm eff}$ chosen from the literature. We adopted luminosities and $T_{\rm eff}$ for four stars from Petigura et al. 2022, which reported the stellar radii determined via the Stefan-Boltzmann relation. The authors calculated the

luminosity for this purpose, but did not report the value. Rather than independently calculating the luminosity, we backed out their value using the reported radii and $T_{\rm eff}$. In order to determine their original uncertainties on the luminosities, we "subtracted in quadrature" using the uncertainties in the radii and $T_{\rm eff}$. Similarly for Kepler-441, we backed out the calculated luminosity from the radius and $T_{\rm eff}$ reported in Berger et al. 2018.

Table 3.1. Selected terrestrial habitable zone exoplanets

Planets	$M_\oplus$	$R_\oplus$	Period [d]	Ref.	α [AU][a]	NexSci Conf.?[b]
Kepler-441 b	...	1.462	207.24871 ± 0.00057	1,2	0.558 ± 0.012	Y
Kepler-442 b	...	1.395	112.30341 ± 0.00057	1,2	0.391 ± 0.009	Y
Kepler-1544 b	...	1.685	168.81128 ± 0.00054	1,2	0.541 ± 0.015	Y
Kepler-62 f	...	1.531	267.291 ± 0.005	1,3	0.724 ± 0.017	Y
HD 40307 g	7.1	...	$197.8^{+5.7}_{-9.0}$	4	$0.593^{+0.017}_{-0.024}$	Y[†]
HD 216520 c	9.440	...	154.43 ± 0.44	5	0.527 ± 0.019	Y
Kepler-452 b	...	1.511	$384.843^{+0.007}_{-0.012}$	1,6	1.062 ± 0.023	Y[†]

References: 1. Berger et al. 2018 2. Gajdoš, Vaňko, and Parimucha 2019 3. Borucki et al. 2013 4. Tuomi et al. 2013 5. Burt et al. 2021 6. Jenkins et al. 2015

[a]Semi-major axis calculated from period in Table 3.1 and stellar mass in Table 3.2.

[b]NexSci confirmed exoplanet.

[†]Marked as controversial in the NASA Exoplanet Archive.

For HD 40307, we adopt the mean $T_{\rm eff}$ (4870 K) from the PASTEL catalogue (Soubiran, Brouillet, and Casamiquela 2022), which includes measurements from various high-resolution spectroscopy studies. However, we find their reported uncertainty (18 K) too small. The sources that Soubiran, Brouillet, and Casamiquela 2022 referenced to determine their mean $T_{\rm eff}$ and uncertainty have values ranging 4774-4977 K, a significantly wider spread than the reported uncertainty. To better represent the range of $T_{\rm eff}$ measurements, we assume an uncertainty of 100 K, which is nearly

equivalent to the spread between the mean and the upper and lower extremes of the reference values.

For Kepler-442 we could not find a spectral type reported in the literature. To gain a rough estimate of the spectral type, we visually compared the 2MASS (Cutri et al. 2003) $J - H$ and $H - K_s$ colors to the spectral type table provided by Pecaut and Mamajek 2013. We found the colors and $T_{\rm eff}$ to be consistent with that of a K-dwarf and assume this going forward.

Two confirmed exoplanets in our sample, HD 40307 g and Kepler-452 b, are marked as controversial in the NASA Exoplanet Archive. HD 40307 g was detected by Tuomi et al. 2013 via the radial velocity method and a subsequent follow-up analysis of the system was reported in Díaz et al. 2016, both using publicly available data from the HARPS survey (Mayor et al. 2003). They found in the latter analysis that the signal reported at $P \sim 200$ days is inconclusive, which corresponds to HD 40307 g. To date, no follow-up studies using independent observations have been published to further confirm or reject the candidate. Therefore, we retain HD 40307 g in our sample.

Kepler-452 b was detected by Jenkins et al. 2015 via the transit method using data from the *Kepler* mission. Two follow-up studies (Mullally et al. 2018; Burke et al. 2019) of the *Kepler* data found Kepler-452 b to fall below the 99% confidence threshold required for statistical validation due to problems with systematic false positive in the regime of small, long period *Kepler* planet candidates. As with HD 40307 g, no independent follow-up studies have been published to further confirm or reject the candidate and we therefore retain Kepler-452 b in our sample.

The stellar parameters listed in Table 3.2 are used for comparison to stellar evolution models. We use the measured iron abundance relative to solar, [Fe/H], to compare to the overall metallicity, Z, of the models. It is common for only [Fe/H] to

be reported in the literature and subsequently in stellar modeling to assume Z scales accordingly. However, specific abundances can vary significantly for the same [Fe/H] and Truitt et al. 2015; Truitt and Young 2017 show that the HZ distance can be significantly altered with only changes to abundance ratios. Due to the typically large variation between sources for abundance measurements of the same star, attributable to differences in methods and solar normalization (e.g., Hinkel et al. 2016; Furlan et al. 2018), we adopt conservative 0.15 dex uncertainties in [Fe/H], unless the reported uncertainty is higher.

Table 3.2. Stellar parameters for habitable zone exoplanet host stars

Stars	$T_{\rm eff}$ [K]	$L/L_\odot$	$M/M_\odot$	[Fe/H]
Kepler-441	4340 ± 177 (1)	0.086 ± 0.003 (2)†	0.54 ± 0.02 (3)	-0.57 ± 0.18 (1)
Kepler-442	4427 ± 70 (4)	0.137 ± 0.007 (4)†	0.63 ± 0.02 (3)	-0.59 ± 0.15 (4)
Kepler-1544	4744 ± 110 (4)	0.229 ± 0.009 (4)†	0.74 ± 0.03 (3)	0.00 ± 0.15 (4)
Kepler-62	4863 ± 100 (4)	0.253 ± 0.014 (4)†	0.71 ± 0.03 (3)	-0.34 ± 0.15 (4)
HD 40307	4870 ± 100 (5)	0.260 ± 0.010 (6)	0.71 ± 0.02 (7)	-0.31 ± 0.15 (5)
HD 216520	5103 ± 20 (8)	0.353 ± 0.003 (8)	0.82 ± 0.04 (8)	-0.17 ± 0.15 (8)
Kepler-452	5775 ± 100 (4)	1.143 ± 0.055 (4)†	1.08 ± 0.04 (4)	0.24 ± 0.15 (4)

References: 1. Torres et al. 2015 2.Berger et al. 2018 3. Berger et al. 2020 4. Petigura et al. 2022 5. Soubiran, Brouillet, and Casamiquela 2022 6. Stassun et al. 2019 7. Bonfanti, Ortolani, and Nascimbeni 2016 8. Burt et al. 2021

†Luminosity calculated using radius and effective temperature from reference.

3.2.2 Tycho Stellar Evolution Catalog

We use the stellar evolution code Tycho (Young and Arnett 2005) to update the catalog of evolutionary tracks in Ware et al. 2022. Tycho is a 1D stellar evolution code that utilizes a hydrodynamic formulation of the stellar evolution equations. Tycho

contains OPAL opacities (Alexander and Ferguson 1994; Iglesias and Rogers 1996; Rogers and Nayfonov 2002), utilizes a combined OPAL and Timmes equation of state (Timmes and Arnett 1999; Rogers and Nayfonov 2002), and gravitationally induced diffusion (Thoul, Bahcall, and Loeb 1994). Tycho utilizes an adaptable 177 element reaction network up to ^{74}Ge combined with REACLIB rates (Angulo et al. 1999; Rauscher and Thielemann 2000; Iliadis et al. 2001; Wiescher et al. 2006), weak rates from Langanke and Martínez-Pinedo 2000, and screening from Graboske et al. 1973. Turbulent convection is defined via a hydrodynamic formulation (Meakin and Arnett 2007; Arnett, Meakin, and Young 2009, 2010; Arnett and Meakin 2011) based on 3D, well-resolved simulations of convection between stable layers, which eliminates the need for free convective parameters (i.e., "convective overshoot").

We have updated the Tycho catalog to include a finer resolution grid of model masses, enabling a more precise calculation of the posterior probability distributions described in Section 3.2.4. The catalog contains mass models between $0.5 - 1.3$ $M_{\odot}$, with steps of 0.01 $M_{\odot}$. The model metallicities remain unchanged and are between $0.1 - 3.0$ of $Z_{\odot}$, with steps of 0.1 $Z_{\odot}$ between $0.1 - 1.5$ $Z_{\odot}$ and steps of 0.25 $Z_{\odot}$ between $1.5 - 3.0$ $Z_{\odot}$. We use these models in Section 3.2.3 to determine the HZ boundaries over the evolution of the star. The catalog also varies in [O/Fe] between 0.44×, 1.0×, and 2.28× $(O/Fe)_{\odot}$ for the full metallicity range. However, we leave out those models for this analysis as there are not [O/Fe] measurements available in the literature for all the stars in our sample. When available, we plan to include [O/Fe] ratios as a prior in our Bayesian method, as this can have a significant effect on the evolution of the HZ (Truitt et al. 2015).

3.2.3 Habitable Zone Models

Following Ware et al. 2022, we include the HZ models from Kopparapu et al. 2014. Here, we specifically focus on the conservative 1 $M_\oplus$ model, defined by a runaway greenhouse IHZ and maximum greenhouse OHZ, and the optimistic RV/EM model, assuming the incident solar fluxes for Venus and Mars when liquid water may have been present on the surfaces. The authors parameterize the HZ with respect to the T_{eff} and luminosity of the star. By taking outputs from the Tycho stellar evolution models, we calculate the HZ boundaries for each time-step of the star's main sequence evolution. For a given orbital radius, we can predict how long a planet would remain within the HZ.

As a comparison and complement to the 1D models, we incorporate statistics from a ROCKE-3D GCM PPE of land planet atmospheres (Kiang, N. Y. et al. 2024, in preparation). The authors conducted a Latin hypercube sampling of 10 variables for Earth-size, all land planets in circular orbits: stellar T_{eff}, instellation compared to modern Earth (S_0 = 1361 W $m^{-}2$ from Prša et al. 2016), rotation period, surface pressure, N_2/CO_2 pressure, surface albedo, surface roughness, soil texture, and initial water inventory. Final climatological mean diagnostics are reported for an ensemble of 110 planets, which includes 18 planets that did not reach climatological and/or hydrological equilibrium: 17 planets, with mean surface temperatures $> 115°C$, likely reached a runaway greenhouse state at which the GCM was not designed to account for the change in atmospheric mass; one failed to complete due to numerical issues at extreme conditions not normally handled by the GCM.

In order to define HZ boundaries to combine with outputs from Tycho, we must determine suitable metrics to quantify the potential habitability of a given planet with

respect to the effective temperature and luminosity of the host star. Typically when defining HZ boundaries, a single or limited number of specific planet configurations are tested. Kopparapu et al. 2014 test several planetary masses and background N_2 partial pressures while adjusting the surface temperature or CO_2 partial pressure for the IHZ and OHZ, respectively. Upon reaching the limit of a runaway or maximum greenhouse state, the associated effective incident stellar flux determines the edges of the HZ. The original design of the land planets ensemble was intended to investigate the diversity of climates within the HZ and not to define its edges. The parameter ranges were confined within ranges expected to yield mostly habitable conditions, in particular the instellation range was limited to $0.62 - 1.471$ S_0. This results in few planets outside the HZ, making these boundaries less constrained. For those planets that do not have a habitable climate, we only know that the sampled instellation is outside the HZ and not where the precise boundary is for that specific planetary configuration. Despite these limitations, we can determine simplified HZ definitions for this demonstration with surface temperature diagnostics by performing statistical regressions with respect to the currently observable properties, $T_{\rm eff}$ and instellation. The variance in the mean climate diagnostics includes the effects of the excluded planetary parameters, which is reflected in the standard errors of the regression coefficients. This enables us to place confidence bounds on the HZ boundaries, a significant change from previous HZ studies where a limited number of planetary configurations are tested and the uncertainty is largely unknown.

A combined ensemble of climatologically and hydrologically equilibrated and unequilibrated planets presents difficulties. For models which crashed prior to reaching equilibrium, the climate outputs only diagnose the state of the climate up to that point and do not indicate the eventual equilibrium state. For these reasons, we focus on the

93 equilibrated planets. We note that simulations with numerical instabilities still provide useful information on the extent of the HZ, if indicative of a physically unstable climate, and could be incorporated in future studies. While we exclude the crashed planets, many planets that reached equilibrium also have climates akin to a runaway greenhouse, albeit at lower surface temperatures than Earth-like planets with larger water inventories. These hotter planets have mean surface temperatures exceeding 100°C and the majority of their water is held in the atmosphere, with the remainder being non-interactive water bound to the soil or sub-surface water that requires long computational times to fully evaporate. A combination of more temperate planets with mean surface temperatures < 50°C and those planets in a hotter climate regime creates non-linearity, with respect to instellation, in the temperature and water metrics at the transition point. As this work is largely a demonstration-of-concept, we perform simple linear regressions for the predictive equations used to define the HZ boundaries, with the understanding that this will introduce additional uncertainty. A detailed discussion of alternative methods for non-linear fits to the output climate diagnostics is included in K24. Our goal here is to show the impact on estimates of habitability when considering a large number of parameters and their possible ranges, as well as make recommendations for future ensembles to aid in more comprehensive and robust definitions of the HZ.

3.2.3.1 Habitable Zone Boundaries

One possible metric to define the habitability of a planet is the surface temperature. For the IHZ, the upper temperature limit can be taken to be 100°C, the boiling point of water and disinfection threshold. While the boiling point will depend on

the surface pressure, few organisms on Earth can exist above this temperature. The macromolecules essential to life become unstable on the timescales of cellular metabolism as the temperature approaches the proposed theoretical upper limit for life of ~ 150°C (Bains, Xiao, and Yu 2015; Schulze-Makuch, Airo, and Schirmack 2017). We take 100°C as the upper limit and determine an IHZ based on the mean surface temperature of each planet's coolest grid cell. If the climatological mean surface temperature of a planet is 100°C, some area of the planet remains below the upper limit. The minimum mean surface temperature better represents this variability by determining the average coolest temperature over a climatological period, making use of a GCM's ability to capture the surface heterogeneity of a planet's climatology. We perform a multivariate linear regression on the minimum mean surface temperature, with respect to T_{eff} and instellation, achieving an adjusted $R^2 = 0.453$, indicating about half of the variance is captured by the host star properties.

While the problem of crashed planets is less important for determining the OHZ for the land planets ensemble, low-sampling near the OHZ makes the determination of a definitive threshold for habitability difficult. Kodama et al. 2021 use a GCM to study the OHZ for land planets. The threshold is assumed to be the onset of a globally ice-covered state, where snow cover is maintained at every latitude. For the ROCKE-3D land planets ensemble, snow tends to collect in latitudinal bands rather than being distributed at all latitudes. The location of these bands depends on the obliquity and if the planet is synchronously rotating. Additionally, in the 110-member ensemble no planet maintains 100% of their hydrologically available water inventory in a frozen state, likely due to temporal variability. As mentioned in Section 3.2.3, even for planets that are mostly frozen, we only know the sampled instellation at which this occurs and not the exact boundary. Instead we use the maximum mean surface

temperature (i.e., the mean temperature of the warmest grid cell) to determine if, on average, all grid cells remain below 0°C throughout a climate cycle. Although temporal variability still leads to small amounts of melting, planets below this threshold largely remain frozen. The maximum mean surface temperature is an improvement over the global means used by 1D models, which are not sufficient metrics for potential surface habitability. We again perform a multivariate linear regression, with respect to $T_{\rm eff}$ and instellation, achieving an adjusted $R^2 = 0.532$.

3.2.4 Bayesian Habitable Zone Probabilities

The Bayesian method used in this work follows those described in Truitt et al. 2020; Ware et al. 2022, where we aim to determine the probability that a given orbital distance from the host star has spent 2 Gyr in the HZ. Depending on the known properties of the star, this approach could follow several different cases. In this work, we focus on the case where the metallicity, mass, and age are known to within some uncertainty, assumed to be Gaussian. We apply this method to our sample of potentially habitable planets, with the Bayesian posterior distributions for each star presented in Section 3.3.3. Other potential cases are described in detail in Truitt et al. 2020. Although we only consider metallicity, mass, and age in this work, the flexibility of Bayesian statistics means our method can be expanded to include additional cases considering other properties, such as planetary composition and stellar activity.

The only change from Ware et al. 2022 is that we include the 95% confidence intervals for the land planets ensemble CHZ_2 posterior distributions. The means and standard errors for the ensemble surface temperature metrics' regression coefficients

are used to define HZs by randomly sampling from multivariate Gaussian distributions. For each sampled combination of coefficients and each timestep in a given stellar evolution model, we determine the orbital radius at which the chosen HZ threshold is reached. We then take the median and 95% confidence interval of the orbital radius distribution for each HZ boundary. By considering both the IHZ and OHZ, we define the median, upper and lower 95% confidence interval as three separate HZs. These then determine the range of CHZ_2 posterior probabilities for each orbital radius, allowing us to show the effect of observationally unknown planet parameters on the HZ evolution. In the future, uncertainties in the HZ should be included as a prior probability distribution in the Bayesian framework.

3.2.5 Stellar Ages

As in Ware et al. 2022, we aim to assess the current probability that an exoplanet is within the CHZ_2. This requires we know the age of the star within some uncertainty. Without knowledge of the age, we can only postulate on the continuous habitability of the exoplanet with respect to the full main sequence lifetime of the star up to the maximum age of the model.

Measuring stellar ages for stars in clusters is relatively straightforward (e.g., Sandage 1970; Lastennet and Valls-Gabaud 2002), but is more difficult for field stars (e.g., Soderblom 2010). Ages are often determined via isochrones and/or empirical age-rotation and age-activity relations with uncertainties for Sun-like stars on the order of 1 Gyr or larger (e.g., Soderblom 2010; Torres, Andersen, and Giménez 2010). Although precise ages are preferred, by operating within a Bayesian statistical framework, a poorly known age still provides a useful constraint on the posterior

probability distribution. Assuming a Gaussian distribution, we introduce the age as a prior in the calculation. We were able to retrieve ages from the literature for all of the stars in our sample. For comparison, and to enable the calculation of ages for future analysis where stars may lack age measurements, we estimate ages for our sample of host stars by fitting measured properties to Tycho stellar evolution models.

Using the method described in Ware et al. 2022, we find that the method does not properly capture the sensitivity of age uncertainties to changes in the uncertainties of the measured properties. We have made an adjustment to the fitting algorithm to correct this. Starting with luminosity, $T_{\rm eff}$, and metallicity measurements from the literature, assumed to be Gaussian, we perform χ^2 fits to models from the Tycho stellar evolution catalog:

$$\chi^2 = \frac{(L_{\rm mod} - L_{\rm obs})^2}{\sigma_L^2} + \frac{(T_{\rm mod} - T_{\rm obs})^2}{\sigma_T^2} \frac{(Z_{\rm mod} - Z_{\rm obs})^2}{\sigma_Z^2} \tag{3.1}$$

where $L_{\rm mod}$, $T_{\rm mod}$, and $Z_{\rm mod}$ are the model luminosities, $T_{\rm eff}$, and metallicities. $L_{\rm obs}$, $T_{\rm obs}$, $Z_{\rm obs}$ are the measured luminosities, $T_{\rm eff}$, and metallicities. σ_L, σ_T, σ_Z are the uncertainties in the observations. We keep all model points which fit to within 1σ of the measured values and determine the likelihood, P, of each χ^2 fit:

$$P = exp(-\chi^2/2) \tag{3.2}$$

We take the median and 68% confidence interval of the remaining models points, weighting by the likelihood.

The ages for all host stars derived in this work and from literature sources are provided in Table 3.3. For consistency and comparison to our best-fit ages, we preferred literature ages from the stellar property sources used in this work. The ages from this work fall within the 1-σ errors in the literature sources, except for Kepler-442.

Petigura et al. 2022 report an age of $13.1^{+4.8}_{-7.1}$ for Kepler-442 from fits to isochrones, which places a significant portion of the age distribution above the age of the universe.

We use our age estimates in our CHZ_2 analysis, except for Kepler-441 and HD 216520 for which we use the literature ages. These sources either used empirical gyrochronology relations (Kepler-441) or a compilation of ages from various methods (HD 216520). Lower mass stars evolve slowly, making fits to stellar evolution models difficult without extremely precise measured properties. The relatively large uncertainties for measured stellar properties compared to the evolutionary rate of change in those properties typically results in large age uncertainties for low-mass stars. For this reason, ages from empirical relations currently provide more precise estimates. In Section 3.4.1, we compare the effects on the CHZ_2 for stars similar in mass to Kepler-441 and Kepler-452, which represent the mass range for our sample, at various ages and uncertainties. We then discuss the broader implications for planets in HZ of the lowest and highest mass Sun-like stars.

Table 3.3. Stellar ages for potentially habitable systems

Stars	Age_{Tycho} [Gyr]	Age_{lit} [Gyr]	Ref.	Method[a]
Kepler-441	$1.59^{+7.26}_{-1.49}$	$1.9^{+0.5}_{-0.4}$	1	1,2
Kepler-442	$5.72^{+2.67}_{-4.13}$	$13.1^{+4.8}_{-7.1}$	2	2
Kepler-1544	$3.12^{+3.20}_{-2.76}$	$7.9^{+7.0}_{-5.5}$	2	2
Kepler-62	$4.68^{+4.01}_{-3.37}$	$10.6^{+6.2}_{-6.7}$	2	2
HD 40307	$6.16^{+4.21}_{-4.44}$	6.9 ± 4.0	3	2
HD 216520	$7.13^{+3.63}_{-4.46}$	6 ± 3	4	1,2
Kepler-452	$2.37^{+2.12}_{-2.31}$	$2.9^{+2.2}_{-1.7}$	2	2

References: 1. Torres et al. 2015 2. Petigura et al. 2022 3. Bonfanti, Ortolani, and Nascimbeni 2016 4. Burt et al. 2021

[a]Measurement Methods: 1. Gyrochronology 2. Isochrones

3.3 Results

3.3.1 Inner Habitable Zone Comparison

We compare the HZ boundaries from Kopparapu et al. 2014 versus the land planets ensemble for the IHZ in Figure 3.1(a). The median 100°C minimum mean surface temperature boundary sits entirely inside the 1 $M_{\oplus}$ boundary and extends inside the RV boundary for stars $\gtrsim$ 4400 K. The land planets ensemble boundary shows a stronger $T_{\rm eff}$ dependence than the Kopparapu et al. 2014 models. While it is difficult to make a direct comparison between the Kopparapu et al. 2014 and land planets ensemble boundaries due to differences in their definition and model parameters, it is expected that the HZ will be highly dependent on spectral type (e.g., Rugheimer et al. 2013; Shields et al. 2013; Rugheimer et al. 2015). The land planets ensemble demonstrates that, for the same instellation, planets orbiting cooler stars will be warmer than those around hotter stars. As $T_{\rm eff}$ decreases, the Wien peak of the stellar spectrum moves toward the near-IR where water absorption becomes dominant and Rayleigh scattering becomes less important. This effect is seen for higher $T_{\rm eff}$ in the Kopparapu et al. 2014 models, but tapers off as the planetary albedo approaches a minimum near zero for the coolest stars.

The small instellation range sampled for the land planets ensemble ($0.62-1.471$ S_0) has a large impact on the confidence levels of the HZ boundaries. For the hottest stars, the 100°C boundary is extrapolated outside the sampling range. None of the planets with a G2-type (5772 K) host star that reached equilibrium surface temperatures $>$ 100°C and the population of planets with surface temperatures $>$ 100°C is over represented by M dwarf host stars. While the limited inference allowed by the small

instellation range is compounded by the small sample size, the trend of hotter host stars with cooler surface temperatures, and vice versa, is indicative of the importance of stellar spectral type. With decreasing planetary albedo it becomes easier to heat the planet for a given instellation level, a trend potentially exacerbated by increased stellar activity in late type stars.

Interestingly, while planets with surface temperatures exceeding 100°C are likely uninhabitable, land planets may maintain stable surface water due to limited water inventories coupled with high pressure atmospheres. The hottest planet in the ensemble, with a mean surface temperature of 283°C and orbiting an M8.2-type host star, reached equilibrium, indicating there are likely certain planet configurations that maintain stable, extreme climates. This could present difficulties for determining the potential habitability of land planets without a direct measurement of the surface temperature, as signs of a runaway greenhouse atmosphere may not be readily discernible.

3.3.2 Outer Habitable Zone Comparison

Figure 3.1(b) compares the EM, 1 $M_\oplus$, and ROCKE-3D land planets ensemble 0°C maximum mean surface temperature (complete freezing point) OHZs. The median land planets ensemble boundary is shifted inwards for all spectral types, most significantly for Sun-like stars. As before, a stronger $T_{\rm eff}$ dependence is present in the land planets ensemble boundary than is seen with the Kopparapu et al. 2014 models. The 1 $M_\oplus$ OHZ is defined by the maximum greenhouse, where the CO_2 partial pressure was increased until Rayleigh scattering became dominant over the greenhouse effect. For the coolest M dwarf host stars, Rayleigh scattering never becomes an important factor as the stellar spectrum peak shifts into the near-IR. While considering the effects of

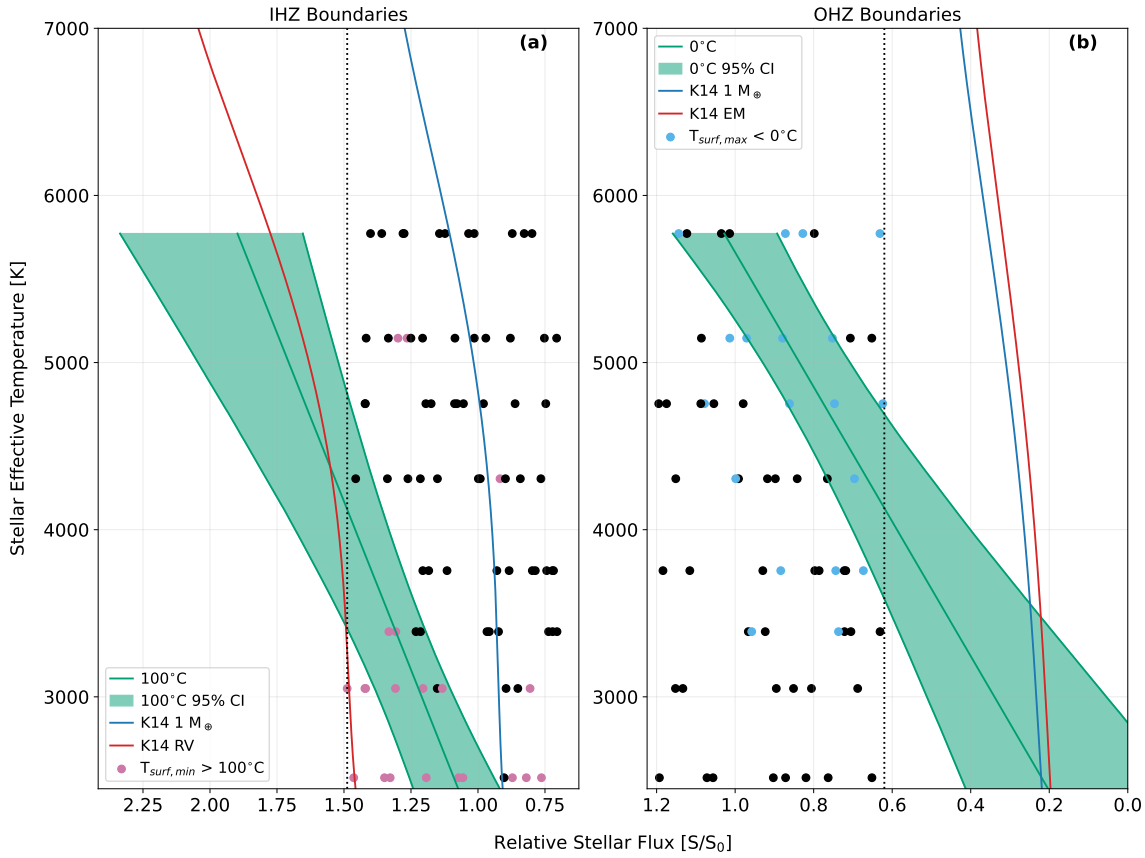

Figure 3.1. Comparison of the RV/EM, 1 $M_{\oplus}$, and ROCKE-3D land planets ensemble HZ boundaries. The land planets ensemble HZ boundaries are defined by (a) the 100°C minimum mean surface temperature for the IHZ and (b) the 0°C maximum mean surface temperature (complete freezing point) for the OHZ. The shaded regions represent the 95% confidence intervals on the land planets ensemble HZ boundaries. The vertical dotted lines represent the land planets ensemble sampling range for the instellation ($0.62 - 1.471$ S_0). Over-plotted are the land planets ensemble models, with (a) pink indicating planets with minimum mean surface temperatures > 100°C and (b) light blue indicating planets with maximum mean surface temperatures < 0°C.

clouds and surface ice is likely to push the OHZ closer than is seen in these 1D models, drawing firm conclusions for the land planets ensemble boundary is complicated by a number of factors.

By pushing planets to the maximum CO_2 greenhouse in the Kopparapu et al. 2014 models, the final CO_2 partial pressure for an Earth-like planet orbiting the Sun is ~ 8

bars and increases with decreasing $T_{\rm eff}$. The land planets ensemble sampled up to 10 bars of CO_2, but only two planets ended up with > 8 bars and only 10 have > 1 bar. Again, the goal of the land planets ensemble was not to push ever configuration to the extremes, but to instead sample from the possible ranges of parameters. The land planets ensemble OHZ is extrapolated past the instellation sampling range for stars $\lesssim 4200$ K. The coldest 20 planets with maximum mean surface temperatures $< 0°$C are dominated by K and G dwarf hosts, with only five of these having M dwarf hosts. This leaves the OHZ to be based mainly on hotter planets for the cooler host stars.

3.3.3 CHZ_2 Planet Profiles

We use the Kopparapu et al. 2014 and ROCKE-3D GCM land planets ensemble HZ boundaries combined with Tycho stellar evolution models and a Bayesian framework to determine posterior likelihood distributions for the CHZ_2 around 7 K and G dwarf host stars with potentially habitable exoplanets, as well as for the Sun. The land planets ensemble HZ boundaries are defined by the 93 planets that reached equilibrium. Figure 3.2 shows the CHZ_2 posterior distributions for the full 8 star sample with the 1 $M_\oplus$ and RV/EM HZ boundaries compared against the land planets ensemble 100°C minimum mean surface temperature IHZ and 0°C maximum mean surface temperature OHZ. CHZ_2 posterior likelihoods for each planet are provided in Table 3.4, which are determined by taking the average of the posterior distributions over the 1σ semi-major ranges listed in Table 3.1. Average posterior likelihoods for the land planets ensemble HZ boundaries have upper and lower "uncertainties". While this is unconventional to place an uncertainty on a probability, inherently a measure of uncertainty itself, this allows us to show the range of estimates given by the 95% confidence intervals. In the

future, HZ boundaries with uncertainties should be integrated as a prior probability distribution, resulting in a single likelihood for each orbital radius.

As we are only considering host stars with $T_{\rm eff} \gtrsim 4300$ K, the land planets ensemble CHZ_2 is generally shifted inwards relative to Kopparapu et al. 2014. The RV IHZ is typically within the 100°C minimum mean surface temperature 95% confidence interval, with the 1 $M_\oplus$ IHZ being less optimistic for all stars. This results in an increased CHZ_2 probability for Kepler-442 b ($P \sim 0.375$) and HD 216520 c ($P \sim 0.491$), a significant increase over the 1 $M_\oplus$ model and on par with the RV/EM model. The median probability for Venus does not increase relative to the Kopparapu et al. 2014 models, but ranges from $P = 0 - 1$ based on the 95% confidence intervals.

The largest differences result from the significantly more conservative land planets ensemble OHZ, reducing the outer extent of the CHZ_2 by > 0.5 AU for the Sun and Kepler-452. The probabilities for Kepler-441 b, Kepler-62 f, and Mars decrease to $P \sim 0$, while HD 40307 g drops from $P \sim 0.55$ for Kopparapu et al. 2014 to $P = 0.114$. Kepler-1544 b remains largely constant and Kepler-452 b still increases over the 1 $M_\oplus$ model due to orbiting relatively close in. Earth is notable in that the Kopparapu et al. 2014 models gives a 100% chance of being in the CHZ_2, but straddles the lower 95% confidence for the outer land planets ensemble CHZ_2, with a range of $P = 0 - 0.710$. This is due to the restricted land planets OHZ, which is heavily impacted by the small sampled instellation range and sample size relative the number of sample parameters. While the Earth sits within the land planets ensemble HZ, taking into account the Sun's evolutionary history results in Earth not being within the median CHZ_2.

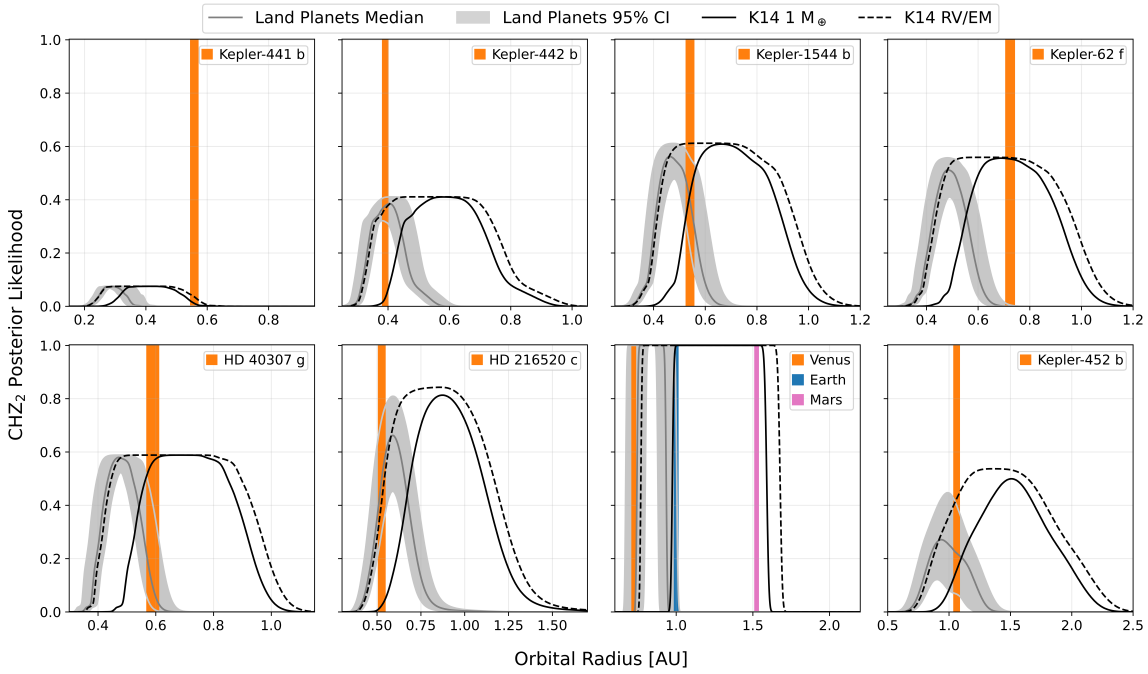

Figure 3.2. CHZ_2 posterior likelihood distributions for the sample of host stars in 3.2 and the Sun using the 1 $M_\oplus$ and RV/EM models and the land planets ensemble 100°C minimum mean surface temperature IHZ and 0°C maximum mean surface temperature OHZ. Grey shaded regions denote the 95% confidence interval. Colored vertical bars correspond to the 1σ semi-major axis range for the sample of exoplanets in Table 3.1. Bars for Venus, Earth, and Mars are widened for clarity.

3.4 Discussion

CHZ_2 posterior likelihoods for exoplanets in the HZ are meant to aid in prioritization of observations by considering the likelihood that life has both evolved and made a detectable impact on the atmosphere. Exoplanets can be ranked or separated into tiers based on their associated CHZ_2 probability. Considering average posterior likelihoods in Table 3.4 for the 100°C minimum mean surface temperature IHZ and 0°C maximum mean surface temperature OHZ, Kepler-442 b, Kepler-1544 b, and HD 216520 c would be the highest priority targets for follow-up observations aimed at detecting biosignatures. Although further work is needed to improve the reliability

Table 3.4. Planetary CHZ_2 posterior likelihoods

Planets	$< P_{1M_\oplus} >$	$< P_{RV/EM} >$	$< P_{Land\ Planets} >$
Kepler-441 b	0.012	0.035	0
Kepler-442 b	0.038	0.365	$0.375^{+0.033}_{-0.060}$
Kepler-1544 b	0.415	0.611	$0.390^{+0.169}_{-0.169}$
Kepler-62 f	0.552	0.557	$0.000^{+0.007}_{-0.000}$
HD 40307 g	0.547	0.588	$0.114^{+0.258}_{-0.083}$
HD 216520 c	0.029	0.418	$0.491^{+0.223}_{-0.193}$
Venus	0	0	$0.000^{+1.000}_{-0.000}$
Earth	1	1	$0.000^{+0.710}_{-0.000}$
Mars	1	1	0
Kepler-452 b	0.156	0.424	$0.221^{+0.177}_{-0.156}$

Note: CHZ_2 posterior likelihoods for the sample of planets. These are calculated by taking the average of each posterior likelihood distribution over the 1σ range of the semi-major axis given in Table 3.1. For Venus, Earth, and Mars their semi-major axes are taken to be 0.723, 1, and 1.524 AU, respectively. Uncertainties in the averages for the land planets ensemble HZ boundaries correspond to the upper and lower 95% confidence intervals.

of the HZs defined using the land planets ensemble, we show the advantages of HZs based on a variety of planetary configurations taking into account current unknowns that will affect habitability. Determining if exoplanets are currently in the HZ and their likelihood of continuous habitability is benefited by having a single HZ definition with confidence intervals rather than a HZ for each possible scenario. The confidence intervals can be taken as conservative and optimistic HZ limits or integrated as priors into models to place a single probability on the continuous habitability for a given exoplanet. Here we discuss the importance of stellar age when determining the CHZ, HZs for land planets in the literature, potential alternative metrics for defining the HZ from GCM ensembles, and recommended changes for future ensembles to enable more robust determinations of the HZ boundaries.

3.4.1 Effect of Age and Spectral Type on the CHZ_2

Solar-type stars with solar metallicity have main sequence lifetimes of ~ 10 Gyr. As a result, the HZ evolves significantly over the age of the universe, but the CHZ is wide enough to provide a stable radiation environment for life to evolve and make a detectable impact on the atmosphere. For M, late-type K, and F dwarfs, the HZ evolution differs substantially. In Figure 3.3, we compare the CHZ_2 posterior probability distributions for solar metallicity 0.55 and 1.1 $M_\odot$ stars with various ages and uncertainties. These model stars are similar in mass to Kepler-441 and Kepler-452, representing the upper and lower mass range of the sample considered in this work. For low-mass stars, the effects of the age and uncertainty are insignificant, only becoming important for young stars where planets have not yet reached 2 Gyr of continuous habitability. For higher mass stars, the age is critical to constraining the CHZ_2 as the HZ shifts outward with time, increased uncertainty contributes to significant broadening of the probability distribution and reduces the maximum possible CHZ_2 probability.

M and late-type K dwarfs evolve slowly, with main sequence lifetimes far exceeding the age of the universe. Therefore, the HZs of even the oldest stars have remained relatively constant until now. Over the 8 Gyr considered in Figure 3.3(a), the CHZ_2 shifts outward only a few hundredths of an AU for the 0.55 $M_\odot$ model. The age precision is less important as well, generally only affecting the maximum CHZ_2 probability with increasing uncertainty (Figure 3.3(b)). Unless a planet orbits at the inner or outer edge of HZ, it will remain in the HZ with little change in instellation or spectral energy distribution (SED). The continuous habitability is therefore nearly independent of the luminosity and $T_{\rm eff}$ evolution of the host star. Planets in the HZ of

these low-mass stars are orbiting close in, likely leading to tidal locking and significant effects from stellar activity. Without knowledge of the planetary properties and stellar activity evolution, the current model becomes less informative for determining the CHZ_2.

Planets orbiting in the HZ of F dwarfs encounter the opposite problem. For the 1.1 $M_\odot$ model, the outer edge of the CHZ_2 shift outwards nearly 0.5 AU over the 4 Gyr considered (Figure 3.3(c)). The IHZ evolves slower due to the parameterization in Kopparapu et al. 2014, but still increases > 0.2 AU. The age precision becomes more important, with increasing uncertainty significantly decreasing the maximum CHZ_2 probability and increasing the posterior distribution width (Figure 3.3(d)). The rapid evolution of the HZ decreases the likelihood of HZ planets remaining continuously habitable and reduces the total lifetime of the HZ over the main sequence. The 1.1 $M_\odot$ model has a main sequence lifetime of ~ 7 Gyr, still long enough for 2 Gyr to remain a feasible threshold for continuous habitability. For stars $\gtrsim 1.4$ $M_\odot$, depending on the metallicity, the main sequence lifetime can drop below 2 Gyr. While 2 Gyr is a conservative threshold for the time life needs to evolve and make a detectable impact, the likelihood of finding detectable life on planets in the HZs of early-type F dwarfs is substantially decreased even for more optimistic thresholds. Luckily, only a small fraction ($\sim 2\%$) of the stars in the current NASA ExEP mission star list for HWO (Mamajek and Stapelfeldt 2024) exist in this regime. However, $\sim 40\%$ of the current target sample are F dwarfs and precise stellar ages will be needed to properly constrain the area of continuous habitability.

Mello and Friaça 2023 combine a minimal mantle and atmospheric model to study the evolution of the CHZ for various planetary parameters and stellar types. Although they consider the CHZ with respect to the full main sequence lifetime,

more conservative than the CHZ_2 considered in this work, they similarly caution the potential continuous habitability of planets orbiting F dwarfs with stellar masses $>\gtrsim 1.1$ $M_\odot$. When considering both the rapid luminosity evolution of higher mass stars and the cooling timescales of the planetary interior, the CHZ becomes restricted or even nonexistent for small planets ($\lesssim 0.5$ $M_\oplus$) and those orbiting F dwarfs. We do not consider the planetary interior evolution in this work, but combining an interior model and GCM would be fruitful for future studies on continuous habitability.

3.4.2 Habitable Zone for Land Planets in the Literature

While most studies of planetary habitability focus on aqua planets like Earth with surfaces dominated by oceans, a handful of works have explored the limits of habitability for land planets and the water inventories or land fractions that divide these two populations. Abe et al. 2011 use a GCM to study the IHZ and OHZ for land planets with 1 $R_\oplus$ around a Solar-type star. The initial water inventories vary between 20, 40, and 60 cm of water, falling within the range sampled by K24. The IHZ is defined by the runaway greenhouse case and the OHZ is defined by the complete freezing point, where permanent snow is present at every latitude. They find IHZ limits of 1.7 S_0, regardless of the initial water inventory, and OHZ limits of 0.77 S_0 and 0.58 S_0 for low- and high-obliquity planets, respectively. This compares to $1.90^{+0.44}_{-0.24}$ and $1.03^{+0.13}_{-0.13}$ S_0 for the 100°C minimum mean surface temperature and 0°C maximum mean surface temperature boundaries at $T_{\rm eff} = 5772$. While their OHZ falls outside the 0°C maximum mean surface temperature 95% confidence interval, this is unsurprising given the differences in definition, parameters sampled, sampling ranges.

Kodama et al. 2018; Kodama et al. 2019; Kodama et al. 2021 built off the work

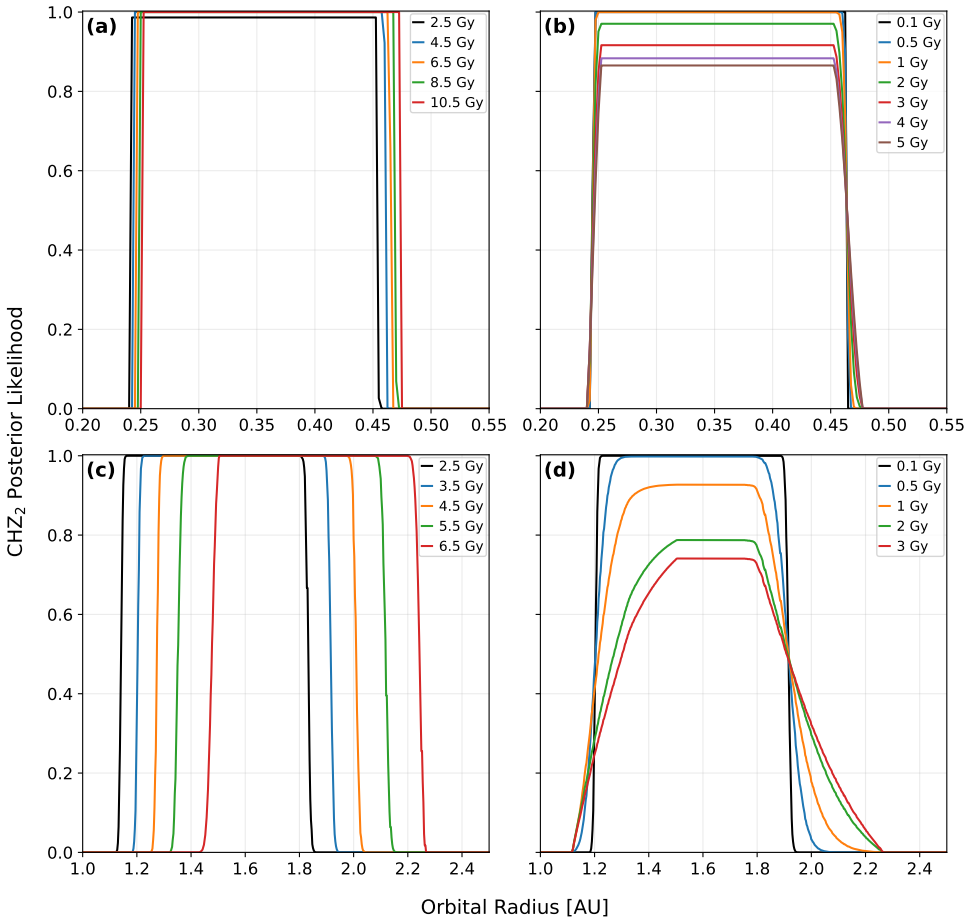

Figure 3.3. CHZ_2 posterior likelihood distributions using the Kopparapu et al. 2014 1 $M_\oplus$ HZ model for solar metallicity, 0.55 (top) and 1.1 (bottom) $M_\odot$ stars, assuming an insignificant uncertainty in the mass and metallicity. The ages start from 2.5 Gyr to ensure 2 Gyr has passed since the end of the pre-main sequence. The left plots show posteriors for various ages and assume a small 0.1 Gyr uncertainty. The right plots show posteriors for a constant age with various uncertainties. The ages are 6 and 3.5 Gyr, respectively, which are approximately half the maximum model age or main sequence lifetime.

of Abe et al. 2011 and explored the relationship between the HZ boundaries and the surface water distribution or water inventory for Earth-sized land planets orbiting Solar-type stars. They find that the runaway greenhouse IHZ ranges from $\sim$ 1.3 S_0 for planets with larger water inventories and meridionally dispersed distributions (water pools at equally spaced longitudes) to $\sim$ 1.8 S_0 for planets with small water

inventories ($\sim 1\%$ Earth's oceans) and zonally uniform distributions concentrated at the poles. At the IHZ, they find a clear division between the climate regimes of aqua planets and land planets as the tropics dry out. This is occurs at a water inventory of $\sim 10\%$ Earth's oceans or a land fraction of $\sim 40\%$. Higher water inventories or smaller land fractions than these thresholds result in a generally constant IHZ instellation of ~ 1.3 S_0. At the OHZ, the division between aqua and land planets is less clear. The complete freezing point follows the same trend for water distribution or inventory as the IHZ and varies between $0.92 - 0.77$ S_0, with the lower limit in agreement with Abe et al. 2011 for a planet with 0° obliquity. Kodama et al. 2019; Kodama et al. 2021 also tested planets with the topographies of Venus, Earth, and Mars. They found that the limiting instellations for the IHZ and OHZ generally fall between the meridionally dispersed and zonally uniform cases. Overall, these studies show similar results to the IHZ boundary in this work, but future work is needed to determine the level of agreement between these models, especially for the OHZ.

3.4.3 Alternative Habitable Zone Metrics

We focused on temperature metrics from the ROCKE-3D land planets ensemble to define the IHZ and OHZ. There are a multitude of other metrics we did not explore which help describe the relative habitability of a planet. For one, we only considered the maximum mean and minimum mean surface temperatures of the planets. The mean surface temperature is the first and most common reference point for describing the overall climate of a planet. For planets with relatively small differences in surface temperature between zones (e.g., fast rotators with denser atmospheres), the mean surface temperature should be sufficient. If the planet has a large surface temperature

gradient (e.g., tidally locked planets or those with higher obliquities), the mean surface temperature may neglect these variations. The absolute maximum and minimum surface temperatures may be better choices in these cases.

One could also explore HZ boundaries based on the phase distribution of water or the availability of water for life. The fraction of total water that exists as ice versus ground and lake liquid water can probe the outer edge. Similarly, the total atmospheric water could define planets that have reached the complete evaporation point, where all water not molecularly bound to the soil is evaporated. However, both the coldest and hottest planets still maintain unbounded liquid surface water in the land planets ensemble. At a minimum instellation of 0.62 S_0, temporal surface temperature variations on cold planets still cause melting. For hot planets with surface temperature exceeding 100°C, liquid surface water persists due to the long model times required to fully evaporate all water, which is a consequence of ROCKE-3D preventing evaporation from deep surface layers.

A common obstacle for all of the aforementioned metrics of habitability is what threshold should be used to distinguish a habitable and uninhabitable planet. For surface temperature, the OHZ is easiest as a planet which remains permanently below freezing will either be in a state of global glaciation for aqua planets or with a fully frozen water inventory for land planets, save for briny water or water heated geothermally which may remain unfrozen. At the IHZ, the exact boundary of habitability is less clear. While planets with temperatures exceeding boiling, with respect to the surface pressure, or the maximum temperature threshold for life are likely uninhabitable, the runaway greenhouse or rapid water loss states should occur prior to reaching these thresholds. For the distribution of water between phases, small amounts of liquid surface water could still exist with temporal variations, even if the planet

is largely uninhabitable. For example, with decreasing instellation the land planets ensemble asymptotically approaches 100% frozen water inventory. These metrics are therefore best used in combination to diagnose a planets habitability holistically. This is why the runaway greenhouse and maximum greenhouse or complete freezing point are the most attractive options, by setting clear boundaries between planets which may still have detectable surface life and those where only sub-surface life may still remain. However, we plan to explore these alternative metrics in the future with an expanded ensemble and with an updated version of ROCKE-3D that is able to handle planets entering a runaway greenhouse state.

3.4.4 Recommendations for Future Ensembles

The original intent of K24 was to explore the relative habitability and distribution of water for planets with small water inventories and various configurations within the typical range of instellations consistent with HZ planets. Defining HZ boundaries would always be complicated for this sample, but it presented an opportunity to understand how this could be done for a more holistic sample than previous studies, demonstrate the uncertainty in the HZ and continuous habitability introduced by a large set of possible parameters, and plan for future large ensembles to define the HZ in a more robust manner. Recommended updates for future ensembles include a wider range of instellations, adding host stars with spectral types earlier than G2, introducing additional greenhouse gases, a range of planetary masses and radii, sampling various surface water distributions or ocean and continent configurations, and a wider range of water inventories.

For exploring HZ boundaries, the most relevant change to the parameter sampling

would be an increase in the range of instellations. Based on the results of Abe et al. 2011; Kodama et al. 2018; Kodama et al. 2019; Kodama et al. 2021, this range should at least span $0.58 - 1.8$ S_0. However, there is a lack of studies using GCMs to define the HZ for land planets orbiting stars other than the Sun. While the results of this work are limited by the sampling, a stronger $T_{\rm eff}$ dependence for land planets could push the boundaries beyond these limits for the hottest and coolest host stars. For the OHZ in particular, this range should likely extend to 0.2 S_0, the approximate edge of the EM boundary for a $T_{\rm eff} = 2516$ K host star. These recommended instellation ranges assume a similar method is used for future ensembles, where instellations are sampled rather than incrementally increasing or decreasing the incident flux until a runaway greenhouse or complete freezing point is reached. Based on the difficulty of defining HZs in this work, the IHZ in particular, it may be best to instead institute the former method. This will require significantly more computational time, but would provide more robust results for the instantaneous edges of the HZ.

The current ensemble covers the sub-solar regime of stars that could host potentially habitable planets, with *JWST* and near-term missions focused on characterizing planets around late-type M dwarfs. HWO and future missions will seek to characterize planets in the HZ of Sun-like stars, up to early-type F stars. Taking into account the preliminary NASA ExEP mission star list for HWO (Mamajek and Stapelfeldt 2024), the $T_{\rm eff}$ range should extend up to 7000 K, the approximate upper limit for solar metallicity F1V stars.

Variation in the initial atmospheric composition is limited to N_2 and CO_2 in the land planets ensemble. Secondary greenhouse gases, such as CH_4, are typically ignored for HZ studies, focusing solely on the effects of H_2O and CO_2. Ramirez and Kaltenegger 2018 find that CH_4 has a significant effect on the OHZ Earth-like planets

using 1D models, with a net greenhouse effect due to increased IR absorption for host stars hotter than 4500 K. Below 4500 K, increased near-IR stellar flux leads to absorption by CH_4 and a net cooling effect. While CH_4 is efficiently lost through photolysis and diffusion limited escape, significant abiotic and biotic sources could maintain higher CH_4 concentrations (Ramirez and Kaltenegger 2018). In fact, a previously higher level of CH_4 is a proposed solution to the faint young Sun problem for both early Earth (e.g., Haqq-Misra et al. 2008; Wolf and Toon 2013) and Mars (e.g., Ramirez 2017; Wordsworth et al. 2017). Although Ramirez and Kaltenegger 2018 focused on the OHZ, the land planets ensemble shows that greenhouse gases other than H_2O cannot be ignored for the IHZ of planets with low water inventories. The runaway greenhouse for Earth-like planets with significant water inventories occurs when surface temperatures exceed the critical point of water ($\sim$ 647 K at 220 bars, Kasting, Whitmire, and Reynolds 1993) and the oceans fully evaporate. Water dominates the atmospheres of these planets near the IHZ, making the effects of additional greenhouse gases negligible. The land planets considered in K24 do not have enough water to reach this pressure threshold. The hottest planets in the ensemble with fully evaporated surface water, neglecting non-interactive and sub-surface water, do not even reach the water volume mixing ratios of the classic moist greenhouse limit for Earth (1E-3,). The runaway greenhouse can be better defined as the complete evaporation point for these dry planets and additional greenhouse gases play a larger role in determining this limit. Therefore, it may be beneficial to explore the climate sensitivity, at both the IHZ and OHZ, to CH_4 or other greenhouse gases in future ensembles.

A key parameter included in Kopparapu et al. 2014, but absent from the land planets ensemble and most other HZ parameterizations, is variance in planetary mass

and radius. Kopparapu et al. 2014 tested both increasing the background N_2 partial pressure with increasing radius, under the assumption that larger planets will have denser atmospheres, and the effect of increased gravity with increasing mass. The largest effect was seen for the IHZ with increasing gravity. Increased gravity led to a smaller H_2O column depth, which increases the outgoing longwave radiation and enables more efficient cooling. The land planets ensemble included variation in N_2 partial pressure, but the results of Kopparapu et al. 2014 demonstrate that planetary mass and radius should be considered as well.

K24 assume a flat topography for all planets in the ensemble and water is allowed to pool in a single lake in each grid cell, but can redistribute through general circulation. The results of Kodama et al. 2018; Kodama et al. 2019; Kodama et al. 2021 show that the prescribed water body distribution can have a significant effect on the HZ limits. It may be useful to sample the extremes explored in these works: zonally uniform water pool regions versus the meridionally uniform dispersed case and fully ocean-covered versus continent-bearing planets with a variety of continental configurations (e.g., Venus, early to modern Earth, and Mars). Kodama et al. 2019 also found that the initial water inventory will impact the HZ limits, with a transition between the behaviors of aqua and land planet climates occurring at $\sim 10\%$ of Earth's oceans for the IHZ. While a comprehensive study of both aqua and land planets would be best, future land planet ensembles should sample up to this transition point, or at least high enough for a circulating ocean to form, in order to consider the full range of potential land planets.

3.5 Conclusions

In this work, we used a Bayesian framework, combined with statistics from a 3D GCM perturbed parameter ensemble (Kiang, N. Y. et al. 2024, in preparation) and a grid of stellar evolution models, to determine posterior probabilities for the location of the CHZ_2 for G and K stars with known potentially habitable exoplanets. The GCM ensemble focused on Earth-sized land planets with minimal water inventories as opposed to Earth-like aqua planets, for which HZ boundaries are typically defined. Land planets are better suited to maintain habitable conditions due to drier atmospheres, which increase radiative cooling at the IHZ and reduce cloud fractions (albedo) at the OHZ. We performed multivariate linear regressions on surface temperature metrics, with respect to stellar T_{eff} and planetary instellation, to define HZ boundaries for the IHZ and OHZ. Our regressions did not include perturbed parameters that would be unknowns for near-term missions, such as CO_2 partial pressure and surface albedo. The variance from these parameters in the is included in the standard errors of the regression coefficients, enabling us to determine confidence intervals for the HZ boundaries. Other studies of HZ limits typically focused on specific planetary configurations, where a single limiting instellation is found for each stellar spectral type.

For the IHZ, we defined boundaries using the 100°C minimum mean surface temperature threshold. For the OHZ, we defined a boundary using the 0°C maximum mean surface temperature threshold, where each GCM grid cell remains below freezing on average. We found significant differences in the HZ range when comparing to the conservative runaway/maximum greenhouse 1 $M_\oplus$ and optimistic RV/EM HZs defined by Kopparapu et al. 2014. In general, the IHZ and OHZ boundaries defined using

the land planets ensemble extended inwards to those from Kopparapu et al. 2014 for hotter G and K host stars, but predicted comparable HZs for M stars. This is a result of the stronger stellar $T_{\rm eff}$ dependence for the land planets ensemble HZ boundaries. While the differences between the HZs are expected due to separate definitions of the HZ boundaries, the use of 1D versus 3D models, and the planetary configurations considered (e.g., aqua versus land planets), the sampling of parameters in the land planets ensemble made a significant impact on the robustness of the HZ boundaries defined in this work. The limited instellation range ($0.62 - 1.471$ S_0) sampled in K24 caused the majority of planets around hotter G and early-type K host stars to maintain temperate climates. For planets with late-type K and M host stars, the shift in the stellar spectrum towards the near-IR leads to lower planetary albedos and higher surface temperatures at the same instellation. This caused a large number of models near the IHZ to crash upon reaching a hotter climate state beyond the capabilities of ROCKE-3D and those near the OHZ never reached the complete freezing point.

Although our results were impacted by the sampling in the land planets ensemble, we still demonstrated the benefit of determining HZs with large GCM perturbed parameter ensembles and pairing these within a Bayesian framework for predicting continuous habitability. Our comparison of CHZ_2 posterior probability distributions for the sample of selected known potentially habitable systems followed the same trends seen in the HZ boundaries, with the land planets ensemble CHZ_2 shifting inward relative to Kopparapu et al. 2014 for these hotter G and K host stars. However, by including the 95% confidence intervals in the land planets ensemble HZ boundaries we show the range of CHZ_2 probabilities predicted by the variance in perturbed parameters. For planets orbiting in the middle of the HZ around lower mass stars, which evolve more slowly, their CHZ_2 probabilities may only differ by $\sim 1\%$ (e.g.,

Kepler-442 b). For planets orbiting closer to the edge of the HZ around higher mass and more quickly evolving stars, their range of CHZ_2 probabilities could be $0 - 100\%$ (e.g., Venus). Caution should be exercised in prioritizing exoplanets near the edge of the HZ, since taking into account the possible range of unknown planetary parameters and uncertainties in stellar properties reduces the likelihood of continuous habitability.

Perturbed parameter ensembles present a means to approach planetary habitability in a more holistic and robust manner. We look forward to future ensembles covering a broader range of planetary parameters, with a recommendation to prioritize a larger range of instellations to aid in determination of the HZ boundaries. Based on the results of prior HZ studies and the preliminary target list for the future HWO NASA direct imaging mission, it would be beneficial to include spectral types up to early F stars, additional greenhouse gases, a range of planetary masses and radii, various surface water distributions, and a large range of initial water inventories. We only included prior probabilities on the stellar mass, metallicity, and age in our CHZ_2 calculations, but the flexibility of Bayesian statistics encourages the introduction of additional constraint on planetary and stellar parameters. Consideration of the impact of geological and biological processes on the atmospheric composition and climate regulation are critical to determining the potential habitability of a planet. By incorporating models of outgassing rates, we could better constrain the likely range of atmospheric compositions with additional input from measurements of planetary mass and bulk compositions. As the ultimate goal of this work is to develop a more comprehensive method for prioritizing planets most likely to host detectable life for future missions, additional work is needed to predict the continuous habitability of exoplanets orbiting low mass stars. Since the luminosity evolution is slow over billion

year timescales, the effects of stellar activity and synchronous rotation are of greater importance.

Chapter 4

CONTINUOUS HABITABLE ZONE PREDICTIONS FOR POTENTIAL HABITABLE WORLDS OBSERVATORY TARGET STARS

4.1 Introduction

Future direct imaging space telescopes, such as NASA's UV/O/IR direct imaging mission, coined the Habitable Worlds Observatory (HWO), will be the first telescopes capable of both detecting and characterizing Earth-sized exoplanets in the habitable zones (HZ) of nearby Sun-like (F-, G-, K-type) stars. Currently, the *James Webb Space Telescope* (*JWST*) will seek to characterize the atmospheres of transiting terrestrial exoplanets orbiting the smallest, nearby M dwarf stars. However, to access exoplanets at any orbital inclination, those with longer orbital periods, and to probe down to surface, direct imaging of reflected light is required (The LUVOIR Team 2019; Gaudi et al. 2020). For an Earth-like exoplanet orbiting in the HZ of a G2-dwarf, detection of reflected light requires a sensitivity of $\sim 10^{-10}$ for the planet-star contrast at visible wavelengths (Fujii et al. 2018). Achieving this level of contrast and surveying the entire HZ to initially detect terrestrial HZ exoplanets, not including detailed spectroscopic characterization, will require a significant amount of time and resources for even a single system. This makes prioritization based on the likelihood that discovered exoplanets will host detectable life critical to consider.

With the release of the NASA ExEP mission star list (EMSL) for HWO (Mamajek and Stapelfeldt 2024), we now have a sample of the 164 stars with HZs most accessible to a future direct imaging survey with a 6-m-class telescope. The current system for

ranking these targets is based on the conservative moist greenhouse inner habitable zone (IHZ) and maximum greenhouse outer habitable zone (OHZ) boundaries for our solar system from Kasting, Whitmire, and Reynolds 1993 and Kopparapu et al. 2013. These boundaries are then combined with a simple luminosity scaling relation to determine the current HZ boundaries for other stars. There is no consideration of the effect of stellar effective temperature, other HZ models, or the evolution of the HZ. Stellar effective temperature will have a significant effect on the extent of the HZ (e.g., Rugheimer et al. 2013; Shields et al. 2013; Rugheimer et al. 2015) and 1D and 3D climate models have shown a wide range of possible HZ limits (e.g., see Wolf et al. 2017, and references therein). Further, the use of the moist greenhouse IHZ boundary should be reexamined. Studies with 3D GCMs and energy balance models have shown that Earth would transition directly to a runaway greenhouse for F-, G-, K-, and M-type stars (Leconte, Forget, Charnay, Wordsworth, and Pottier 2013; Ramirez 2020). Additionally, the moist greenhouse does not imply that a planet is uninhabitable, only that the stratosphere is wet enough for the planet to lose the volume of Earth's oceans to photolysis in ~ 4.5 Gyr.

As this sample is composed mainly of F-, G-, and K-type stars where HZ evolution with respect to stellar luminosity plays a more significant role over billion year timeframes, this presents a perfect opportunity to extend our Bayesian 2 Gyr continuous habitable zone (CHZ_2) method to the EMSL. We apply this method to the 164 stars in the EMSL, combining an updated grid of Tycho stellar evolution tracks with the runaway greenhouse and maximum greenhouse HZ definitions of Kopparapu et al. 2014. In addition, we incorporate the IHZ definition from Turbet et al. 2023, which defines the initial IHZ boundary where Earth-like planets will be able to form oceans following formation. For targets in the EMSL, which lack discovered terrestrial

HZ exoplanets, we must instead consider the total extent of the CHZ_2 to prioritize targets. By integrating over the posterior CHZ_2 distribution outside hypothetical HWO coronagraph inner working angles (Mamajek and Stapelfeldt 2024), we demonstrate a method for prioritizing targets according to the accessibility of the CHZ_2 through a single CHZ_2 metric for each star.

To streamline the process of determining stellar ages and CHZ_2 posterior likelihood distributions, we combine both methods inside the open-source stellar model grid interpolation code `kiauhoku` (Claytor et al. 2020). This enables us to determine stellar ages, masses, and CHZ_2 posteriors together, greatly improving the efficiency and robustness of our results. We compare our results to the SPORES (Stellar/System Properties & Observational Reconnaissance for Exoplanet Studies with HWO) catalog (Harada et al. 2024), which determined masses and ages in a similar manner for all of the EMSL stars.

In Section 4.2, we discuss updates to the Tycho stellar evolution code and model grid, the HZ definitions used, our updated Bayesian CHZ_2 method, and the process for calculating the CHZ_2 metric. Section 4.3 reports our results and comparison of masses and ages to those in the SPORES catalog. Section 4.4 discusses issues with determining stellar masses and ages for the lowest mass stars in the EMSL, trends and implications for the derived CHZ_2 metrics, and future work. Finally, Section 4.5 presents a summary of our work.

4.2 Methods

4.2.1 Tycho Stellar Evolution Catalog

We use the stellar evolution code Tycho (Young and Arnett 2005) to generate a new catalog of stellar evolution tracks. Tycho is a 1D stellar evolution code that utilizes a hydrodynamic formulation of the stellar evolution equations. We have updated Tycho to include the latest Los Alamos OPLIB high temperature opacities (Colgan et al. 2016) and ÆSOPUS 2.0 low temperature opacities (Marigo et al. 2022), a 522 element reaction network up to ^{99}Tc utilizing the latest REACLIB rates (Cyburt et al. 2010), and the Asplund, Amarsi, and Grevesse 2021 protosolar abundances as our reference solar mixture. As with previous versions, Tycho uses a combined OPAL and Timmes equation of state (Timmes and Arnett 1999; Rogers and Nayfonov 2002), gravitationally induced diffusion (Thoul, Bahcall, and Loeb 1994), general relativistic gravity, time lapse, curvature, and automatic rezoning. The reaction network uses weak rates from Langanke and Martínez-Pinedo 2000 and screening from Graboske et al. 1973. Neutrino cooling and mass loss are included, but the latter is trivial for the low mass stars considered in this work. Tycho avoids the need for free convective parameters (i.e., "convective overshoot") by utilizing a description of turbulent convection based on 3D, well-resolved simulations of convection between stable layers (Meakin and Arnett 2007; Arnett, Meakin, and Young 2009, 2010; Arnett and Meakin 2011).

The new Tycho stellar evolution catalog spans masses of $0.2 - 1.6$ M$_\odot$ in steps of 0.01 M$_\odot$, metallicities ([M/H]) of $-1.75 - 0.5$ dex in steps of 0.25 dex, and evolutionary phases from the pre-main sequence birth to the first convective dredge-up or a maximum

age of 15 Gyr. These parameter ranges are sufficient for the studying the 164 F, G, K and early-M main sequence and subgiant stars in the EMSL, with the caveat that we neglect rotation and departures from the initial scaled solar abundances.

In Section 4.2.4, we use stellar model grid interpolation to determine the stellar age, mass, and CHZ_2 posterior likelihood distributions for all stars in the EMSL. When interpolating between tracks, stellar age is not an optimal dimension for comparison. Depending on the initial mass and metallicity, consecutive tracks can vary substantially in the lifetime of each evolutionary phase and which phases are reached. In order to simplify and improve the accuracy of interpolation, the original tracks output by the stellar evolution model are transformed onto a uniform basis, with an equal number of steps for each evolutionary phase. We transform the Tycho stellar evolution catalog tracks to an equivalent evolutionary phase (EEP) basis, using the EEP definitions of Dotter 2016. The main difference is that we do not go up to or past the tip of the red giant branch (RGB). We only need to simulate up to the end of the subgiant branch for the EMSL stars, so we stop the tracks at the maximum extent of the first convective dredge-up. The first dredge-up is an event in the first half of the RGB where the convective envelope extends deep enough to bring the products of Hydrogen burning to the surface. The maximum convective depth provides an easily distinguishable feature when examining the total convective mass in the stellar interior (Figure 4.1) and we apply this as the final EEP for all tracks in our grid that reach the RGB. We recommend this EEP for studies focused on earlier phases of evolution to avoid the large computational time required to reach the Helium flash at the tip of the RGB.

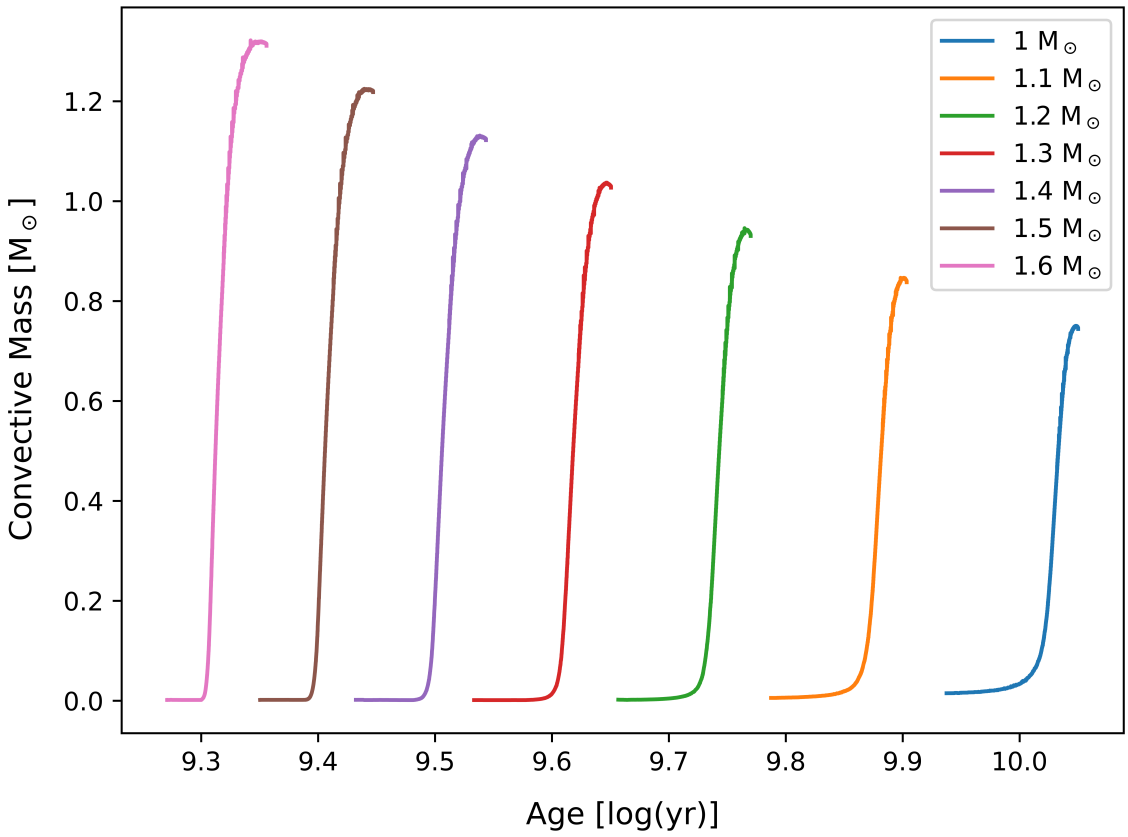

Figure 4.1. Evolution of the total convective mass for $1 - 1.6$ $M_{\odot}$, solar metallicity Tycho stellar evolution tracks. Here, tracks start from the base of the RGB and end just after the maximum convective depth is reached during the first dredge-up. The maximum convective mass provides a common final EEP for all tracks that reach the RGB in our model grid.

4.2.2 SPORES Catalog

Following the publication of the EMSL for HWO, the SPORES collaboration created a catalog of system properties for all 164 stars (Harada et al. 2024). This includes averaged spectroscopic abundances from the Hypatia Catalog (Hinkel et al. 2014) and independently, uniformly derived stellar properties via spectral energy distribution modeling. We adopt the stellar radii ($R_{\star}$), effective temperatures ($T_{\rm eff}$), and iron abundances ([Fe/H]) for use in Section 4.2.4 to calculate stellar ages, masses,

and CHZ_2 posterior likelihood distributions. The [Fe/H] values reported in the SPORES Catalog are normalized to the solar photospheric iron abundance reported in Asplund et al. 2009. We normalize the photospheric [Fe/H] for each timestep in the Tycho stellar evolution tracks to the same scale as the SPORES catalog to avoid introducing systematic errors when fitting to the Tycho models. For stars in the SPORES catalog without [Fe/H] from Hypatia, we use the values reported in the EMSL. The SPORES catalog also report masses and ages from sampling of the MIST (MESA Isochrones and Stellar Tracks) isochrone grid (Dotter 2016), which we compare to in Section 4.3.1.

4.2.3 Habitable Zone Models

Following Ware et al. 2022, we include the 1 $M_\oplus$ HZ model from Kopparapu et al. 2014, defined by a runaway greenhouse IHZ and maximum greenhouse OHZ. The authors parameterize the HZ with respect to the $T_{\rm eff}$ and luminosity of the star. By taking outputs from the Tycho stellar evolution models, we calculate the HZ boundaries for each time-step of the star's main sequence evolution.

We also include a new IHZ boundary from Turbet et al. 2023, determined using a 3D general circulation model (GCM), as a compliment to the 1D HZ model from Kopparapu et al. 2014. Climate models often assume the planet's initial water begins condensed on the surface. Turbet et al. 2021 showed that if water is assumed to initially be fully vaporized following the magma ocean phase, a new IHZ instellation limit can be determined where atmospheric water vapor condenses on the surface. The authors find that this so-called "water condensation limit" (WCL) is always at a lower instellation than the runaway greenhouse limit at the zero-age main sequence (ZAMS).

If a planet has an instellation exceeding the WCL at the ZAMS, that planet will be unable to ever form oceans on its surface and will lose its water through photolysis and atmospheric escape. This has significant consequences for planets near the IHZ, such as Venus. Figure 4.2 shows the HZ definitions along with the instellations for Venus and Earth at the ZAMS and at solar age (4.57 Gyr). While Earth would have been outside the WCL at the ZAMS, Venus has always been inside the WCL. This implies Venus would never have been able to form oceans. This result is crucial to take into account when determining the potential habitability of exoplanets and prioritizing exoplanets and stellar systems for detailed biosignature searches. We incorporate these results into our model, with the WCL defining the initial IHZ at the ZAMS. We keep the IHZ distance constant as the star evolves until the stellar luminosity increase causes the runaway greenhouse limit to exceed the WCL.

4.2.4 Stellar Masses, Ages, and CHZ_2 Posterior Likelihood Distributions

Previously, we calculated stellar ages and CHZ_2 posterior likelihood distributions separately. This involved first performing χ^2 fits to Tycho stellar evolution tracks to obtain best-fit stellar ages and/or retrieving literature measurements of stellar age determined via empirical age relations. We then combined the age with measured stellar masses and metallicities from the literature, in order to avoid fitting the Tycho best-fit mass to the stellar evolution tracks a second time, to place prior probabilities on our HZ evolution models. By calculating the Bayesian likelihood that a range of orbital radii are within the CHZ_2 we produced posterior likelihood distributions for the location of the CHZ_2 around a given star. While this method is functional and effective, we have significantly improved the efficiency, robustness, and reproducibility

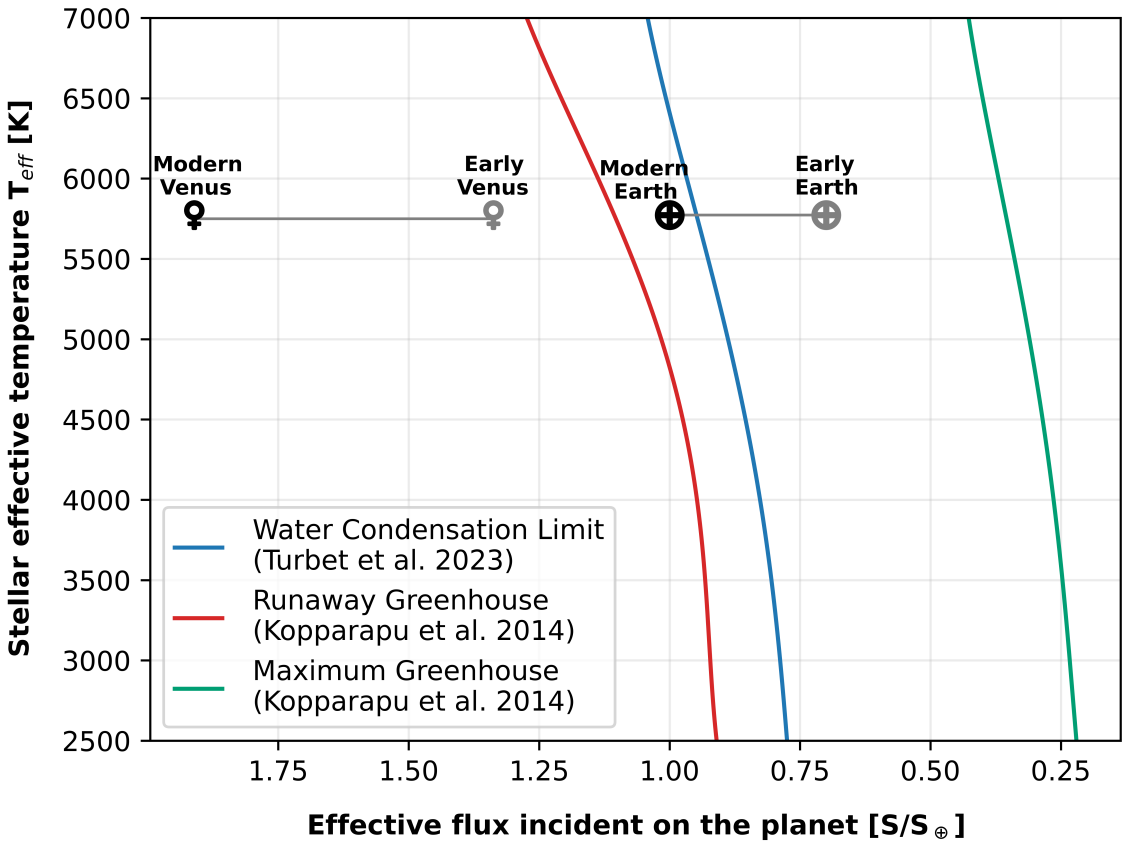

Figure 4.2. HZ definitions used in this work: runaway greenhouse IHZ and maximum greenhouse OHZ from Kopparapu et al. 2014; water condensation limit IHZ from Turbet et al. 2023. Over-plotted are the instellations for Venus and Earth at the ZAMS and solar age (4.57 Gyr).

of our method by combining both calculations within the open-source `kiauhoku`[1] stellar model grid interpolator.

First presented in Claytor et al. 2020, `kiauhoku` performs interpolation between stellar evolution tracks that have been transformed to an EEP basis and maps stellar observables, in this case effective temperature, radius, and [Fe/H], onto the stellar model fundamental properties of mass, metallicity, and age. Combined with the Markov Chain Monte Carlo (MCMC) sampling Python package `emcee` (Foreman-

[1]https://github.com/zclaytor/kiauhoku

Mackey et al. 2013; Foreman-Mackey et al. 2019), this results in sampled posterior distributions for each parameter of interest. In order to include the location of the CHZ_2 as a sampled parameter, we calculate the CHZ_2 boundaries for each timestep in the stellar evolution tracks, starting from the ZAMS. We then use an ensemble of walkers running individual Markov chains to sample the posterior distributions for mass, age and CHZ_2 location.

We place priors on the initial mass, initial metallicity, age, and EEP range. For mass and metallicity, we restrict the sampling to within the bounds of the Tycho model grid and use the joint log-normal and power-law Chabrier initial mass function (Chabrier 2003) to positively weight lower mass models. For age, we use the Gaussian Q-function to constrain samples below the age of the universe (13.787±0.020 Gyr, Planck Collaboration et al. 2020), which takes the form

$$P = \frac{1}{2}(1 + erf(\frac{Age_{\rm mod} - Age_{\rm uni}}{\sigma_{\rm uni}\sqrt{2}})) \tag{4.1}$$

where erf is the error function, $Age_{\rm mod}$ is the model age, and $Age_{\rm uni}$ is the age of the universe. For the EEP range, we use the luminosity classes reported in the EMSL to determine the upper and lower limits: the ZAMS to terminal-age main sequence (TAMS) for dwarfs (V), the TAMS to first dredge-up for subgiants (IV), and the ZAMS to first dredge-up for uncertain classifications (IV-V). We use a χ^2 distribution to calculate the log-likelihood for each model grid point:

$$ln(P) = -\frac{1}{2}\sum_i (\frac{x_{{\rm obs},i} - x_{{\rm mod},i}}{\sigma_{{\rm obs},i}})^2 \tag{4.2}$$

where $x_{{\rm obs},i}$ and $x_{{\rm mod},i}$ are the SPORES catalog measured and Tycho modeled stellar effective temperatures, radii, and [Fe/H], respectively. After obtaining a sampled posterior distribution for the CHZ_2 boundaries, we compare a range of orbital radii to

the posterior distribution to determine the likelihood that any given orbital distance around a star is within the CHZ_2.

This combined method for determining stellar ages and CHZ_2 locations enables us to generalize the Bayesian CHZ_2 routine from Ware et al. 2022 to any stellar model grid. This also eliminates additional uncertainty introduced by fitting ages separately and using literature masses to constrain the HZ evolution models. Alongside the published version of this chapter, we will be releasing a GitHub module within `kiauhoku` to enable users to calculate CHZ_2 boundaries for any stellar model grid with options for various published HZ models, sample full CHZ_2 posterior distributions for a range orbital radii, and calculate CHZ_2 posterior likelihoods for individual planets. Additionally, the Tycho stellar model grid will be included as an option to use within `kiauhoku`.

4.2.5 Determining a CHZ_2 Metric

The goal of determining CHZ_2 posterior distributions for each star in the EMSL is to demonstrate a method for further prioritizing observations based on the likelihood a terrestrial HZ exoplanet in the system will host detectable signatures of life. However, at the time of this writing none of the EMSL star have any candidate or confirmed terrestrial HZ exoplanets, assuming an upper radius limit of 1.8 $M_\oplus$ and the HZ definitions from Kopparapu et al. 2014. Therefore, instead of ranking exoplanets within each system based on their CHZ_2 likelihoods, we must derive a metric for prioritization by considering the full CHZ_2 posterior distribution for each system. For a star with exact knowledge of the stellar properties, such as the Sun, this metric would be defined by the total range of the CHZ_2 given by the inner and outer boundaries.

For the stars in the EMSL with significant associated uncertainties for measured stellar properties, we must integrate over the full CHZ_2 posterior distribution. In this case, each orbital radius is weighted by the likelihood of being within the CHZ_2.

HWO will be a direct imaging mission, in which a coronagraph will be used to block the light from star and reveal the faint reflected light of the planets. Coronagraphs have an associated inner working angle (IWA), inside of which any planets would be hidden behind the coronagraph or the diffracted light from the host star. We must take into account the IWA when integrating over the CHZ_2 posterior distribution, with the IWA defining the lower integration limit. The metric equation then takes the form

$$metric = \int_{IWA}^{\infty} P(CHZ_2)dr \tag{4.3}$$

where the IWA is converted from a projected angle on the sky to an orbital radius using the distance reported in the EMSL, typically from Gaia. Currently, we do not know the final specifications for HWO, but we can utilize the IWA estimates from the EMSL for each tier of targets. The EMSL used three separate IWAs to determine the accessibility of the HZ, ranging from conservative to optimistic: 83 mas for tier A, 72 mas for tier B, and 65 mas for tier C. We use these IWA estimates to calculate the CHZ_2 metric for each star and then rank the stars within their respective tiers. The CHZ_2 can be interpreted as a proxy for the range of the CHZ_2 with a higher metric indicating a combination of a more accessible CHZ_2 for HWO and a higher likelihood of continuous habitability for terrestrial exoplanets in the HZ. We retain each star within their respective EMSL tiers to account for the additional factors used to initially rank them, such as the presence of a disk or close stellar companion.

4.3 Results

We used 50 walkers, a burn-in phase of 1,000 iterations, and 10,000 final iterations with the MCMC sampler for each of the 164 stars in the EMSL. We used long chains to ensure convergence, with longer computational times not being an issue for this relatively small sample. To check the quality of the final samples, we compared the SPORES catalog effective temperature, radius, and [Fe/H] to the sampled posterior distribution for each star. If the literature values fell within the 2σ, we flagged the samples as reliable. The effective temperatures and radii reported in the SPORES catalog have median uncertainties of $\sim 0.8\%$ and $\sim 1.9\%$, respectively. These are more than two times lower than the systematic noise floors of $\sim 2.4\%$ and $\sim 4.2\%$ set by measured interferometric angular diameters and bolometric fluxes (Tayar et al. 2022). Further, the SPORES catalog uses the means of the log iron abundance measurements in Hypatia, which will skew the mean and uncertainty relative to the linear mean. When taking the mean of log abundances, one should first convert the abundances to a linear scale then take the log of the mean value. Additionally, the median and spread about the median often better represent the range of abundance measurements, where significant systematic differences between methods are common (Hinkel et al. 2016). For these reasons, we use a more conservative 2σ threshold to determine reliable samples.

In total, 153 stars were flagged as reliable. For these stars, we calculated the mean, median, and root median square offset (RMedS) between the sample median and input effective temperatures, radii, and [Fe/H]. These are shown in Table 4.1 and demonstrate that the samples are well converged, with the mean, median, and RMedS offsets being close to zero for all parameters.

Table 4.1. MCMC sample offsets compared to SPORES catalog

Parameter	Mean	Median	RMedS
$\Delta T_{\rm eff}$ (K)	15	7	7
ΔR ($R_\odot$)	0.01	0	0
Δ[Fe/H] (dex)	0.033	0.01	0.01
ΔM ($M_\odot$)	0.03	0.03	0.03
ΔAge (Gyr)	1.84	1.29	1.29

Note: Offsets were only calculated for stars with samples flagged as reliable.

4.3.1 Stellar Masses and Ages

From our sampling of effective temperature, radius, and [Fe/H], we obtained posterior distributions for the masses and ages of the EMSL stars. We report the SPORES catalog inputs and the median and 68% credible intervals for the masses and ages of all 164 stars in Table B.1. Figure 4.3 compares the masses derived in this work, for the 153 stars with samples flagged as reliable, to those in the SPORES catalog. We find a generally tight correlation, with virtually all of the masses having a $< 2\sigma$ discrepancy as determined by the residuals normalized by the quadrature sum of the uncertainties. We compare the median uncertainties between both sets of masses in Table 4.2. We achieve a median uncertainty of 0.03 $M_\odot$ (2.8%) from our sampling, compared to 0.05 $M_\odot$ (4.6%) for the SPORES catalog. Aside from differences in the stellar model physics and inputs, one obvious factor could have influenced the tighter constraints for our samples. We applied priors on the evolutionary phases in the MCMC sampling generally according to the spectral types reported in the EMSL. However, after an initial round of sampling without any EEP priors, we also checked the posterior distributions to determine if stars near the TAMS were more likely to be dwarfs or subgiants and adjusted the EEP priors accordingly. Overall, the two sets

of mass agree well, with a RMedS offset of 0.03 $M_\odot$, well within the quadrature sum of the median uncertainties (0.06 $M_\odot$). The mean, median, and RMedS offsets for both the masses and ages are listed in Table 4.1.

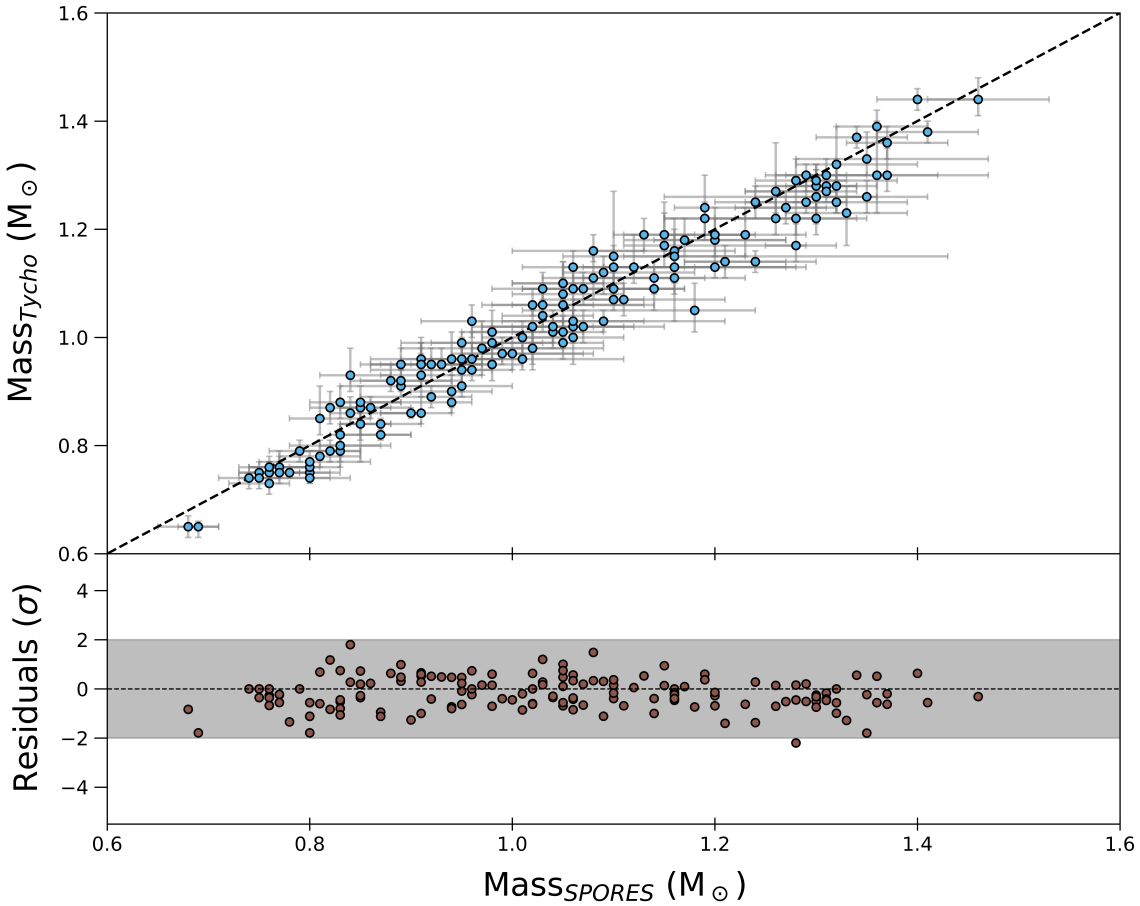

Figure 4.3. (top) Median masses from MCMC sampling of Tycho stellar model grid compared to masses from the SPORES catalog. Only stars with samples flagged as reliable are shown. The black dashed line represents a 1:1 correlation. (bottom) Residuals normalized by the quadrature sum of the uncertainties. The grey shaded region shows stars with $< 2\sigma$ discrepancy.

Figure 4.4 compares the ages derived in this work to those in the SPORES catalog. While there initially appears to be significant discrepancies between the two sets of ages, accounting for the uncertainties results in all but four of the 153 stars having

discrepancies $< 2\sigma$. The Tycho ages systematically skew older for younger stars in the SPORES catalog and vice versa. This is likely due to the EEP priors previously mentioned, along with the prior for the age of universe, which limits the range of possible ages relative to the SPORES catalog. We compare the median uncertainties between boths sets of ages in Table 4.2. We achieve a median uncertainty of 1.15 Gyr (25.3%) from our sampling, compared to 1.89 Gyr (41.2%) for the SPORES catalog. An additional factor influencing the tighter age constraints is our method of calculating the log-likelihood with respect to the measured [Fe/H]. We compared the photospheric [Fe/H] at each EEP step in the Tycho tracks to the measured [Fe/H] rather than the initial metallicity of the model, which is the more commonly used method. This places an additional constraint on the age beyond effective temperature and radius. Since Tycho includes both gravitational settling and a more realistic treatment of convection, the photospheric abundances are more likely to be predictive than models lacking one or both of these effects. Further, this avoids the problem of fitting to the initial uniform bulk composition, which is based on a protosolar abundance mixture and will change over time due to nucleosynthesis, mixing, and gravitational settling of heavier elements in the envelope. As with the masses, the overall ages of the two sets agree well, with a RMedS offset of 1.29 Gyr, which is within the quadrature sum of the median uncertainties (2.21 Gyr).

4.3.2 CHZ_2 Posterior Likelihoods

From our sampling of the Tycho stellar model grid, we also obtained posterior distributions for the CHZ_2 boundaries. By comparing a range of orbital radii to

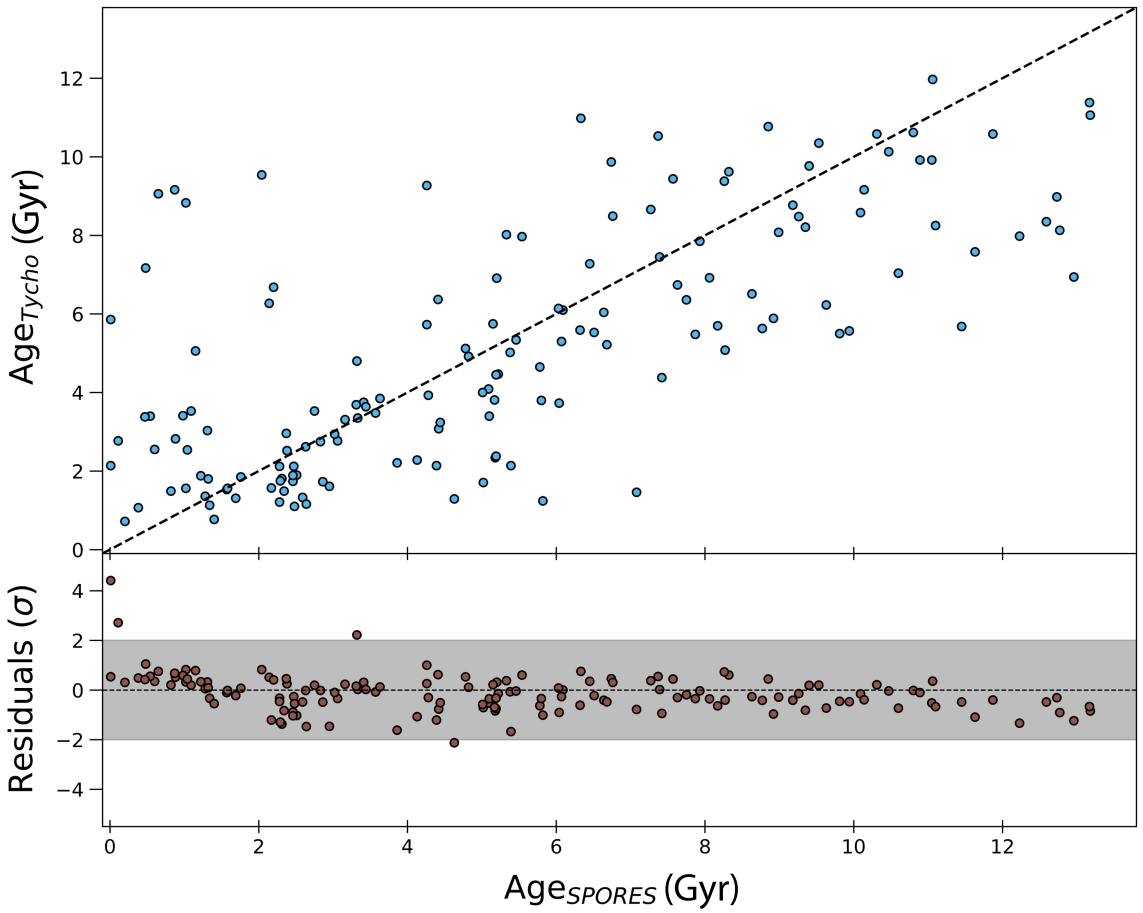

Figure 4.4. (top) Median ages from MCMC sampling of Tycho stellar model grid compared to ages from the SPORES catalog. Only stars with samples flagged as reliable are shown. The black dashed line represents a 1:1 correlation. Error bars are excluded for clarity. (bottom) Residuals normalized by the quadrature sum of the uncertainties. The grey shaded region shows stars with $< 2\sigma$ discrepancy.

the inner and outer CHZ_2 posteriors, we calculate the CHZ_2 posterior likelihood distributions for all 164 stars in the EMSL. We convert the likelihood posteriors to a single CHZ_2 metric value using the method described in Section 4.2.5. Here we focus on the 153 stars with samples flagged as reliable, but the full list of CHZ_2 metric results is provided in Table B.2 with stars separated into their EMSL tiers and ranked according to the metric value.

Figure 4.5 shows the CHZ_2 metric with respect to the age derived in this work

Table 4.2. Median mass and age uncertainties

Parameter	Median	Median$_{SPORES}$
σ_M ($M_\odot$)	0.03 (2.8%)	0.05 (4.6%)
σ_{Age} (Gyr)	1.15 (25.3%)	1.89 (41.2%)

Note: Median uncertainties were only calculated for stars with samples flagged as reliable.

and spectral type for EMSL Tier A, B, and C stars. Results are comparable between tiers, with minimal difference in the overall trends. This is expected, as we are only considering the properties of the star irrespective of distance, binarity, the presence of a disk, or other factors that are already accounted for with their separation into tiers. The CHZ_2 metric begins close to 0 for stars < 2 Gyr in age, as these stars are not yet old enough to obtain a CHZ_2. The CHZ_2 metric then increases with age, peaking close to solar age between $3 - 4$ Gyr with late-F to early-G stars typically having the highest values of $\sim 0.8 - 0.9$, before slightly tapering off for the oldest stars. We mark stars with $\log g < 4$, determined by the mass derived in this work and the SPORES catalog radius, as these are likely to be subgiants. Although the sample of potential subgiants is small (~ 9), these stars follow the same general trends as the sample of dwarf stars, albeit with lower CHZ_2 metrics than the peak as they tend to be older. We discuss these trends further in Section 4.4 along with how these metrics can factor into future prioritization and future work that is needed.

4.4 Discussion

We determined masses, ages, and CHZ_2 metrics for the 164 stars in EMSL through MCMC sampling of our Tycho stellar model grid. Sampled posterior distributions for

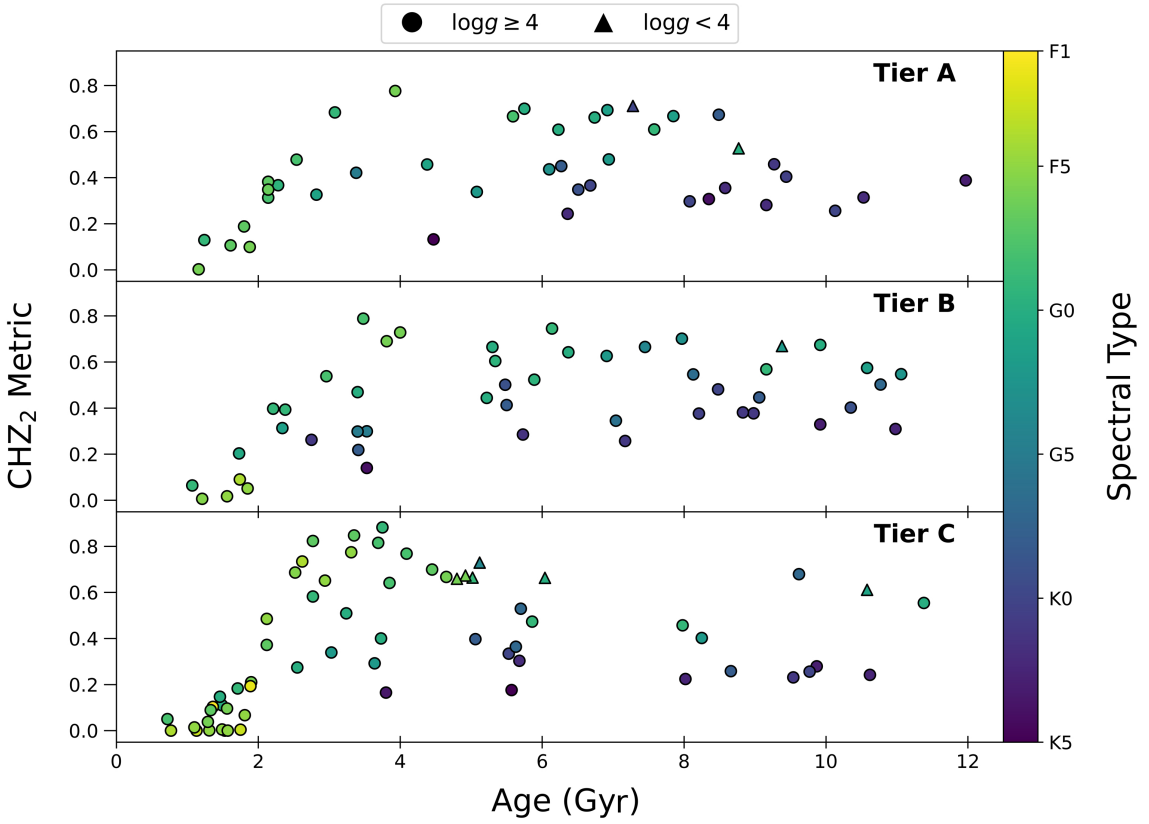

Figure 4.5. CHZ_2 metric vs. age for stars with samples flagged as reliable, separated into tiers A (top), B (middle), and C (bottom) according to the EMSL. Stars with log$g < 4$, determined by the Tycho derived mass and SPORES catalog radius, are marked by triangles to denote likely subgiants. Stars are colored according to the spectral type from the EMSL.

153 of the stars were deemed reliable with the median sampled effective temperatures, radii, and [Fe/H] falling within 2σ of the inputs. We examine here the other 11 stars for which the samples were deemed unreliable. These stars were all K- and M-type dwarfs, typically with sub-solar [Fe/H]. Stellar evolution models are known to struggle simulating low-mass stars, with radii underestimated by $\sim 5\%$ for stars < 0.7 $R_\odot$ and effective temperature overestimated by $\sim 3\%$ for stars < 5000 K (Boyajian et al. 2012). A major contributing factor is likely the exclusion of the effects of magnetic fields and starspots (e.g., Morales, Ribas, and Jordi 2008; Somers, Cao, and Pinsonneault 2020),

which lead to inflated radii and cooler effective temperatures relative to predictions. This is exacerbated for lower metallicity stars as decreasing opacity causes smaller model radii and higher model temperatures.

While insufficient models likely explain the majority of the offset between the input and sampled radii and effective temperatures for these 11 stars, we also compare the SPORES catalog properties to those derived from interferometric angular diameters and bolometric luminosities. 8 of the 11 stars have interferometric radii and effective temperatures reported in the literature, with the effective temperatures being generally consistent with those in the SPORES catalog. However, radii are found to be systematically overestimated in the SPORES catalog, with a median offset of 0.03 $R_\odot$ compared to the literature for HD 88230 (Boyajian et al. 2012), HD 95735 (Boyajian et al. 2012), HD 103095 (Karovicova et al. 2020), HD 165341 (Boyajian et al. 2012), HD 201091 (Boyajian et al. 2012), HD 201092 (Boyajian et al. 2012), HD 209100 (Demory et al. 2009), and HD 217987 (Boyajian et al. 2012). As the posterior distributions skewed toward smaller radii for these stars, the input radii may have contributed to the tension between the sampled radii and effective temperatures.

4.4.1 Trends and Implications for CHZ_2 Metrics

The CHZ_2 metrics show expected trends with respect to age and spectral type. Older stars in this sample tend to have slightly lower CHZ_2 metrics, likely due to two factors. The CHZ_2 shrinks as stars evolve, with more rapid changes in luminosity as hydrogen is depleted in the core. Based on the ages derived in this work, the oldest stars are typically K dwarfs, which biases the CHZ_2 metric towards lower values. For F, G, and K dwarfs, the median values are 0.297, 0.448, and 0.382, respectively. While

K dwarfs have longer main sequence lifetimes, the size of the HZ scales with $(\frac{L}{L_\odot})^{0.5}$ and hence results in a smaller CHZ_2. The opposite is true for F dwarfs, with G dwarfs striking a balance between these two with both long main sequence lifetimes and larger HZs.

Notably, the CHZ_2 metric peaks between $3-4$ Gyr for early-G and late-F dwarfs, which is most exemplified by Tier C stars. Stars close in spectral type to the Sun may have the largest zones of continuous habitability, combining the benefits of long lifetimes, large HZs, and slow evolution rates. This result matches that found in Mello and Friaça 2023, in which the authors combine a minimal mantle and atmospheric model to study the evolution of the CHZ for various planetary parameters and stellar types. In their model, the IHZ expands as the luminosity increases and the OHZ contracts as geologic activity, and hence CO_2 outgassing, decreases with time. This results in planets becoming geologically dead within $\sim 5-7$ Gyr for those between $0.5-1$ $M_\oplus$, after which the planets rely solely on their host star's luminosity to maintain habitable surface temperatures. The authors speculate that the average age for habitable planets is therefore younger than the age of the Earth, with only super-Earth's maintaining habitable conditions for longer periods.

One may expect subgiants in this sample to have significantly lower CHZ_2 metrics than dwarfs as they leave the main sequence and begin to rapidly evolve. However, the luminosity remains relatively constant on the subgiant branch, only changing once the star nears the RGB. The effective temperature decreases significantly throughout the subgiant branch, reaching ~ 4000 K for a solar twin at the base of the RGB. While this will have a slight effect on the HZ boundaries, pushing the HZ further out as the Wien peak shifts towards the infrared, the overall shift is marginal relative to the luminosity of the star at the TAMS. The impact this shift in peak wavelength would have on life

is less clear, but increased interest in the potential for life on exoplanets has spurred further research. A recent study (Vilović, Schulze-Makuch, and Heller 2024) explored the effects of two photosynthetic organisms grown under a solar spectrum and a simulated K dwarf spectrum (4,300 K). Garden cress *Lepidium sativum*, a common garden plant, exhibited comparable growth and photosynthetic efficiency, a measure of how effectively an organism converts photons to chemical energy, under both spectra. Surprisingly, the cyanobacterium *Chroococcidiopsis* exhibited increased culture growth and photosynthetic efficiency under the K dwarf spectrum. While further research is needed to apply a broad consensus for life on Earth, these results are encouraging for the prospects of life on other worlds surviving the spectral shift during the subgiant branch.

Overall, the three highest ranked stars according to the EMSL tier and CHZ_2 metric are HD 142860 (F6V), HD 23249 (K0IV), and HD 19373 (G0V). These stars cover a range of ages from $3.93 - 7.28$ Gyr, providing an excellent sub-sample of systems for comparative planetology from younger to older than the Earth. Further, HD 23249 provides the opportunity explore the potential habitability of systems with evolved subgiant host stars.

4.4.2 Future Work

In this work we have only focused on using the Tycho grid of stellar evolution models, combined with the HZ definitions of Kopparapu et al. 2014 and Turbet et al. 2023, to estimate ages, masses, and CHZ_2 posterior likelihood distributions for stars in the EMSL. There are a plethora of stellar model grids that exist, with some taking into account effects of rotation (e.g., YREC, Claytor et al. 2020) and

magnetic fields (e.g., SPOTS, Somers, Cao, and Pinsonneault 2020). Considering our difficulties with sampling for the lowest mass K and M dwarfs and the known systematic offsets between model grids (e.g., Tayar et al. 2022), it will be essential to compare to predictions from a variety of stellar models. While the Kopparapu et al. 2014 HZ definitions are some of the most commonly used in the exoplanet community, a large number of HZ definitions have been reported in the literature over the past two decades (e.g., see Wolf et al. 2017, and references therein). Considering the limitations of 1D climate models in realistically simulating planetary atmospheres and the various planetary parameters that can impact the climate as discussed in Chapter 3, comparisons with HZ definitions determined with 3D GCMs and alternative planetary configurations will better inform target prioritization for HWO. A benefit of using `kiauhoku` is that we can easily compare offsets between stellar model grids for derived masses and ages. With the addition of our module for computing CHZ_2 posterior distributions, we will also be able to compare offsets between grids for the CHZ_2 metrics.

As discussed in Chapters 2 and 3, stellar ages are notoriously difficult to constrain for field dwarfs, especially low-mass K and M dwarfs with long main sequence lifetimes. Alternative methods to fitting surface properties to stellar model grids often provide more precise estimates, such as through asteroseismology (e.g., Huber et al. 2022) or empirical relations between age and rotation (e.g., Barnes and Kim 2010), activity (e.g., Lorenzo-Oliveira et al. 2018), or elemental abundances (e.g., Nissen 2015). We plan to incorporate age estimates from these sources in the future to enable better constraints on the current location of the CHZ_2.

4.5 Conclusion

Searching for terrestrial HZ exoplanets around Sun-like stars and probing their atmospheres for biosignatures through direct imaging will be a daunting task, but represents our best chance at constraining the prevalence of life in our galaxy. Considering the potential for life to have made a detectable impact on the atmosphere presents a means to prioritize targets in the lead-up to future missions. For the targets in the EMSL (Mamajek and Stapelfeldt 2024), which have been determined to be best targets for the HWO direct imaging mission, only the present-day HZ was used in separating targets in priority tiers. This presented a clear opportunity to demonstrate how consideration of the continuous HZ could be used to further prioritize targets. The goal of this work was to determine the likelihood of terrestrial HZ exoplanets remaining continuously habitable and the accessibility of the CHZ_2 for the EMSL stars. Here we provide a summary of the updates to our methods, our results, and key takeaways:

- As in Ware et al. 2022, we used the 1 $M_\oplus$ runaway greenhouse and maximum greenhouse HZ definitions from Kopparapu et al. 2014, but with the addition of the WCL initial IHZ boundary from Turbet et al. 2023. This is a critical addition as it defines the boundary at the ZAMS where Earth-like planets will be able to form oceans following the magma ocean phase.
- We updated our Bayesian CHZ_2 method to work with the open-source stellar model grid interpolation code `kiauhoku` (Claytor et al. 2020), enabling the simultaneous sampling of stellar age, mass, and the CHZ_2 boundaries.
- With the need for a means to easily compare the CHZ_2 posterior distributions for stars in the EMSL, as there are not currently discovered terrestrial HZ

exoplanets for this sample, we developed a CHZ_2 metric. By integrating over the CHZ_2 posterior distributions outside hypothetical HWO IWAs, we could directly compare likelihood and accessibility of the CHZ_2 for each star.

- Comparison of our derived masses and ages to those in the SPORES catalog (Harada et al. 2024) showed generally good agreement, with RMedS offsets comparable to the median uncertainties for each set. We do achieve improved median uncertainties compared to the SPORES catalog, most likely due our additional prior on the evolutionary phases.
- We note that we fail to achieve reliable MCMC samples for 11 K and M dwarfs, a well known problem for stellar evolution models (e.g., Boyajian et al. 2012). The addition of the effects of magnetic fields and starspots to Tycho or the use of a model grid which already accounts for some of these effects (Somers, Cao, and Pinsonneault 2020) may be necessary to achieve reliable sampling for these stars.
- We report CHZ_2 metrics results for the 164 stars in the EMSL. Our results show that late-F and early-G dwarfs near solar may be the best targets for habitable exoplanet searches. The median CHZ_2 metric is highest for F- and G-type and the CHZ_2 distribution with age peaks between $3 - 4$ Gyr. This result is backed up by Mello and Friaça 2023, where the combined evolution of the geosphere and atmosphere shows that the continuous HZ begins to shrink for Earth-twins soon after solar age due to a decrease in geologic activity. However, the highest ranked stars in Tier A of the EMSL are HD 142860 (F6V), HD 23249 (K0IV), and HD 19373 (G0V). The inclusion of an evolved subgiant among the stars in Tier A with the highest CHZ_2 metric may be unrealistic due to decreased rates of outgassing for Earth-sized planets, but recent results show that photosynthetic

organisms on Earth may withstand the shift in the spectral energy distribution during the subgiant branch (Vilović, Schulze-Makuch, and Heller 2024).

- Future work is needed to compare our CHZ_2 metrics results between stellar model grids and for various HZ definitions. While the overall trends may be similar since the HZ will always move outward with increasing luminosity and the HZ boundaries shift outward with decreasing effective temperature, results for individual stars will certainly vary. Examining the effects from the inclusion of stellar ages derived using more precise methods will also be a worthwhile investigation.

In conclusion, we presented an updated version of Bayesian CHZ_2 method from Ware et al. 2022, where we determine the likelihood that any given orbital radius around a star is within the CHZ_2, and applied this method to the 164 stars in the EMSL. Using a CHZ_2 metric to compare the likelihood and accessibility of the CHZ_2 between stars, we demonstrate a method for prioritizing future direct imaging searches habitable exoplanets and biosignatures. We emphasize the need for alternative stellar evolution models to better simulate the lowest mass K and M dwarfs, as well as the need for comparisons between stellar model grids and HZ definitions to explore offsets in the CHZ_2 metrics. We hope that the future release of an open-source module for calculating CHZ_2 posterior distributions will be useful to the community and spur increased interest in the study of continuous HZ evolution.

Chapter 5

EPILOGUE

This thesis dissertation presented three studies on the extension and application of a Bayesian continuous habitable (CHZ) method for estimating the long-term habitability potential of terrestrial habitable zone (HZ) exoplanets. Future direct imaging searches of systems with Sun-like host stars for habitable exoplanets and biosignatures will present significant difficulties for even the best of targets, requiring extensive vetting and target prioritization to maximize our chances of detection. With NASA funding both precursor and preparatory science for the Habitable Worlds Observatory (HWO) and establishing a working group dedicated to host star characterization, consideration of the long-term habitability of potential target systems will be beneficial to these efforts.

Chapter 2 expanded upon the Bayesian method for estimating the 2 Gyr continuous habitable zone (CHZ_2) likelihood for exoplanets from Truitt et al. 2020. The authors only considered the measured mass and metallicity of the host star, combining Tycho (Young and Arnett 2005) stellar evolution tracks with the HZ prescriptions from Kopparapu et al. 2013; Kopparapu et al. 2014 to calculate the CHZ_2 likelihood for the full main sequence lifetime. By adding a prior for the stellar age into the posterior likelihood calculation, we improved upon this method by calculating the current CHZ_2 likelihood. This was most exemplified for the Sun for which the astrophysical age has been measured to high precision (4.57 ± 0.11, Bonanno, Schlattl, and Paternò 2002), increasing the CHZ_2 likelihood for Earth from $\sim 20\%$ without an age prior to 100% with the age prior.

Chapter 3 explored using the results of a perturbed parameter ensemble (PPE) of general circulation models (GCM) for land planet atmospheres (Kiang et al. 2024, in prep) to define HZ boundaries. We performed multivariate linear regressions on surface temperature metrics, with respect to stellar effective temperature and planetary instellation, to determine prescriptions for the inner HZ (IHZ) and outer HZ (OHZ). The HZ boundaries were defined by the instellations at which planets reached 0°C (complete freezing point) at the OHZ and 100°C at the IHZ, since a runaway greenhouse threshold could not be used as the GCM, ROCKE-3D, crashes at this point. The regressions did not include parameters from the PPE that would be unknowns for near-term missions, such as CO_2 partial pressure and surface albedo. The variance from these parameters was included in the standard errors of the regression coefficients, enabling calculation of confidence intervals for the HZ boundaries that can be propagated through the Bayesian CHZ_2 calculation. This was a novel way of determining the HZ boundaries as other studies typically focused on a limited set of planetary configurations for aqua planets like Earth, where a single limiting instellation was found for each stellar spectral type.

We found significant offsets relative to the commonly used HZ prescriptions of Kopparapu et al. 2014, with the IHZ and OHZ boundaries derived in this work generally being shifted inward towards higher instellations. A direct comparison of the HZs was difficult due to a number of factors, such as the differences in HZ boundary definitions, the small PPE sample size (93 planets reached equilibrium), and the small PPE instellation range ($0.62 - 1.471$ S_0). The small sample size and instellation range also affected the robustness of the derived HZ prescriptions. For planets with late-type K and M host stars, the shift in the stellar spectrum towards the near-IR leads to lower planetary albedos and higher surface temperatures at the same instellation. This

caused a large number of models near the IHZ to crash upon reaching a hotter climate state and those near the OHZ never reached the complete freezing point. The opposite was true for planets with hotter host stars, causing the IHZ and OHZ boundaries to be dominated by lower and higher mass host stars, respectively. While the HZ results were impacted, we still demonstrated the usefulness of defining HZ boundaries that take into account a large number of planetary parameters that may effect habitability, as current HZ prescriptions for limited sets of planetary configurations give a massive range of possible HZ boundaries (e.g., Wolf et al. 2017). Combined within a Bayesian framework for calculating CHZ_2 likelihoods, this enables various stellar and planetary uncertainties to be taken into account when estimating the long-term habitability potential of exoplanets.

Chapter 4 applied our Bayesian CHZ_2 method to the samples of stars in the NASA Exoplanet Exploration Program mission star list (EMSL) for HWO (Mamajek and Stapelfeldt 2024), the current highest priority targets for a future direct imaging survey of potentially habitable exoplanets orbiting Sun-like stars. We used an updated grid of stellar evolution tracks combined with the HZ prescriptions from Kopparapu et al. 2014 and Turbet et al. 2023 to calculate CHZ_2 posterior likelihood distributions for all 164 stars in the EMSL. We also combined our CHZ_2 method with the open-source stellar model grid interpolation code `kiauhoku` (Claytor et al. 2020), enabling the simultaneously calculation of stellar mass, age, and CHZ_2 likelihood. Comparing our derived masses and ages to those from the SPORES (Stellar/System Properties & Observational Reconnaissance for Exoplanet Studies with HWO) catalog (Harada et al. 2024), we found generally good agreement, but with increased precision in this work.

As the stars in the EMSL lack known terrestrial HZ exoplanets, we derived a CHZ_2

metric to be able to compare the CHZ_2 posterior likelihood distributions between stars. We used our CHZ_2 metric results to rank stars within their respective EMSL tiers, demonstrating a method for further prioritizing observations based on the long-term habitability potential and the accessibility for HWO. Overall, our results showed that late-F and early-G dwarfs near solar age are likely the best targets. However, subgiants should not be discounted, as the second-highest ranked star in EMSL Tier A is the K0IV star HD 23249. For some of the lowest mass stars in the sample, we had difficulty determining reliable masses, ages, and CHZ_2 metrics. This reflects the need for stellar model grids better suited for active, slowly evolving low-mass stars.

From the recommendation for the Terrestrial Planet Finder in 2000 to what is now known as the Habitable Worlds Observatory in 2020, the search for habitable exoplanets and life on other worlds has been a major point of emphasis in the Astrophysics Decadal Surveys for the past two decades. As the community dedicates to a mission that may finally answer fundamental questions about life in the universe, we must consider the vast array of variables that could influence our ability to find habitable, and inhabited, exoplanets. Considering of long-term habitability is one such variable and a flexible Bayesian framework for continuous habitability can aid in factoring in the small amounts of information we do have about what makes a planet Earth-like. Future work is needed to account for other stellar and planetary aspects of habitability, such as the influences of stellar activity and the coupled evolution of the atmosphere and geosphere that likely play a significant role in the ability for habitable conditions to be maintained over billions of years. However, we are hopeful the work detailed in this dissertation can aid in this collective endeavor and look forward to what is to come.

Abe, Yutaka, Ayako Abe-Ouchi, Norman H. Sleep, and Kevin J. Zahnle. 2011. "Habitable Zone Limits for Dry Planets." *Astrobiology* 11, no. 5 (June): 443–460. https://doi.org/10.1089/ast.2010.0545.

Alexander, D. R., and J. W. Ferguson. 1994. "Low-Temperature Rosseland Opacities." *The Astrophysical Journal* 437 (December): 879. https://doi.org/10.1086/175039.

Anbar, Ariel D., Yun Duan, Timothy W. Lyons, Gail L. Arnold, Brian Kendall, Robert A. Creaser, Alan J. Kaufman, et al. 2007. "A Whiff of Oxygen Before the Great Oxidation Event?" *Science* 317, no. 5846 (September): 1903. https://doi.org/10.1126/science.1140325.

Angulo, C., M. Arnould, M. Rayet, P. Descouvemont, D. Baye, C. Leclercq-Willain, A. Coc, et al. 1999. "A compilation of charged-particle induced thermonuclear reaction rates." *Nuclear Physics A* 656, no. 1 (August): 3–183. https://doi.org/10.1016/S0375-9474(99)00030-5.

Apai, Dániel, Benjamin V. Rackham, Mark S. Giampapa, Daniel Angerhausen, Johanna Teske, Joanna Barstow, Ludmila Carone, et al. 2018. "Understanding Stellar Contamination in Exoplanet Transmission Spectra as an Essential Step in Small Planet Characterization." *arXiv e-prints* (March): arXiv:1803.08708. https://doi.org/10.48550/arXiv.1803.08708. arXiv: 1803.08708 [astro-ph.EP].

Arnett, David, Casey Meakin, and Patrick A. Young. 2009. "Turbulent Convection in Stellar Interiors. II. The Velocity Field." *The Astrophysical Journal* 690, no. 2 (January): 1715–1729. https://doi.org/10.1088/0004-637X/690/2/1715. arXiv: 0809.1625 [astro-ph].

———. 2010. "Convection Theory and Sub-Photospheric Stratification." *The Astrophysical Journal* 710, no. 2 (February): 1619–1626. https://doi.org/10.1088/0004-637X/710/2/1619. arXiv: 0910.0821 [astro-ph.SR].

Arnett, W. David, and Casey Meakin. 2011. "Toward Realistic Progenitors of Core-collapse Supernovae." *The Astrophysical Journal* 733, no. 2 (June): 78. https://doi.org/10.1088/0004-637X/733/2/78. arXiv: 1101.5646 [astro-ph.SR].

Asplund, M., A. M. Amarsi, and N. Grevesse. 2021. "The chemical make-up of the Sun: A 2020 vision." *Astronomy & Astrophysics* 653 (September): A141. https://doi.org/10.1051/0004-6361/202140445. arXiv: 2105.01661 [astro-ph.SR].

Asplund, Martin, Nicolas Grevesse, A. Jacques Sauval, and Pat Scott. 2009. "The Chemical Composition of the Sun." *Annual Review of Astronomy and Astrophysics* 47, no. 1 (September): 481–522. https://doi.org/10.1146/annurev.astro.46.060407.145222. arXiv: 0909.0948 [astro-ph.SR].

Bains, William, Yao Xiao, and Changyong Yu. 2015. "Prediction of the Maximum Temperature for Life Based on the Stability of Metabolites to Decomposition in Water." *Life* 5, no. 2 (March): 1054–1100. https://doi.org/10.3390/life5021054.

Barclay, Thomas, Joshua Pepper, and Elisa V. Quintana. 2018. "A Revised Exoplanet Yield from the Transiting Exoplanet Survey Satellite (TESS)." *The Astrophysical Journal Supplement* 239, no. 1 (November): 2. https://doi.org/10.3847/1538-4365/aae3e9. arXiv: 1804.05050 [astro-ph.EP].

Barnes, Rory. 2017. "Tidal locking of habitable exoplanets." *Celestial Mechanics and Dynamical Astronomy* 129, no. 4 (December): 509–536. https://doi.org/10.1007/s10569-017-9783-7. arXiv: 1708.02981 [astro-ph.EP].

Barnes, Sydney A. 2007. "Ages for Illustrative Field Stars Using Gyrochronology: Viability, Limitations, and Errors." *The Astrophysical Journal* 669, no. 2 (November): 1167–1189. https://doi.org/10.1086/519295. arXiv: 0704.3068 [astro-ph].

Barnes, Sydney A., and Yong-Cheol Kim. 2010. "Angular Momentum Loss from Cool Stars: An Empirical Expression and Connection to Stellar Activity." *The Astrophysical Journal* 721, no. 1 (September): 675–685. https://doi.org/10.1088/0004-637X/721/1/675. arXiv: 1104.2350 [astro-ph.SR].

Batalha, Natalie M., William J. Borucki, Stephen T. Bryson, Lars A. Buchhave, Douglas A. Caldwell, Jørgen Christensen-Dalsgaard, David Ciardi, et al. 2011. "Kepler's First Rocky Planet: Kepler-10b." *The Astrophysical Journal* 729, no. 1 (March): 27. https://doi.org/10.1088/0004-637X/729/1/27. arXiv: 1102.0605 [astro-ph.EP].

Bean, Jacob L., Dorian S. Abbot, and Eliza M. -R. Kempton. 2017. "A Statistical Comparative Planetology Approach to the Hunt for Habitable Exoplanets and Life Beyond the Solar System." *The Astrophysical Journal Letters* 841, no. 2 (June): L24. https://doi.org/10.3847/2041-8213/aa738a. arXiv: 1705.06288 [astro-ph.EP].

Berger, Travis A., Daniel Huber, Eric Gaidos, and Jennifer L. van Saders. 2018. "Revised Radii of Kepler Stars and Planets Using Gaia Data Release 2." *The Astrophysical Journal* 866, no. 2 (October): 99. https://doi.org/10.3847/1538-4357/aada83. arXiv: 1805.00231 [astro-ph.EP].

Berger, Travis A., Daniel Huber, Jennifer L. van Saders, Eric Gaidos, Jamie Tayar, and Adam L. Kraus. 2020. "The Gaia-Kepler Stellar Properties Catalog. I. Homogeneous Fundamental Properties for 186,301 Kepler Stars." *The Astronomical Journal* 159, no. 6 (June): 280. https://doi.org/10.3847/1538-3881/159/6/280. arXiv: 2001.07737 [astro-ph.SR].

Bonanno, A., H. Schlattl, and L. Paternò. 2002. "The age of the Sun and the relativistic corrections in the EOS." *Astronomy & Astrophysics* 390 (August): 1115–1118. https://doi.org/10.1051/0004-6361:20020749. arXiv: astro-ph/0204331 [astro-ph].

Bonfanti, A., S. Ortolani, and V. Nascimbeni. 2016. "Age consistency between exoplanet hosts and field stars." *Astronomy & Astrophysics* 585 (January): A5. https://doi.org/10.1051/0004-6361/201527297. arXiv: 1511.01744 [astro-ph.SR].

Bonomo, A. S., X. Dumusque, A. Massa, A. Mortier, R. Bongiolatti, L. Malavolta, A. Sozzetti, et al. 2023. "Cold Jupiters and improved masses in 38 Kepler and K2 small planet systems from 3661 HARPS-N radial velocities. No excess of cold Jupiters in small planet systems." *Astronomy & Astrophysics* 677 (September): A33. https://doi.org/10.1051/0004-6361/202346211. arXiv: 2304.05773 [astro-ph.EP].

Borucki, William J., Eric Agol, Francois Fressin, Lisa Kaltenegger, Jason Rowe, Howard Isaacson, Debra Fischer, et al. 2013. "Kepler-62: A Five-Planet System with Planets of 1.4 and 1.6 Earth Radii in the Habitable Zone." *Science* 340, no. 6132 (May): 587–590. https://doi.org/10.1126/science.1234702. arXiv: 1304.7387 [astro-ph.EP].

Borucki, William J., David Koch, Gibor Basri, Natalie Batalha, Timothy Brown, Douglas Caldwell, John Caldwell, et al. 2010. "Kepler Planet-Detection Mission: Introduction and First Results." *Science* 327, no. 5968 (February): 977. https://doi.org/10.1126/science.1185402.

Boyajian, Tabetha S., Kaspar von Braun, Gerard van Belle, Harold A. McAlister, Theo A. ten Brummelaar, Stephen R. Kane, Philip S. Muirhead, et al. 2012. "Stellar Diameters and Temperatures. II. Main-sequence K- and M-stars." *The Astrophysical Journal* 757, no. 2 (October): 112. https://doi.org/10.1088/0004-637X/757/2/112. arXiv: 1208.2431 [astro-ph.SR].

Brocks, Jochen J., Graham A. Logan, Roger Buick, and Roger E. Summons. 1999. "Archean Molecular Fossils and the Early Rise of Eukaryotes." *Science* 285 (5430): 1033–1036. https://doi.org/10.1126/science.285.5430.1033. eprint: https://science.sciencemag.org/content/285/5430/1033.full.pdf.

Bryson, S., J. Coughlin, N. M. Batalha, T. Berger, D. Huber, C. Burke, J. Dotson, and S. E. Mullally. 2020. "A Probabilistic Approach to Kepler Completeness and Reliability for Exoplanet Occurrence Rates." *The Astronomical Journal* 159, no. 6 (June): 279. https://doi.org/10.3847/1538-3881/ab8a30. arXiv: 1906.03575 [astro-ph.EP].

Bryson, Steve, Michelle Kunimoto, Ravi K. Kopparapu, Jeffrey L. Coughlin, William J. Borucki, David Koch, Victor Silva Aguirre, et al. 2021. "The Occurrence of Rocky Habitable-zone Planets around Solar-like Stars from Kepler Data." *The Astronomical Journal* 161, no. 1 (January): 36. https://doi.org/10.3847/1538-3881/abc418. arXiv: 2010.14812 [astro-ph.EP].

Burke, Christopher J., F. Mullally, Susan E. Thompson, Jeffrey L. Coughlin, and Jason F. Rowe. 2019. "Re-evaluating Small Long-period Confirmed Planets from Kepler." *The Astronomical Journal* 157, no. 4 (April): 143. https://doi.org/10.3847/1538-3881/aafb79. arXiv: 1901.00506 [astro-ph.EP].

Burt, Jennifer, Fabo Feng, Bradford Holden, Eric E. Mamajek, Chelsea X. Huang, Mickey M. Rosenthal, Songhu Wang, et al. 2021. "A Collage of Small Planets from the Lick-Carnegie Exoplanet Survey: Exploring the Super-Earth and Sub-Neptune Mass Regime." *The Astronomical Journal* 161, no. 1 (January): 10. https://doi.org/10.3847/1538-3881/abc2d0. arXiv: 2011.08867 [astro-ph.EP].

Cadieux, Charles, René Doyon, Ryan J. MacDonald, Martin Turbet, Étienne Artigau, Olivia Lim, Michael Radica, et al. 2024. "Transmission Spectroscopy of the Habitable Zone Exoplanet LHS 1140 b with JWST/NIRISS." *The Astrophysical Journal Letters* 970, no. 1 (July): L2. https://doi.org/10.3847/2041-8213/ad5afa. arXiv: 2406.15136 [astro-ph.EP].

Chabrier, Gilles. 2003. "Galactic Stellar and Substellar Initial Mass Function." *Publications of the Astronomical Society of the Pacific* 115, no. 809 (July): 763–795. https://doi.org/10.1086/376392. arXiv: astro-ph/0304382 [astro-ph].

Chen, Howard, Eric T. Wolf, Zhuchang Zhan, and Daniel E. Horton. 2019. "Habitability and Spectroscopic Observability of Warm M-dwarf Exoplanets Evaluated with a 3D Chemistry-Climate Model." *The Astrophysical Journal* 886, no. 1 (November): 16. https://doi.org/10.3847/1538-4357/ab4f7e. arXiv: 1907.10048 [astro-ph.EP].

Christie, Duncan A., Elspeth K. H. Lee, Hamish Innes, Pascal A. Noti, Benjamin Charnay, Thomas J. Fauchez, Nathan J. Mayne, et al. 2022. "CAMEMBERT: A Mini-Neptunes General Circulation Model Intercomparison, Protocol Version 1.0.A CUISINES Model Intercomparison Project." *The Planetary Science Journal*

3, no. 11 (November): 261. https://doi.org/10.3847/PSJ/ac9dfe. arXiv: 2211.04048 [astro-ph.EP].

Claytor, Zachary R., Jennifer L. van Saders, Ângela R. G. Santos, Rafael A. García, Savita Mathur, Jamie Tayar, Marc H. Pinsonneault, and Matthew Shetrone. 2020. "Chemical Evolution in the Milky Way: Rotation-based Ages for APOGEE-Kepler Cool Dwarf Stars." *The Astrophysical Journal* 888, no. 1 (January): 43. https://doi.org/10.3847/1538-4357/ab5c24. arXiv: 1911.04518 [astro-ph.SR].

Cloutier, Ryan. 2024. "Exoplanet Demographics: Physical and Orbital Properties." *arXiv e-prints* (September): arXiv:2409.13062. https://doi.org/10.48550/arXiv.2409.13062. arXiv: 2409.13062 [astro-ph.EP].

Cloutier, Ryan, and Kristen Menou. 2020. "Evolution of the Radius Valley around Low-mass Stars from Kepler and K2." *The Astronomical Journal* 159, no. 5 (May): 211. https://doi.org/10.3847/1538-3881/ab8237. arXiv: 1912.02170 [astro-ph.EP].

Colgan, J., D. P. Kilcrease, N. H. Magee, M. E. Sherrill, Jr. Abdallah J., P. Hakel, C. J. Fontes, J. A. Guzik, and K. A. Mussack. 2016. "A New Generation of Los Alamos Opacity Tables." *The Astrophysical Journal* 817, no. 2 (February): 116. https://doi.org/10.3847/0004-637X/817/2/116. arXiv: 1601.01005 [astro-ph.SR].

Crowe, Sean A., Lasse N. Døssing, Nicolas J. Beukes, Michael Bau, Stephanus J. Kruger, Robert Frei, and Donald E. Canfield. 2013. "Atmospheric oxygenation three billion years ago." *Nature* 501, no. 7468 (September): 535–538. https://doi.org/10.1038/nature12426.

Cutri, R. M., M. F. Skrutskie, S. van Dyk, C. A. Beichman, J. M. Carpenter, T. Chester, L. Cambresy, et al. 2003. "VizieR Online Data Catalog: 2MASS All-Sky Catalog of Point Sources (Cutri+ 2003)." *VizieR Online Data Catalog* (June): II/246.

Cyburt, Richard H., A. Matthew Amthor, Ryan Ferguson, Zach Meisel, Karl Smith, Scott Warren, Alexander Heger, et al. 2010. "The JINA REACLIB Database: Its Recent Updates and Impact on Type-I X-ray Bursts." *The Astrophysical Journal Supplement* 189, no. 1 (July): 240–252. https://doi.org/10.1088/0067-0049/189/1/240.

Damiano, Mario, Aaron Bello-Arufe, Jeehyun Yang, and Renyu Hu. 2024. "LHS 1140 b Is a Potentially Habitable Water World." *The Astrophysical Journal Letters* 968,

no. 2 (June): L22. https://doi.org/10.3847/2041-8213/ad5204. arXiv: 2403.13265 [astro-ph.EP].

Del Genio, Anthony D., Michael J. Way, David S. Amundsen, Igor Aleinov, Maxwell Kelley, Nancy Y. Kiang, and Thomas L. Clune. 2019. "Habitable Climate Scenarios for Proxima Centauri b with a Dynamic Ocean." *Astrobiology* 19, no. 1 (January): 99–125. https://doi.org/10.1089/ast.2017.1760.

Demory, B. -O., D. Ségransan, T. Forveille, D. Queloz, J. -L. Beuzit, X. Delfosse, E. di Folco, et al. 2009. "Mass-radius relation of low and very low-mass stars revisited with the VLTI." *Astronomy & Astrophysics* 505, no. 1 (October): 205–215. https://doi.org/10.1051/0004-6361/200911976. arXiv: 0906.0602 [astro-ph.SR].

Díaz, R. F., D. Ségransan, S. Udry, C. Lovis, F. Pepe, X. Dumusque, M. Marmier, et al. 2016. "The HARPS search for southern extra-solar planets. XXXVIII. Bayesian re-analysis of three systems. New super-Earths, unconfirmed signals, and magnetic cycles." *Astronomy & Astrophysics* 585 (January): A134. https://doi.org/10.1051/0004-6361/201526729. arXiv: 1510.06446 [astro-ph.EP].

Dittmann, Jason A., Jonathan M. Irwin, David Charbonneau, Xavier Bonfils, Nicola Astudillo-Defru, Raphaëlle D. Haywood, Zachory K. Berta-Thompson, et al. 2017. "A temperate rocky super-Earth transiting a nearby cool star." *Nature* 544, no. 7650 (April): 333–336. https://doi.org/10.1038/nature22055. arXiv: 1704.05556 [astro-ph.EP].

Dong, Chuanfei, Meng Jin, Manasvi Lingam, Vladimir S. Airapetian, Yingjuan Ma, and Bart van der Holst. 2018. "Atmospheric escape from the TRAPPIST-1 planets and implications for habitability." *Proceedings of the National Academy of Science* 115, no. 2 (January): 260–265. https://doi.org/10.1073/pnas.1708010115. arXiv: 1705.05535 [astro-ph.EP].

Dotter, Aaron. 2016. "MESA Isochrones and Stellar Tracks (MIST) 0: Methods for the Construction of Stellar Isochrones." *The Astrophysical Journal Supplement* 222, no. 1 (January): 8. https://doi.org/10.3847/0067-0049/222/1/8. arXiv: 1601.05144 [astro-ph.SR].

Dressing, Courtney D., and David Charbonneau. 2015. "The Occurrence of Potentially Habitable Planets Orbiting M Dwarfs Estimated from the Full Kepler Dataset and an Empirical Measurement of the Detection Sensitivity." *The Astrophysical Journal* 807, no. 1 (July): 45. https://doi.org/10.1088/0004-637X/807/1/45. arXiv: 1501.01623 [astro-ph.EP].

Eyring, Veronika, Sandrine Bony, Gerald A. Meehl, Catherine A. Senior, Bjorn Stevens, Ronald J. Stouffer, and Karl E. Taylor. 2016. "Overview of the Coupled Model Intercomparison Project Phase 6 (CMIP6) experimental design and organization." *Geoscientific Model Development* 9, no. 5 (May): 1937–1958. https://doi.org/10.5194/gmd-9-1937-2016.

Fauchez, Thomas J., Martin Turbet, Denis E. Sergeev, Nathan J. Mayne, Aymeric Spiga, Linda Sohl, Prabal Saxena, et al. 2021. "TRAPPIST Habitable Atmosphere Intercomparison (THAI) Workshop Report." *The Planetary Science Journal* 2, no. 3 (June): 106. https://doi.org/10.3847/PSJ/abf4df. arXiv: 2104.01091 [astro-ph.EP].

Ferguson, Jason W., David R. Alexander, France Allard, Travis Barman, Julia G. Bodnarik, Peter H. Hauschildt, Amanda Heffner-Wong, and Akemi Tamanai. 2005. "Low-Temperature Opacities." *The Astrophysical Journal* 623, no. 1 (April): 585–596. https://doi.org/10.1086/428642. arXiv: astro-ph/0502045 [astro-ph].

Foreman-Mackey, Daniel, Will Farr, Manodeep Sinha, Anne Archibald, David Hogg, Jeremy Sanders, Joe Zuntz, et al. 2019. "emcee v3: A Python ensemble sampling toolkit for affine-invariant MCMC." *The Journal of Open Source Software* 4, no. 43 (November): 1864. https://doi.org/10.21105/joss.01864. arXiv: 1911.07688 [astro-ph.IM].

Foreman-Mackey, Daniel, David W. Hogg, Dustin Lang, and Jonathan Goodman. 2013. "emcee: The MCMC Hammer." *Publications of the Astronomical Society of the Pacific* 125, no. 925 (March): 306. https://doi.org/10.1086/670067. arXiv: 1202.3665 [astro-ph.IM].

Fujii, Yuka, Daniel Angerhausen, Russell Deitrick, Shawn Domagal-Goldman, John Lee Grenfell, Yasunori Hori, Stephen R. Kane, et al. 2018. "Exoplanet Biosignatures: Observational Prospects." *Astrobiology* 18, no. 6 (June): 739–778. https://doi.org/10.1089/ast.2017.1733. arXiv: 1705.07098 [astro-ph.EP].

Fulton, Benjamin J., Erik A. Petigura, Andrew W. Howard, Howard Isaacson, Geoffrey W. Marcy, Phillip A. Cargile, Leslie Hebb, et al. 2017. "The California-Kepler Survey. III. A Gap in the Radius Distribution of Small Planets." *The Astronomical Journal* 154, no. 3 (September): 109. https://doi.org/10.3847/1538-3881/aa80eb. arXiv: 1703.10375 [astro-ph.EP].

Furlan, E., D. R. Ciardi, W. D. Cochran, M. E. Everett, D. W. Latham, G. W. Marcy, L. A. Buchhave, et al. 2018. "The Kepler Follow-up Observation Program. II. Stellar Parameters from Medium- and High-resolution Spectroscopy." *The*

Astrophysical Journal 861, no. 2 (July): 149. https://doi.org/10.3847/1538-4357/aaca34. arXiv: 1805.12089 [astro-ph.SR].

Gaidos, E., A. W. Mann, A. L. Kraus, and M. Ireland. 2016. "They are small worlds after all: revised properties of Kepler M dwarf stars and their planets." *Monthly Notices of the Royal Astronomical Society* 457, no. 3 (April): 2877–2899. https://doi.org/10.1093/mnras/stw097. arXiv: 1512.04437 [astro-ph.EP].

Gajdoš, Pavol, Martin Vaňko, and Štefan Parimucha. 2019. "Transit timing variations and linear ephemerides of confirmed Kepler transiting exoplanets." *Research in Astronomy and Astrophysics* 19, no. 3 (March): 041. https://doi.org/10.1088/1674-4527/19/3/41. arXiv: 1809.11104 [astro-ph.EP].

Gallet, F., C. Charbonnel, L. Amard, S. Brun, A. Palacios, and S. Mathis. 2017. "Impacts of stellar evolution and dynamics on the habitable zone: The role of rotation and magnetic activity." *Astronomy & Astrophysics* 597 (January): A14. https://doi.org/10.1051/0004-6361/201629034. arXiv: 1608.06772 [astro-ph.EP].

Gaudi, B. Scott, Sara Seager, Bertrand Mennesson, Alina Kiessling, Keith Warfield, Kerri Cahoy, John T. Clarke, et al. 2020. "The Habitable Exoplanet Observatory (HabEx) Mission Concept Study Final Report." *arXiv e-prints* (January): arXiv:2001.06683. arXiv: 2001.06683 [astro-ph.IM].

Gilbert, Emily A., Andrew Vanderburg, Joseph E. Rodriguez, Benjamin J. Hord, Matthew S. Clement, Thomas Barclay, Elisa V. Quintana, et al. 2023. "A Second Earth-sized Planet in the Habitable Zone of the M Dwarf, TOI-700." *The Astrophysical Journal Letters* 944, no. 2 (February): L35. https://doi.org/10.3847/2041-8213/acb599. arXiv: 2301.03617 [astro-ph.EP].

Gillon, Michaël, Amaury H. M. J. Triaud, Brice-Olivier Demory, Emmanuël Jehin, Eric Agol, Katherine M. Deck, Susan M. Lederer, et al. 2017. "Seven temperate terrestrial planets around the nearby ultracool dwarf star TRAPPIST-1." *Nature* 542, no. 7642 (February): 456–460. https://doi.org/10.1038/nature21360. arXiv: 1703.01424 [astro-ph.EP].

Graboske, H. C., H. E. Dewitt, A. S. Grossman, and M. S. Cooper. 1973. "Screening Factors for Nuclear Reactions. II. Intermediate Screen-Ing and Astrophysical Applications." *The Astrophysical Journal* 181 (April): 457–474. https://doi.org/10.1086/152062.

Greene, Thomas P., Michael R. Line, Cezar Montero, Jonathan J. Fortney, Jacob Lustig-Yaeger, and Kyle Luther. 2016. "Characterizing Transiting Exoplanet

Atmospheres with JWST." *The Astrophysical Journal* 817, no. 1 (January): 17. https://doi.org/10.3847/0004-637X/817/1/17. arXiv: 1511.05528 [astro-ph.EP].

Güdel, M., R. Dvorak, N. Erkaev, J. Kasting, M. Khodachenko, H. Lammer, E. Pilat-Lohinger, H. Rauer, I. Ribas, and B. E. Wood. 2014. "Astrophysical Conditions for Planetary Habitability." In *Protostars and Planets VI,* edited by Henrik Beuther, Ralf S. Klessen, Cornelis P. Dullemond, and Thomas Henning, 883–906. January. https://doi.org/10.2458/azu_uapress_9780816531240-ch038. arXiv: 1407.8174 [astro-ph.EP].

Gupta, Akash, and Hilke E. Schlichting. 2019. "Sculpting the valley in the radius distribution of small exoplanets as a by-product of planet formation: the core-powered mass-loss mechanism." *Monthly Notices of the Royal Astronomical Society* 487, no. 1 (July): 24–33. https://doi.org/10.1093/mnras/stz1230. arXiv: 1811.03202 [astro-ph.EP].

Haqq-Misra, Jacob, Eric T. Wolf, Thomas J. Fauchez, Aomawa L. Shields, and Ravi K. Kopparapu. 2022. "The Sparse Atmospheric Model Sampling Analysis (SAMOSA) Intercomparison: Motivations and Protocol Version 1.0: A CUISINES Model Intercomparison Project." *The Planetary Science Journal* 3, no. 11 (November): 260. https://doi.org/10.3847/PSJ/ac9479. arXiv: 2209.10480 [astro-ph.EP].

Haqq-Misra, Jacob D., Shawn D. Domagal-Goldman, Patrick J. Kasting, and James F. Kasting. 2008. "A Revised, Hazy Methane Greenhouse for the Archean Earth." *Astrobiology* 8, no. 6 (December): 1127–1137. https://doi.org/10.1089/ast.2007.0197.

Harada, Caleb K., Courtney D. Dressing, Stephen R. Kane, and Bahareh Adami Ardestani. 2024. "Setting the Stage for the Search for Life with the Habitable Worlds Observatory: Properties of 164 Promising Planet-survey Targets." *The Astrophysical Journal Supplement* 272, no. 2 (June): 30. https://doi.org/10.3847/1538-4365/ad3e81. arXiv: 2401.03047 [astro-ph.EP].

Hawker, George A., and Ian R. Parry. 2019. "High-resolution spectroscopy and high contrast imaging with the ELT: looking for O_2 in Proxima b." *Monthly Notices of the Royal Astronomical Society* 484, no. 4 (April): 4855–4864. https://doi.org/10.1093/mnras/stz323. arXiv: 1901.10833 [astro-ph.EP].

Hayden, Michael R., Jo Bovy, Jon A. Holtzman, David L. Nidever, Jonathan C. Bird, David H. Weinberg, Brett H. Andrews, et al. 2015. "Chemical Cartography with APOGEE: Metallicity Distribution Functions and the Chemical Structure of the Milky Way Disk." *The Astrophysical Journal* 808, no. 2 (August): 132. https://doi.org/10.1088/0004-637X/808/2/132. arXiv: 1503.02110 [astro-ph.GA].

Hill, Michelle L., Kimberly Bott, Paul A. Dalba, Tara Fetherolf, Stephen R. Kane, Ravi Kopparapu, Zhexing Li, and Colby Ostberg. 2023. "A Catalog of Habitable Zone Exoplanets." *The Astronomical Journal* 165, no. 2 (February): 34. https://doi.org/10.3847/1538-3881/aca1c0.

Hinkel, Natalie R., F. X. Timmes, Patrick A. Young, Michael D. Pagano, and Margaret C. Turnbull. 2014. "Stellar Abundances in the Solar Neighborhood: The Hypatia Catalog." *The Astronomical Journal* 148, no. 3 (September): 54. https://doi.org/10.1088/0004-6256/148/3/54. arXiv: 1405.6719 [astro-ph.SR].

Hinkel, Natalie R., Patrick A. Young, Michael D. Pagano, Steven J. Desch, Ariel D. Anbar, Vardan Adibekyan, Sergi Blanco-Cuaresma, et al. 2016. "A Comparison of Stellar Elemental Abundance Techniques and Measurements." *The Astrophysical Journal Supplement* 226, no. 1 (September): 4. https://doi.org/10.3847/0067-0049/226/1/4. arXiv: 1607.03130 [astro-ph.SR].

Holland, Heinrich D. 2006. "The oxygenation of the atmosphere and oceans." *Philosophical Transactions of the Royal Society B: Biological Sciences* 361 (1470): 903–915. https://doi.org/10.1098/rstb.2006.1838. eprint: https://royalsocietypublishing.org/doi/pdf/10.1098/rstb.2006.1838.

Huber, Daniel, Timothy R. White, Travis S. Metcalfe, Ashley Chontos, Michael M. Fausnaugh, Cynthia S. K. Ho, Vincent Van Eylen, et al. 2022. "A 20 Second Cadence View of Solar-type Stars and Their Planets with TESS: Asteroseismology of Solar Analogs and a Recharacterization of π Men c." *The Astrophysical Journal* 163, no. 2 (February): 79. https://doi.org/10.3847/1538-3881/ac3000. arXiv: 2108.09109 [astro-ph.SR].

Iglesias, Carlos A., and Forrest J. Rogers. 1996. "Updated Opal Opacities." *The Astrophysical Journal* 464 (June): 943. https://doi.org/10.1086/177381.

Iliadis, Christian, John M. D'Auria, Sumner Starrfield, William J. Thompson, and Michael Wiescher. 2001. "Proton-induced Thermonuclear Reaction Rates for A=20-40 Nuclei." *The Astrophysical Journal Supplement* 134, no. 1 (May): 151–171. https://doi.org/10.1086/320364.

Jansen, Tiffany, Caleb Scharf, Michael Way, and Anthony Del Genio. 2019. "Climates of Warm Earth-like Planets. II. Rotational "Goldilocks" Zones for Fractional Habitability and Silicate Weathering." *The Astrophysical Journal* 875, no. 2 (April): 79. https://doi.org/10.3847/1538-4357/ab113d. arXiv: 1810.05139 [astro-ph.EP].

Jenkins, Jon M., Joseph D. Twicken, Natalie M. Batalha, Douglas A. Caldwell, William D. Cochran, Michael Endl, David W. Latham, et al. 2015. "Discovery and Validation of Kepler-452b: A 1.6 $R_\oplus$ Super Earth Exoplanet in the Habitable Zone of a G2 Star." *The Astronomical Journal* 150, no. 2 (August): 56. https://doi.org/10.1088/0004-6256/150/2/56. arXiv: 1507.06723 [astro-ph.EP].

Johnson, John Asher, Erik A. Petigura, Benjamin J. Fulton, Geoffrey W. Marcy, Andrew W. Howard, Howard Isaacson, Leslie Hebb, et al. 2017. "The California-Kepler Survey. II. Precise Physical Properties of 2025 Kepler Planets and Their Host Stars." *The Astronomical Journal* 154, no. 3 (September): 108. https://doi.org/10.3847/1538-3881/aa80e7. arXiv: 1703.10402 [astro-ph.EP].

Kaltenegger, Lisa, and Wesley A. Traub. 2009. "Transits of Earth-like Planets." *The Astrophysical Journal* 698, no. 1 (June): 519–527. https://doi.org/10.1088/0004-637X/698/1/519. arXiv: 0903.3371 [astro-ph.IM].

Karovicova, I., T. R. White, T. Nordlander, L. Casagrande, M. Ireland, D. Huber, and P. Jofré. 2020. "Fundamental stellar parameters of benchmark stars from CHARA interferometry. I. Metal-poor stars." *Astronomy & Astrophysics* 640 (August): A25. https://doi.org/10.1051/0004-6361/202037590. arXiv: 2006.05411 [astro-ph.SR].

Kasting, James F., and David Catling. 2003. "Evolution of a Habitable Planet." *Annual Review of Astronomy and Astrophysics* 41 (January): 429–463. https://doi.org/10.1146/annurev.astro.41.071601.170049.

Kasting, James F., Daniel P. Whitmire, and Ray T. Reynolds. 1993. "Habitable Zones around Main Sequence Stars." *Icarus* 101, no. 1 (January): 108–128. https://doi.org/10.1006/icar.1993.1010.

Kodama, T., H. Genda, J. Leconte, and A. Abe-Ouchi. 2021. "The Onset of a Globally Ice-Covered State for a Land Planet." *Journal of Geophysical Research (Planets)* 126, no. 12 (December): e06975. https://doi.org/10.1029/2021JE006975.

Kodama, T., H. Genda, R. O'ishi, A. Abe-Ouchi, and Y. Abe. 2019. "Inner Edge of Habitable Zones for Earth-Sized Planets With Various Surface Water Distributions." *Journal of Geophysical Research (Planets)* 124, no. 8 (August): 2306–2324. https://doi.org/10.1029/2019JE006037. arXiv: 1908.05909 [astro-ph.EP].

Kodama, T., A. Nitta, H. Genda, Y. Takao, R. O'ishi, A. Abe-Ouchi, and Y. Abe. 2018. "Dependence of the Onset of the Runaway Greenhouse Effect on the Latitudinal Surface Water Distribution of Earth-Like Planets." *Journal of Geophysical*

Research (Planets) 123, no. 2 (February): 559–574. https://doi.org/10.1002/2017JE005383. arXiv: 1801.07202 [astro-ph.EP].

Kopp, Robert E., Joseph L. Kirschvink, Isaac A. Hilburn, and Cody Z. Nash. 2005. "The Paleoproterozoic snowball Earth: A climate disaster triggered by the evolution of oxygenic photosynthesis." *Proceedings of the National Academy of Science* 102, no. 32 (August): 11131–11136. https://doi.org/10.1073/pnas.0504878102.

Kopparapu, Ravi Kumar, Eric Hébrard, Rus Belikov, Natalie M. Batalha, Gijs D. Mulders, Chris Stark, Dillon Teal, Shawn Domagal-Goldman, and Avi Mandell. 2018. "Exoplanet Classification and Yield Estimates for Direct Imaging Missions." *The Astrophysical Journal* 856, no. 2 (April): 122. https://doi.org/10.3847/1538-4357/aab205. arXiv: 1802.09602 [astro-ph.EP].

Kopparapu, Ravi Kumar, Ramses Ramirez, James F. Kasting, Vincent Eymet, Tyler D. Robinson, Suvrath Mahadevan, Ryan C. Terrien, Shawn Domagal-Goldman, Victoria Meadows, and Rohit Deshpande. 2013. "Habitable Zones around Main-sequence Stars: New Estimates." *The Astrophysical Journal* 765, no. 2 (March): 131. https://doi.org/10.1088/0004-637X/765/2/131. arXiv: 1301.6674 [astro-ph.EP].

Kopparapu, Ravi Kumar, Ramses M. Ramirez, James SchottelKotte, James F. Kasting, Shawn Domagal-Goldman, and Vincent Eymet. 2014. "Habitable Zones around Main-sequence Stars: Dependence on Planetary Mass." *The Astrophysical Journal Letters* 787, no. 2 (June): L29. https://doi.org/10.1088/2041-8205/787/2/L29. arXiv: 1404.5292 [astro-ph.EP].

Kopparapu, Ravi kumar, Eric T. Wolf, Giada Arney, Natasha E. Batalha, Jacob Haqq-Misra, Simon L. Grimm, and Kevin Heng. 2017. "Habitable Moist Atmospheres on Terrestrial Planets near the Inner Edge of the Habitable Zone around M Dwarfs." *The Astrophysical Journal* 845, no. 1 (August): 5. https://doi.org/10.3847/1538-4357/aa7cf9. arXiv: 1705.10362 [astro-ph.EP].

Kopparapu, Ravi kumar, Eric T. Wolf, Jacob Haqq-Misra, Jun Yang, James F. Kasting, Victoria Meadows, Ryan Terrien, and Suvrath Mahadevan. 2016. "The Inner Edge of the Habitable Zone for Synchronously Rotating Planets around Low-mass Stars Using General Circulation Models." *The Astrophysical Journal* 819, no. 1 (March): 84. https://doi.org/10.3847/0004-637X/819/1/84. arXiv: 1602.05176 [astro-ph.EP].

Krissansen-Totton, Joshua, Stephanie Olson, and David C. Catling. 2018. "Disequilibrium biosignatures over Earth history and implications for detecting exoplanet

life." *Science Advances* 4, no. 1 (January): eaao5747. https://doi.org/10.1126/sciadv.aao5747. arXiv: 1801.08211 [astro-ph.EP].

Kunimoto, Michelle, Jaymie M. Matthews, and Henry Ngo. 2020. "Searching the Entirety of Kepler Data. I. 17 New Planet Candidates Including One Habitable Zone World." *The Astronomical Journal* 159, no. 3 (March): 124. https://doi.org/10.3847/1538-3881/ab6cf8. arXiv: 2003.04397 [astro-ph.EP].

Laliotis, Katherine, Jennifer A. Burt, Eric E. Mamajek, Zhexing Li, Volker Perdelwitz, Jinglin Zhao, R. Paul Butler, et al. 2023. "Doppler Constraints on Planetary Companions to Nearby Sun-like Stars: An Archival Radial Velocity Survey of Southern Targets for Proposed NASA Direct Imaging Missions." *The Astronomical Journal* 165, no. 4 (April): 176. https://doi.org/10.3847/1538-3881/acc067. arXiv: 2302.10310 [astro-ph.EP].

Lammer, H., J. H. Bredehöft, A. Coustenis, M. L. Khodachenko, L. Kaltenegger, O. Grasset, D. Prieur, et al. 2009. "What makes a planet habitable?" *The Astronomy and Astrophysics Review* 17, no. 2 (June): 181–249. https://doi.org/10.1007/s00159-009-0019-z.

Langanke, K., and G. Martínez-Pinedo. 2000. "Shell-model calculations of stellar weak interaction rates: II. Weak rates for nuclei in the mass range /A=45-65 in supernovae environments." *Nuclear Physics A* 673, nos. 1-4 (June): 481–508. https://doi.org/10.1016/S0375-9474(00)00131-7. arXiv: nucl-th/0001018 [nucl-th].

Lastennet, E., and D. Valls-Gabaud. 2002. "Detached double-lined eclipsing binaries as critical tests of stellar evolution. Age and metallicity determinations from the HR diagram." *Astronomy & Astrophysics* 396 (December): 551–580. https://doi.org/10.1051/0004-6361:20021312. arXiv: astro-ph/0211501 [astro-ph].

Leconte, J., F. Forget, B. Charnay, R. Wordsworth, F. Selsis, E. Millour, and A. Spiga. 2013. "3D climate modeling of close-in land planets: Circulation patterns, climate moist bistability, and habitability." *Astronomy & Astrophysics* 554 (June): A69. https://doi.org/10.1051/0004-6361/201321042. arXiv: 1303.7079 [astro-ph.EP].

Leconte, Jérémy, Francois Forget, Benjamin Charnay, Robin Wordsworth, and Alizée Pottier. 2013. "Increased insolation threshold for runaway greenhouse processes on Earth-like planets." *Nature* 504, no. 7479 (December): 268–271. https://doi.org/10.1038/nature12827. arXiv: 1312.3337 [astro-ph.EP].

Lorenzo-Oliveira, Diego, Fabrício C. Freitas, Jorge Meléndez, Megan Bedell, Iván Ramírez, Jacob L. Bean, Martin Asplund, et al. 2018. "The Solar Twin Planet

Search. The age-chromospheric activity relation." *Astronomy & Astrophysics* 619 (November): A73. https://doi.org/10.1051/0004-6361/201629294. arXiv: 1806.08014 [astro-ph.SR].

Loyd, R. O. Parke, Evgenya L. Shkolnik, Adam C. Schneider, Travis S. Barman, Victoria S. Meadows, Isabella Pagano, and Sarah Peacock. 2018. "HAZMAT. IV. Flares and Superflares on Young M Stars in the Far Ultraviolet." *The Astrophysical Journal* 867, no. 1 (November): 70. https://doi.org/10.3847/1538-4357/aae2ae. arXiv: 1810.03277 [astro-ph.SR].

Luque, R., E. Pallé, D. Kossakowski, S. Dreizler, J. Kemmer, N. Espinoza, J. Burt, et al. 2019. "Planetary system around the nearby M dwarf GJ 357 including a transiting, hot, Earth-sized planet optimal for atmospheric characterization." *Astronomy & Astrophysics* 628 (August): A39. https://doi.org/10.1051/0004-6361/201935801. arXiv: 1904.12818 [astro-ph.EP].

Mamajek, Eric, and Karl Stapelfeldt. 2024. "NASA Exoplanet Exploration Program (ExEP) Mission Star List for the Habitable Worlds Observatory (2023)." *arXiv e-prints* (February): arXiv:2402.12414. https://doi.org/10.48550/arXiv.2402.12414. arXiv: 2402.12414 [astro-ph.IM].

Mamajek, Eric E., and Lynne A. Hillenbrand. 2008. "Improved Age Estimation for Solar-Type Dwarfs Using Activity-Rotation Diagnostics." *The Astrophysical Journal* 687, no. 2 (November): 1264–1293. https://doi.org/10.1086/591785. arXiv: 0807.1686 [astro-ph].

Marigo, Paola, Bernhard Aringer, Léo Girardi, and Alessandro Bressan. 2022. "Updated Low-temperature Gas Opacities with ÆSOPUS 2.0." *The Astrophysical Journal* 940, no. 2 (December): 129. https://doi.org/10.3847/1538-4357/ac9b40. arXiv: 2210.08587 [astro-ph.SR].

Mathur, Savita, Daniel Huber, Natalie M. Batalha, David R. Ciardi, Fabienne A. Bastien, Allyson Bieryla, Lars A. Buchhave, et al. 2017. "Revised Stellar Properties of Kepler Targets for the Q1-17 (DR25) Transit Detection Run." *The Astrophysical Journal Supplement* 229, no. 2 (April): 30. https://doi.org/10.3847/1538-4365/229/2/30. arXiv: 1609.04128 [astro-ph.SR].

Mayor, M., F. Pepe, D. Queloz, F. Bouchy, G. Rupprecht, G. Lo Curto, G. Avila, et al. 2003. "Setting New Standards with HARPS." *The Messenger* 114 (December): 20–24.

McKay, Christopher P. 2014. "Requirements and limits for life in the context of exoplanets." *Proceedings of the National Academy of Science* 111, no. 35 (September): 12628–12633. https://doi.org/10.1073/pnas.1304212111.

Meakin, Casey A., and David Arnett. 2007. "Turbulent Convection in Stellar Interiors. I. Hydrodynamic Simulation." *The Astrophysical Journal* 667, no. 1 (September): 448–475. https://doi.org/10.1086/520318. arXiv: astro-ph/0611315 [astro-ph].

Mello, Fernando de Sousa, and Amâncio César Santos Friaça. 2023. "Planetary geodynamics and age constraints on circumstellar habitable zones around main sequence stars." *International Journal of Astrobiology* 22, no. 4 (August): 272–316. https://doi.org/10.1017/S1473550423000083.

Miles, Brittany E., and Evgenya L. Shkolnik. 2017. "HAZMAT. II. Ultraviolet Variability of Low-mass Stars in the GALEX Archive." *The Astronomical Journal* 154, no. 2 (August): 67. https://doi.org/10.3847/1538-3881/aa71ab. arXiv: 1705.03583 [astro-ph.SR].

Morales, J. C., I. Ribas, and C. Jordi. 2008. "The effect of activity on stellar temperatures and radii." *Astronomy & Astrophysics* 478, no. 2 (February): 507–512. https://doi.org/10.1051/0004-6361:20078324. arXiv: 0711.3523 [astro-ph].

Morley, Caroline V., Laura Kreidberg, Zafar Rustamkulov, Tyler Robinson, and Jonathan J. Fortney. 2017. "Observing the Atmospheres of Known Temperate Earth-sized Planets with JWST." *The Astrophysical Journal* 850, no. 2 (December): 121. https://doi.org/10.3847/1538-4357/aa927b. arXiv: 1708.04239 [astro-ph.EP].

Mullally, Fergal, Susan E. Thompson, Jeffrey L. Coughlin, Christopher J. Burke, and Jason F. Rowe. 2018. "Kepler's Earth-like Planets Should Not Be Confirmed without Independent Detection: The Case of Kepler-452b." *The Astronomical Journal* 155, no. 5 (May): 210. https://doi.org/10.3847/1538-3881/aabae3. arXiv: 1803.11307 [astro-ph.EP].

Newman, Patrick D., Peter Plavchan, Jennifer A. Burt, Johanna Teske, Eric E. Mamajek, Stephanie Leifer, B. Scott Gaudi, Gary Blackwood, and Rhonda Morgan. 2023. "Simulations for Planning Next-generation Exoplanet Radial Velocity Surveys." *The Astronomical Journal* 165, no. 4 (April): 151. https://doi.org/10.3847/1538-3881/acad07. arXiv: 2204.13968 [astro-ph.EP].

Nissen, P. E. 2015. "High-precision abundances of elements in solar twin stars. Trends with stellar age and elemental condensation temperature." *Astronomy & Astro-*

physics 579 (July): A52. https://doi.org/10.1051/0004-6361/201526269. arXiv: 1504.07598 [astro-ph.SR].

Owen, James E., and Yanqin Wu. 2017. "The Evaporation Valley in the Kepler Planets." *The Astrophysical Journal* 847, no. 1 (September): 29. https://doi.org/10.3847/1538-4357/aa890a. arXiv: 1705.10810 [astro-ph.EP].

Pagano, Michael, Amanda Truitt, Patrick A. Young, and Sang-Heon Shim. 2015. "The Chemical Composition of τ Ceti and Possible Effects on Terrestrial Planets." *The Astrophysical Journal* 803, no. 2 (April): 90. https://doi.org/10.1088/0004-637X/803/2/90. arXiv: 1503.04189 [astro-ph.EP].

Pecaut, Mark J., and Eric E. Mamajek. 2013. "Intrinsic Colors, Temperatures, and Bolometric Corrections of Pre-main-sequence Stars." *The Astrophysical Journal Supplement* 208, no. 1 (September): 9. https://doi.org/10.1088/0067-0049/208/1/9. arXiv: 1307.2657 [astro-ph.SR].

Petigura, Erik A., Andrew W. Howard, and Geoffrey W. Marcy. 2013. "Prevalence of Earth-size planets orbiting Sun-like stars." *Proceedings of the National Academy of Science* 110, no. 48 (November): 19273–19278. https://doi.org/10.1073/pnas.1319909110. arXiv: 1311.6806 [astro-ph.EP].

Petigura, Erik A., James G. Rogers, Howard Isaacson, James E. Owen, Adam L. Kraus, Joshua N. Winn, Mason G. MacDougall, et al. 2022. "The California-Kepler Survey. X. The Radius Gap as a Function of Stellar Mass, Metallicity, and Age." *The Astronomical Journal* 163, no. 4 (April): 179. https://doi.org/10.3847/1538-3881/ac51e3. arXiv: 2201.10020 [astro-ph.EP].

Planck Collaboration, N. Aghanim, Y. Akrami, M. Ashdown, J. Aumont, C. Baccigalupi, M. Ballardini, et al. 2020. "Planck 2018 results. VI. Cosmological parameters." *Astronomy & Astrophysics* 641 (September): A6. https://doi.org/10.1051/0004-6361/201833910. arXiv: 1807.06209 [astro-ph.CO].

Prša, Andrej, Petr Harmanec, Guillermo Torres, Eric Mamajek, Martin Asplund, Nicole Capitaine, Jørgen Christensen-Dalsgaard, et al. 2016. "Nominal Values for Selected Solar and Planetary Quantities: IAU 2015 Resolution B3." *The Astronomical Journal* 152, no. 2 (August): 41. https://doi.org/10.3847/0004-6256/152/2/41. arXiv: 1605.09788 [astro-ph.SR].

Rackham, Benjamin V., Dániel Apai, and Mark S. Giampapa. 2018. "The Transit Light Source Effect: False Spectral Features and Incorrect Densities for M-dwarf Transiting Planets." *The Astrophysical Journal* 853, no. 2 (February): 122. https://doi.org/10.3847/1538-4357/aaa08c. arXiv: 1711.05691 [astro-ph.EP].

Ramirez, Ramses M. 2017. "A warmer and wetter solution for early Mars and the challenges with transient warming." *Icarus* 297 (November): 71–82. https://doi.org/10.1016/j.icarus.2017.06.025. arXiv: 1706.08639 [astro-ph.EP].

———. 2020. "The effect of high nitrogen pressures on the habitable zone and an appraisal of greenhouse states." *Monthly Notices of the Royal Astronomical Society* 494, no. 1 (May): 259–270. https://doi.org/10.1093/mnras/staa603. arXiv: 2004.00229 [astro-ph.EP].

Ramirez, Ramses M., and Lisa Kaltenegger. 2018. "A Methane Extension to the Classical Habitable Zone." *The Astrophysical Journal* 858, no. 2 (May): 72. https://doi.org/10.3847/1538-4357/aab8fa. arXiv: 1805.02801 [astro-ph.EP].

Rauscher, Thomas, and Friedrich-Karl Thielemann. 2000. "Astrophysical Reaction Rates From Statistical Model Calculations." *Atomic Data and Nuclear Data Tables* 75, nos. 1-2 (May): 1–351. https://doi.org/10.1006/adnd.2000.0834. arXiv: astro-ph/0004059 [astro-ph].

Ricker, George R., Joshua N. Winn, Roland Vanderspek, David W. Latham, Gáspár. Á. Bakos, Jacob L. Bean, Zachory K. Berta-Thompson, et al. 2014. "Transiting Exoplanet Survey Satellite (TESS)." In *Space Telescopes and Instrumentation 2014: Optical, Infrared, and Millimeter Wave,* edited by Jr. Oschmann Jacobus M., Mark Clampin, Giovanni G. Fazio, and Howard A. MacEwen, 9143:914320. Society of Photo-Optical Instrumentation Engineers (SPIE) Conference Series. August. https://doi.org/10.1117/12.2063489. arXiv: 1406.0151 [astro-ph.EP].

Rogers, F. J., and A. Nayfonov. 2002. "Updated and Expanded OPAL Equation-of-State Tables: Implications for Helioseismology." *The Astrophysical Journal* 576, no. 2 (September): 1064–1074. https://doi.org/10.1086/341894.

Rugheimer, S., A. Segura, L. Kaltenegger, and D. Sasselov. 2015. "UV Surface Environment of Earth-like Planets Orbiting FGKM Stars through Geological Evolution." *The Astrophysical Journal* 806, no. 1 (June): 137. https://doi.org/10.1088/0004-637X/806/1/137. arXiv: 1506.07200 [astro-ph.EP].

Rugheimer, Sarah, Lisa Kaltenegger, Andras Zsom, Antígona Segura, and Dimitar Sasselov. 2013. "Spectral Fingerprints of Earth-like Planets Around FGK Stars." *Astrobiology* 13, no. 3 (March): 251–269. https://doi.org/10.1089/ast.2012.0888. arXiv: 1212.2638 [astro-ph.EP].

Rushby, Andrew J., Mark W. Claire, Hugh Osborn, and Andrew J. Watson. 2013. "Habitable Zone Lifetimes of Exoplanets around Main Sequence Stars." *Astrobiology* 13, no. 9 (September): 833–849. https://doi.org/10.1089/ast.2012.0938.

Sandage, A. 1970. "Main-sequence photometry, color-magnitude diagrams, and ages for the globular clusters M3, M13, M15 and M92." *The Astrophysical Journal* 162 (December): 841. https://doi.org/10.1086/150715.

Schulze-Makuch, Dirk, Alessandro Airo, and Janosch Schirmack. 2017. "The Adaptability of Life on Earth and the Diversity of Planetary Habitats." *Frontiers in Microbiology* 8. https://doi.org/10.3389/fmicb.2017.02011.

Schwieterman, Edward W., Nancy Y. Kiang, Mary N. Parenteau, Chester E. Harman, Shiladitya DasSarma, Theresa M. Fisher, Giada N. Arney, et al. 2018. "Exoplanet Biosignatures: A Review of Remotely Detectable Signs of Life." *Astrobiology* 18, no. 6 (June): 663–708. https://doi.org/10.1089/ast.2017.1729. arXiv: 1705.05791 [astro-ph.EP].

Seager, Sara, and Drake Deming. 2010. "Exoplanet Atmospheres." *Annual Review of Astronomy and Astrophysics* 48 (September): 631–672. https://doi.org/10.1146/annurev-astro-081309-130837. arXiv: 1005.4037 [astro-ph.EP].

Seager, Sara, N. Jeremy Kasdin, Jeff Booth, Matt Greenhouse, Doug Lisman, Bruce Macintosh, Stuart Shaklan, et al. 2019. "Starshade Rendezvous Probe Mission." In *Bulletin of the American Astronomical Society,* 51:106. September.

Serenelli, Aldo M., Sarbani Basu, Jason W. Ferguson, and Martin Asplund. 2009. "New Solar Composition: The Problem with Solar Models Revisited." *The Astrophysical Journal Letters* 705, no. 2 (November): L123–L127. https://doi.org/10.1088/0004-637X/705/2/L123. arXiv: 0909.2668 [astro-ph.SR].

Shields, Aomawa L., Victoria S. Meadows, Cecilia M. Bitz, Raymond T. Pierrehumbert, Manoj M. Joshi, and Tyler D. Robinson. 2013. "The Effect of Host Star Spectral Energy Distribution and Ice-Albedo Feedback on the Climate of Extrasolar Planets." *Astrobiology* 13, no. 8 (August): 715–739. https://doi.org/10.1089/ast.2012.0961. arXiv: 1305.6926 [astro-ph.EP].

Silburt, Ari, Eric Gaidos, and Yanqin Wu. 2015. "A Statistical Reconstruction of the Planet Population around Kepler Solar-type Stars." *The Astrophysical Journal* 799, no. 2 (February): 180. https://doi.org/10.1088/0004-637X/799/2/180. arXiv: 1406.6048 [astro-ph.EP].

Sing, David K. 2018. "Observational Techniques With Transiting Exoplanetary Atmospheres." *arXiv e-prints* (April): arXiv:1804.07357. https://doi.org/10.48550/arXiv.1804.07357. arXiv: 1804.07357 [astro-ph.EP].

Skumanich, A. 1972. "Time Scales for Ca II Emission Decay, Rotational Braking, and Lithium Depletion." *The Astrophysical Journal* 171 (February): 565. https://doi.org/10.1086/151310.

Snellen, I., R. de Kok, J. L. Birkby, B. Brandl, M. Brogi, C. Keller, M. Kenworthy, H. Schwarz, and R. Stuik. 2015. "Combining high-dispersion spectroscopy with high contrast imaging: Probing rocky planets around our nearest neighbors." *Astronomy & Astrophysics* 576 (April): A59. https://doi.org/10.1051/0004-6361/201425018. arXiv: 1503.01136 [astro-ph.EP].

Soderblom, David R. 2010. "The Ages of Stars." *Annual Review of Astronomy and Astrophysics* 48 (September): 581–629. https://doi.org/10.1146/annurev-astro-081309-130806. arXiv: 1003.6074 [astro-ph.SR].

Somers, Garrett, Lyra Cao, and Marc H. Pinsonneault. 2020. "The SPOTS Models: A Grid of Theoretical Stellar Evolution Tracks and Isochrones for Testing the Effects of Starspots on Structure and Colors." *The Astrophysical Journal* 891, no. 1 (March): 29. https://doi.org/10.3847/1538-4357/ab722e. arXiv: 2002.10644 [astro-ph.SR].

Soubiran, C., N. Brouillet, and L. Casamiquela. 2022. "Assessment of [Fe/H] determinations for FGK stars in spectroscopic surveys." *Astronomy & Astrophysics* 663 (July): A4. https://doi.org/10.1051/0004-6361/202142409. arXiv: 2112.07545 [astro-ph.SR].

Sousa, S. G., N. C. Santos, M. Mayor, S. Udry, L. Casagrande, G. Israelian, F. Pepe, D. Queloz, and M. J. P. F. G. Monteiro. 2008. "Spectroscopic parameters for 451 stars in the HARPS GTO planet search program. Stellar [Fe/H] and the frequency of exo-Neptunes." *Astronomy & Astrophysics* 487, no. 1 (August): 373–381. https://doi.org/10.1051/0004-6361:200809698. arXiv: 0805.4826 [astro-ph].

Spiegel, David S., and Edwin L. Turner. 2012. "Bayesian analysis of the astrobiological implications of life's early emergence on Earth." *Proceedings of the National Academy of Science* 109, no. 2 (January): 395–400. https://doi.org/10.1073/pnas.1111694108. arXiv: 1107.3835 [astro-ph.EP].

Stassun, Keivan G., Ryan J. Oelkers, Martin Paegert, Guillermo Torres, Joshua Pepper, Nathan De Lee, Kevin Collins, et al. 2019. "The Revised TESS Input Catalog and Candidate Target List." *The Astronomical Journal* 158, no. 4 (October): 138. https://doi.org/10.3847/1538-3881/ab3467. arXiv: 1905.10694 [astro-ph.SR].

Stevenson, Kevin B., Nikole K. Lewis, Jacob L. Bean, Charles Beichman, Jonathan Fraine, Brian M. Kilpatrick, J. E. Krick, et al. 2016. "Transiting Exoplanet Studies and Community Targets for JWST's Early Release Science Program." *Publications of the Astronomical Society of the Pacific* 128, no. 967 (September): 094401. https://doi.org/10.1088/1538-3873/128/967/094401. arXiv: 1602.08389 [astro-ph.EP].

Sullivan, Peter W., Joshua N. Winn, Zachory K. Berta-Thompson, David Charbonneau, Drake Deming, Courtney D. Dressing, David W. Latham, et al. 2015. "The Transiting Exoplanet Survey Satellite: Simulations of Planet Detections and Astrophysical False Positives." *The Astrophysical Journal* 809, no. 1 (August): 77. https://doi.org/10.1088/0004-637X/809/1/77. arXiv: 1506.03845 [astro-ph.EP].

Summons, Roger E., Linda L. Jahnke, Janet M. Hope, and Graham A. Logan. 1999. "2-Methylhopanoids as biomarkers for cyanobacterial oxygenic photosynthesis." *Nature* 400, no. 6744 (August): 554–557. https://doi.org/10.1038/23005.

Tarter, Jill C., Peter R. Backus, Rocco L. Mancinelli, Jonathan M. Aurnou, Dana E. Backman, Gibor S. Basri, Alan P. Boss, et al. 2007. "A Reappraisal of The Habitability of Planets around M Dwarf Stars." *Astrobiology* 7, no. 1 (March): 30–65. https://doi.org/10.1089/ast.2006.0124. arXiv: astro-ph/0609799 [astro-ph].

Tayar, Jamie, Zachary R. Claytor, Daniel Huber, and Jennifer van Saders. 2022. "A Guide to Realistic Uncertainties on the Fundamental Properties of Solar-type Exoplanet Host Stars." *The Astrophysical Journal* 927, no. 1 (March): 31. https://doi.org/10.3847/1538-4357/ac4bbc. arXiv: 2012.07957 [astro-ph.EP].

The LUVOIR Team. 2019. "The LUVOIR Mission Concept Study Final Report." *arXiv e-prints* (December): arXiv:1912.06219. arXiv: 1912.06219 [astro-ph.IM].

Thompson, Susan E., Jeffrey L. Coughlin, Kelsey Hoffman, Fergal Mullally, Jessie L. Christiansen, Christopher J. Burke, Steve Bryson, et al. 2018. "Planetary Candidates Observed by Kepler. VIII. A Fully Automated Catalog with Measured Completeness and Reliability Based on Data Release 25." *The Astrophysical Journal Supplement* 235, no. 2 (April): 38. https://doi.org/10.3847/1538-4365/aab4f9. arXiv: 1710.06758 [astro-ph.EP].

Thoul, Anne A., John N. Bahcall, and Abraham Loeb. 1994. "Element Diffusion in the Solar Interior." *The Astrophysical Journal* 421 (February): 828. https://doi.org/10.1086/173695. arXiv: astro-ph/9304005 [astro-ph].

Timmes, F. X., and Dave Arnett. 1999. "The Accuracy, Consistency, and Speed of Five Equations of State for Stellar Hydrodynamics." *The Astrophysical Journal Supplement* 125, no. 1 (November): 277–294. https://doi.org/10.1086/313271.

Torres, G., J. Andersen, and A. Giménez. 2010. "Accurate masses and radii of normal stars: modern results and applications." *The Astronomy and Astrophysics Review* 18, nos. 1-2 (February): 67–126. https://doi.org/10.1007/s00159-009-0025-1. arXiv: 0908.2624 [astro-ph.SR].

Torres, Guillermo, Stephen R. Kane, Jason F. Rowe, Natalie M. Batalha, Christopher E. Henze, David R. Ciardi, Thomas Barclay, et al. 2017. "Validation of Small Kepler Transiting Planet Candidates in or near the Habitable Zone." *The Astronomical Journal* 154, no. 6 (December): 264. https://doi.org/10.3847/1538-3881/aa984b. arXiv: 1711.01267 [astro-ph.EP].

Torres, Guillermo, David M. Kipping, Francois Fressin, Douglas A. Caldwell, Joseph D. Twicken, Sarah Ballard, Natalie M. Batalha, et al. 2015. "Validation of 12 Small Kepler Transiting Planets in the Habitable Zone." *The Astrophysical Journal* 800, no. 2 (February): 99. https://doi.org/10.1088/0004-637X/800/2/99. arXiv: 1501.01101 [astro-ph.EP].

Truitt, Amanda, and Patrick A. Young. 2017. "Expanding the Catalog: Considering the Importance of Carbon, Magnesium, and Neon in the Evolution of Stars and Habitable Zones." *The Astrophysical Journal* 835, no. 1 (January): 87. https://doi.org/10.3847/1538-4357/835/1/87. arXiv: 1612.03949 [astro-ph.SR].

Truitt, Amanda, Patrick A. Young, Alexander Spacek, Luke Probst, and Jeremy Dietrich. 2015. "A Catalog of Stellar Evolution Profiles and the Effects of Variable Composition on Habitable Systems." *The Astrophysical Journal* 804, no. 2 (May): 145. https://doi.org/10.1088/0004-637X/804/2/145. arXiv: 1504.02145 [astro-ph.SR].

Truitt, Amanda R., Patrick A. Young, Sara I. Walker, and Alexander Spacek. 2020. "A Flexible Bayesian Framework for Assessing Habitability with Joint Observational and Model Constraints." *The Astronomical Journal* 159, no. 2 (February): 55. https://doi.org/10.3847/1538-3881/ab4e93. arXiv: 1910.07137 [astro-ph.EP].

Tuomi, M., G. Anglada-Escudé, E. Gerlach, H. R. A. Jones, A. Reiners, E. J. Rivera, S. S. Vogt, and R. P. Butler. 2013. "Habitable-zone super-Earth candidate in a six-planet system around the K2.5V star HD 40307." *Astronomy & Astrophysics* 549 (January): A48. https://doi.org/10.1051/0004-6361/201220268. arXiv: 1211.1617 [astro-ph.EP].

Turbet, Martin, Emeline Bolmont, Guillaume Chaverot, David Ehrenreich, Jérémy Leconte, and Emmanuel Marcq. 2021. "Day-night cloud asymmetry prevents early oceans on Venus but not on Earth." *Nature* 598, no. 7880 (October): 276–280. https://doi.org/10.1038/s41586-021-03873-w. arXiv: 2110.08801 [astro-ph.EP].

Turbet, Martin, Thomas J. Fauchez, Jeremy Leconte, Emeline Bolmont, Guillaume Chaverot, Francois Forget, Ehouarn Millour, et al. 2023. "Water condensation zones around main sequence stars." *Astronomy & Astrophysics* 679 (November): A126. https://doi.org/10.1051/0004-6361/202347539. arXiv: 2308.15110 [astro-ph.EP].

Unterborn, C. T., S. J. Desch, J. Haldemann, A. Lorenzo, J. G. Schulze, N. R. Hinkel, and W. R. Panero. 2023. "The Nominal Ranges of Rocky Planet Masses, Radii, Surface Gravities, and Bulk Densities." *The Astrophysical Journal* 944, no. 1 (February): 42. https://doi.org/10.3847/1538-4357/acaa3b. arXiv: 2212.03934 [astro-ph.EP].

Valenti, Jeff A., and Debra A. Fischer. 2005. "Spectroscopic Properties of Cool Stars (SPOCS). I. 1040 F, G, and K Dwarfs from Keck, Lick, and AAT Planet Search Programs." *The Astrophysical Journal Supplement* 159, no. 1 (July): 141–166. https://doi.org/10.1086/430500.

Valle, G., M. Dell'Omodarme, P. G. Prada Moroni, and S. Degl'Innocenti. 2014. "Evolution of the habitable zone of low-mass stars. Detailed stellar models and analytical relationships for different masses and chemical compositions." *Astronomy & Astrophysics* 567 (July): A133. https://doi.org/10.1051/0004-6361/201323350. arXiv: 1405.7486 [astro-ph.SR].

Vilović, Iva, Dirk Schulze-Makuch, and René Heller. 2024. "Observation of significant photosynthesis in garden cress and cyanobacteria under simulated illumination from a K dwarf star." *International Journal of Astrobiology* 23 (September): e18. https://doi.org/10.1017/S1473550424000132. arXiv: 2405.19180 [astro-ph.EP].

Waltham, David. 2017. "Star Masses and Star-Planet Distances for Earth-like Habitability." *Astrobiology* 17, no. 1 (January): 61–77. https://doi.org/10.1089/ast.2016.1518.

Ware, Austin, Patrick Young, Amanda Truitt, and Alexander Spacek. 2022. "Continuous Habitable Zones: Using Bayesian Methods to Prioritize Characterization of Potentially Habitable Worlds." *The Astrophysical Journal* 929, no. 2 (April): 143. https://doi.org/10.3847/1538-4357/ac5c4e. arXiv: 2203.06259 [astro-ph.EP].

Way, M. J., I. Aleinov, David S. Amundsen, M. A. Chandler, T. L. Clune, A. D. Del Genio, Y. Fujii, et al. 2017. "Resolving Orbital and Climate Keys of Earth and Extraterrestrial Environments with Dynamics (ROCKE-3D) 1.0: A General Circulation Model for Simulating the Climates of Rocky Planets." *The Astrophysical Journal Supplement* 231, no. 1 (July): 12. https://doi.org/10.3847/1538-4365/aa7a06. arXiv: 1701.02360 [astro-ph.EP].

Weber, Edmund J., and Jr. Davis Leverett. 1967. "The Angular Momentum of the Solar Wind." *The Astrophysical Journal* 148 (April): 217–227. https://doi.org/10.1086/149138.

Wiescher, M., R. E. Azuma, L. Gasques, J. Görres, M. Pignatari, and E. Simpson. 2006. "Charged particle reaction rates from stellar H to C burning." *Memorie della Società Astronomica Italiana* 77 (January): 910.

Wolf, E. T., and O. B. Toon. 2013. "Hospitable Archean Climates Simulated by a General Circulation Model." *Astrobiology* 13, no. 7 (July): 656–673. https://doi.org/10.1089/ast.2012.0936.

Wolf, Eric T., Aomawa L. Shields, Ravi K. Kopparapu, Jacob Haqq-Misra, and Owen B. Toon. 2017. "Constraints on Climate and Habitability for Earth-like Exoplanets Determined from a General Circulation Model." *The Astrophysical Journal* 837, no. 2 (March): 107. https://doi.org/10.3847/1538-4357/aa5ffc. arXiv: 1702.03315 [astro-ph.EP].

Wordsworth, R., Y. Kalugina, S. Lokshtanov, A. Vigasin, B. Ehlmann, J. Head, C. Sanders, and H. Wang. 2017. "Transient reducing greenhouse warming on early Mars." *Geophysical Research Letters* 44, no. 2 (January): 665–671. https://doi.org/10.1002/2016GL071766. arXiv: 1610.09697 [astro-ph.EP].

Wright, D. J., R. A. Wittenmyer, C. G. Tinney, J. S. Bentley, and Jinglin Zhao. 2016. "Three Planets Orbiting Wolf 1061." *The Astrophysical Journal Letters* 817, no. 2 (February): L20. https://doi.org/10.3847/2041-8205/817/2/L20. arXiv: 1512.05154 [astro-ph.EP].

Yang, Jun, Nicolas B. Cowan, and Dorian S. Abbot. 2013. "Stabilizing Cloud Feedback Dramatically Expands the Habitable Zone of Tidally Locked Planets." *The Astrophysical Journal Letters* 771, no. 2 (July): L45. https://doi.org/10.1088/2041-8205/771/2/L45. arXiv: 1307.0515 [astro-ph.EP].

Young, P. A., E. E. Mamajek, David Arnett, and James Liebert. 2001. "Observational Tests and Predictive Stellar Evolution." *The Astrophysical Journal* 556, no. 1

(July): 230–244. https://doi.org/10.1086/321559. arXiv: astro-ph/0103390 [astro-ph].

Young, Patrick A., and David Arnett. 2005. "Observational Tests and Predictive Stellar Evolution. II. Nonstandard Models." *The Astrophysical Journal* 618, no. 2 (January): 908–918. https://doi.org/10.1086/426131. arXiv: astro-ph/0409658 [astro-ph].

Zeng, Li, Dimitar D. Sasselov, and Stein B. Jacobsen. 2016. "Mass-Radius Relation for Rocky Planets Based on PREM." *The Astrophysical Journal* 819, no. 2 (March): 127. https://doi.org/10.3847/0004-637X/819/2/127. arXiv: 1512.08827 [astro-ph.EP].

APPENDIX A

CO-AUTHOR PERMISSIONS FOR PUBLICATIONS IN THIS THESIS

Chapter 2 of this thesis has been published as "Continuous Habitable Zones: Using Bayesian Methods to Prioritize Characterization of Potentially Habitable Worlds" in The Astrophysical Journal 929, 143, in 2022. The authors of this publication are Austin Ware (Arizona State University), Patrick Young (Arizona State University), Amanda Truitt (Los Alamos National Lab), and Alexander Spacek (Los Alamos National Lab).

The papers published in this dissertation have the full acknowledgement and approval of all co-authors.

APPENDIX B

SUPPLEMENTARY TABLES

Table B.1. Derived masses and ages for EMSL stars

Star	SpT	Tier	M	σ_M^+	σ_M^-	Age	σ_{Age}^+	σ_{Age}^-	Flag
			($M_\odot$)	($M_\odot$)	($M_\odot$)	(Gyr)	(Gyr)	(Gyr)	
HD 72673	K1V	C	0.75	0.02	0.02	9.54	1.57	3.55	1
HD 72905	G0.5V	B	1.00	0.03	0.03	1.73	1.80	1.50	1
HD 74576	K2.5V	C	0.78	0.03	0.02	8.02	3.39	4.61	1
HD 75732 A	K0IV-V	C	0.94	0.07	0.02	5.53	1.08	5.48	1
HD 76151	G2V	C	1.01	0.03	0.03	3.03	1.38	1.33	1
HD 78366	G0IV-V	C	1.07	0.03	0.02	1.49	0.92	1.43	1
HD 78154 A	F7V	C	1.30	0.03	0.04	2.77	0.62	0.36	1
HD 82885 A	G9IV-V	B	0.97	0.03	0.02	5.48	1.88	1.95	1
HD 84117	F9V	A	1.12	0.03	0.04	3.08	1.04	0.63	1
HD 84737	G0V	B	1.13	0.06	0.03	6.37	0.68	1.16	1
HD 86728 A	G4IV	B	1.02	0.03	0.03	7.45	1.17	1.15	1
HD 88230	K7V	A	0.63	0.02	0.02	5.45	2.11	2.95	2
HD 89449	F6IV-V	C	1.39	0.03	0.03	1.90	0.27	0.17	1
HD 90589	F3V	C	1.44	0.04	0.03	1.13	0.17	0.34	1
HD 90839	F8V	A	1.09	0.03	0.03	2.14	0.80	1.62	1
HD 90089 A	F4V	C	1.29	0.04	0.04	0.77	0.45	0.74	1
HD 91324	F9V	C	1.15	0.12	0.07	5.02	0.67	1.05	1
HD 95128	G1.5IV-V	A	1.02	0.03	0.03	6.92	1.02	0.96	1
HD 95735	M2V	B	0.20	0.00	0.00	0.02	0.00	0.00	2
HD 100623 A	K0V	A	0.75	0.02	0.01	10.13	1.03	2.06	1
HD 101501	G8V	A	0.88	0.02	0.02	6.27	1.23	2.11	1
HD 102365	G2V	A	0.93	0.05	0.03	6.94	1.67	6.78	1
HD 102870	F9V	C	1.28	0.05	0.05	3.75	0.69	0.74	1
HD 103095	K1V	C	0.63	0.01	0.01	6.66	2.03	1.78	2
HD 105452 A	F1V	C	1.30	0.10	0.07	1.36	0.62	1.33	1
HD 109085	F2V	C	1.38	0.02	0.02	1.53	0.16	0.17	1
HD 109358	G0V	A	0.96	0.04	0.03	6.23	1.67	2.07	1
HD 110897	F9V	C	0.87	0.03	0.03	7.98	1.45	1.43	1
HD 114710	F9.5V	A	1.10	0.04	0.03	2.28	1.05	2.07	1
HD 114613	G4IV	C	1.24	0.03	0.03	5.12	0.35	0.32	1
HD 114837 A	F6V	C	1.11	0.05	0.04	4.65	0.68	0.91	1
HD 115404 A	K2.5V	C	0.75	0.02	0.02	10.62	2.06	3.49	1
HD 115617	G6.5V	B	0.95	0.03	0.01	8.13	1.03	1.99	1
HD 122064	K3V	C	0.79	0.02	0.02	9.87	2.32	4.00	1
HD 125276 A	F9V	C	0.89	0.02	0.02	5.86	1.04	1.21	1

Continued on next page

Table B.1 – continued from previous page

Star	SpT	Tier	M	σ_M^+	σ_M^-	Age	σ_{Age}^+	σ_{Age}^-	Flag
			($M_\odot$)	($M_\odot$)	($M_\odot$)	(Gyr)	(Gyr)	(Gyr)	
HD 126660 A	F7V	C	1.28	0.04	0.04	3.35	0.42	0.56	1
HD 128167	F4V	B	1.22	0.03	0.03	1.74	0.32	0.36	1
HD 128621	K1V	B	0.91	0.02	0.02	2.75	3.60	2.50	1
HD 128620	G2V	B	1.05	0.05	0.04	6.91	1.87	2.44	1
HD 131156 B	K5V	C	0.65	0.01	0.02	5.57	1.70	2.58	1
HD 131156 A	G8V	B	0.86	0.03	0.02	5.50	2.17	3.07	1
HD 131977	K4V	A	0.75	0.02	0.01	8.35	3.40	4.77	1
HD 134083	F5V	B	1.28	0.02	0.02	1.85	0.19	0.29	1
HD 136352	G2.5V	B	0.87	0.01	0.00	11.06	0.51	0.86	1
HD 140538 A	G5V	B	0.97	0.03	0.03	3.53	1.69	2.36	1
HD 141004	G0V	A	1.06	0.05	0.04	6.74	1.06	1.23	1
HD 140901 A	G7IV-V	C	0.95	0.03	0.01	5.63	1.08	5.33	1
HD 142373	G0V	A	0.96	0.05	0.03	8.77	0.83	1.10	1
HD 142860	F6V	A	1.16	0.04	0.03	3.93	0.61	0.64	1
HD 143761	G0IV	B	0.95	0.03	0.03	9.92	1.08	1.04	1
HD 146233	G3V	A	0.98	0.03	0.03	6.10	1.58	1.61	1
HD 147513	G1V	A	1.01	0.03	0.03	2.82	1.51	1.71	1
HD 149661	K0V	A	0.84	0.02	0.02	8.08	1.49	2.73	1
HD 155886	K1V	B	0.74	0.02	0.02	8.98	2.74	4.38	1
HD 155885	K1V	B	0.74	0.02	0.01	8.83	2.74	4.24	1
HD 156026	K5V	A	0.65	0.02	0.02	4.47	2.51	3.46	1
HD 156274 A	G9V	B	0.75	0.01	0.01	10.35	0.75	1.56	1
HD 157214	G0V	C	0.88	0.03	0.01	11.38	0.83	1.69	1
HD 156897 A	F2V	C	1.30	0.02	0.03	1.89	0.37	0.17	1
HD 158633	K0V	C	0.76	0.01	0.01	9.77	0.81	1.56	1
HD 160032	F4V	C	1.26	0.05	0.04	2.62	0.50	0.36	1
HD 160915	F5V	C	1.18	0.04	0.03	2.94	0.49	0.80	1
HD 160691	G3V	B	1.07	0.03	0.03	7.97	1.17	1.17	1
HD 165341 A	K0V	B	0.84	0.01	0.01	8.48	0.80	1.41	1
HD 165341 B	K4V	B	0.67	0.01	0.01	4.89	1.71	2.58	2
HD 165185	G0V	C	1.03	0.03	0.03	1.46	1.52	1.40	1
HD 166620	K2V	C	0.75	0.02	0.01	11.46	1.11	2.17	2
HD 165499	G0V	B	1.06	0.04	0.04	5.30	1.29	1.35	1
HD 168151	F5V	C	1.22	0.04	0.03	3.31	0.43	0.44	1
HD 182572	G7IV-V	C	1.03	0.02	0.02	9.62	1.00	0.89	1

Continued on next page

Table B.1 – continued from previous page

Star	SpT	Tier	M	σ_M^+	σ_M^-	Age	σ_{Age}^+	σ_{Age}^-	Flag
			($M_\odot$)	($M_\odot$)	($M_\odot$)	(Gyr)	(Gyr)	(Gyr)	
HD 185144	K0V	A	0.80	0.03	0.03	6.68	2.93	4.48	1
HD 187013	F5.5IV-V	C	1.26	0.03	0.03	2.52	0.40	0.43	1
HD 187691 A	F8V	B	1.22	0.03	0.03	3.48	0.56	0.41	1
HD 190360	G7V	B	0.96	0.03	0.02	10.77	1.08	1.48	1
HD 189567	G2V	C	0.92	0.03	0.02	8.25	1.05	1.52	1
HD 190248	G8IV-V	A	1.02	0.03	0.03	8.49	1.58	1.44	1
HD 191408 A	K2.5V	C	0.73	0.02	0.01	10.22	2.39	3.78	2
HD 192310	K2V	A	0.82	0.02	0.02	8.58	1.55	2.79	1
HD 193664	G0V	C	0.99	0.02	0.03	3.73	1.14	1.54	1
HD 197692	F5V	C	1.33	0.05	0.03	1.49	0.34	0.69	1
HD 199260	F6V	C	1.14	0.03	0.03	1.56	0.63	1.03	1
HD 201091	K5V	A	0.70	0.01	0.01	4.96	0.79	1.46	2
HD 201092	K7V	A	0.57	0.02	0.02	6.99	3.19	4.83	2
HD 202560	M0V	A	0.55	0.01	0.01	9.48	1.67	3.06	2
HD 203608	F9V	A	0.88	0.03	0.03	7.58	1.34	1.29	1
HD 206860	G0IV-V	C	1.02	0.03	0.03	2.55	1.24	1.41	1
HD 207129	G0V	C	1.04	0.03	0.03	3.24	1.07	1.30	1
HD 209100	K4V	A	0.75	0.01	0.01	9.34	2.75	4.39	2
HD 210302	F6V	A	1.27	0.03	0.02	1.88	0.22	0.50	1
HD 212330 A	G2IV-V	B	1.00	0.05	0.05	9.38	1.03	1.03	1
HD 213845 A	F5V	C	1.32	0.07	0.03	1.31	0.37	1.28	1
HD 215648 A	F6V	C	1.15	0.04	0.04	4.92	0.47	0.47	1
HD 216803	K4V	B	0.74	0.01	0.02	3.53	2.92	3.11	1
HD 217987	M1V	B	0.45	0.05	0.01	7.37	4.57	5.76	2
HD 219134	K3V	A	0.76	0.01	0.01	11.97	1.20	2.33	1
HD 219623	F8V	C	1.13	0.02	0.02	3.85	0.60	1.06	1
HD 166	G8V	B	0.95	0.03	0.03	3.41	2.37	3.06	1
HD 693	F8V	A	1.08	0.03	0.02	5.59	0.45	0.53	1
HD 739	F5V	C	1.25	0.03	0.03	1.81	0.22	0.44	1
HD 1581	F9.5V	B	0.98	0.05	0.05	5.34	2.02	1.78	1
HD 2151	G0V	C	1.13	0.04	0.04	6.04	0.53	0.59	1
HD 3651 A	K0.5V	B	0.86	0.01	0.01	8.21	0.69	1.19	1
HD 4391	G5V	B	0.98	0.04	0.04	3.40	1.84	2.84	1
HD 4628	K2V	A	0.73	0.02	0.02	10.53	2.15	3.46	1
HD 4614 A	F9V	A	0.95	0.02	0.03	1.24	1.50	1.04	1

Continued on next page

Table B.1 – continued from previous page

Star	SpT	Tier	M	σ_M^+	σ_M^-	Age	σ_{Age}^+	σ_{Age}^-	Flag
			($M_\odot$)	($M_\odot$)	($M_\odot$)	(Gyr)	(Gyr)	(Gyr)	
HD 4813	F7V	A	1.13	0.03	0.03	1.80	0.75	1.01	1
HD 5015	F8V	C	1.24	0.06	0.06	4.09	0.77	0.80	1
HD 7570	F9V	B	1.19	0.04	0.03	2.21	0.52	0.91	1
HD 7788 A	F5V	C	1.36	0.03	0.03	2.12	0.26	0.28	1
HD 9826 A	F8V	C	1.26	0.05	0.05	3.69	0.70	0.68	1
HD 10361	K2V	A	0.75	0.02	0.02	6.36	3.96	3.76	1
HD 10360	K2V	A	0.76	0.03	0.02	9.16	2.63	4.61	1
HD 10647	F9V	C	1.10	0.04	0.03	1.71	0.88	1.54	1
HD 10476	K1V	A	0.82	0.02	0.01	9.27	0.92	1.62	1
HD 10700	G8V	B	0.77	0.02	0.02	9.06	0.89	1.73	1
HD 10780	G9V	A	0.87	0.02	0.02	6.51	1.65	2.62	1
HD 14412	G8V	C	0.76	0.02	0.01	8.66	1.37	2.48	1
HD 17051	F9V	B	1.19	0.05	0.04	1.07	0.81	1.04	1
HD 16895 A	F7V	A	1.19	0.03	0.03	2.14	0.58	0.67	1
HD 17206	F7V	A	1.27	0.09	0.04	1.61	0.50	1.59	1
HD 17925	K1.5V	B	0.84	0.03	0.03	5.73	3.32	3.70	1
HD 19373	G0V	A	1.11	0.04	0.03	5.75	0.95	1.05	1
HD 20010 A	F6V	C	1.17	0.04	0.03	4.80	0.51	0.56	1
HD 20766	G2IV	A	0.91	0.03	0.02	5.08	1.28	3.41	1
HD 20807	G1V	A	0.95	0.04	0.04	4.38	1.75	2.33	1
HD 20630	G5V	A	0.99	0.04	0.03	3.38	1.74	2.21	1
HD 20794	G6V	B	0.85	0.06	0.03	7.04	1.22	7.01	1
HD 22001 A	F3V	C	1.37	0.02	0.02	1.75	0.15	1.73	1
HD 22049	K2V	C	0.79	0.03	0.03	5.68	4.40	4.27	1
HD 22484	F9IV-V	B	1.11	0.03	0.03	6.14	0.66	0.63	1
HD 23249	K0IV	A	1.13	0.09	0.10	7.28	2.06	1.39	1
HD 23754	F5IV-V	C	1.44	0.02	0.02	1.57	0.13	0.13	1
HD 25457	F7V	C	1.19	0.05	0.04	1.33	0.73	1.28	1
HD 25998	F8V	C	1.23	0.05	0.06	0.72	1.08	0.68	1
HD 26965 A	K0.5V	A	0.79	0.02	0.02	9.44	1.35	3.29	1
HD 30495	G1.5V	B	1.01	0.04	0.03	2.34	1.73	1.92	1
HD 30652	F6V	A	1.25	0.05	0.02	1.16	0.41	1.02	1
HD 32147	K3V	B	0.80	0.02	0.02	9.92	1.62	2.75	1
HD 33262 A	F9V	B	1.06	0.03	0.02	2.38	0.80	0.89	1
HD 32923	G1V	C	0.96	0.03	0.02	10.58	0.72	0.84	1

Continued on next page

Table B.1 – continued from previous page

Star	SpT	Tier	M	σ_M^+	σ_M^-	Age	σ_{Age}^+	σ_{Age}^-	Flag
			($M_\odot$)	($M_\odot$)	($M_\odot$)	(Gyr)	(Gyr)	(Gyr)	
HD 34411	G1.5V	A	1.03	0.04	0.03	7.85	1.09	1.19	1
HD 33564	F7V	C	1.29	0.03	0.05	2.12	0.64	0.43	1
HD 35296	F8V	A	1.13	0.03	0.03	2.54	0.63	1.08	1
HD 39091	G0V	B	1.09	0.03	0.03	3.40	1.10	0.85	1
HD 37394	K1V	B	0.86	0.03	0.02	7.17	1.79	2.67	1
HD 38392	K2.5V	B	0.76	0.02	0.02	10.98	1.77	3.32	1
HD 38393	F6.5V	A	1.18	0.04	0.03	2.14	0.61	0.64	1
HD 38858	G2V	C	0.94	0.06	0.04	3.64	2.22	3.28	1
HD 43834 A	G7V	C	0.96	0.02	0.02	5.70	1.80	1.75	1
HD 43042	F5.5IV-V	B	1.30	0.05	0.03	1.21	0.49	1.18	1
HD 43386	F5V	B	1.25	0.05	0.02	1.56	0.36	0.76	1
HD 46588 A	F8V	B	1.09	0.04	0.04	2.96	0.92	0.84	1
HD 48682	F9V	C	1.14	0.02	0.02	2.77	0.60	0.81	1
HD 50281	K3.5V	C	0.75	0.02	0.02	3.80	3.43	2.86	1
HD 50692	G0V	B	0.99	0.03	0.03	5.22	1.46	1.23	1
HD 53705	G1.5V	B	0.93	0.05	0.04	10.58	1.32	1.70	1
HD 55575	F9V	B	0.92	0.03	0.02	9.16	1.09	1.17	1
HD 58855	F6V	B	1.09	0.03	0.03	3.81	0.56	0.58	1
HD 64379	F5V	C	1.22	0.04	0.03	1.10	0.54	1.06	1
HD 65907 A	F9.5V	B	0.95	0.04	0.03	5.89	1.27	1.64	1
HD 69830	G8V	C	0.90	0.03	0.03	5.06	1.92	2.87	1
HD 69897	F6V	B	1.09	0.04	0.04	4.00	0.69	0.72	1
HD 219482	F6V	C	1.16	0.03	0.02	1.29	0.59	1.07	1
HD 222368	F7V	C	1.17	0.08	0.04	4.45	0.72	1.15	1

Note: Follows same ordering as EMSL and SPORES catalog. Flag = 1 indicates MCMC sampling was deemed reliable.

Table B.2. CHZ_2 metric for EMSL stars

Star	SpT	Tier	CHZ_2 metric	Flag
HD 142860	F6V	A	0.776	1
HD 23249	K0IV	A	0.711	1
HD 19373	G0V	A	0.699	1
HD 95128	G1.5IV-V	A	0.693	1
HD 84117	F9V	A	0.683	1
HD 190248	G8IV-V	A	0.673	1
HD 34411	G1.5V	A	0.667	1
HD 693	F8V	A	0.666	1
HD 141004	G0V	A	0.661	1
HD 203608	F9V	A	0.609	1
HD 109358	G0V	A	0.608	1
HD 142373	G0V	A	0.527	1
HD 102365	G2V	A	0.479	1
HD 35296	F8V	A	0.478	1
HD 10476	K1V	A	0.458	1
HD 20807	G1V	A	0.457	1
HD 101501	G8V	A	0.450	1
HD 146233	G3V	A	0.436	1
HD 20630	G5V	A	0.421	1
HD 26965 A	K0.5V	A	0.404	1
HD 219134	K3V	A	0.388	1
HD 16895 A	F7V	A	0.382	1
HD 114710	F9.5V	A	0.367	1
HD 185144	K0V	A	0.366	1
HD 192310	K2V	A	0.355	1
HD 10780	G9V	A	0.348	1
HD 38393	F6.5V	A	0.348	1
HD 20766	G2IV	A	0.338	1
HD 147513	G1V	A	0.326	1
HD 209100	K4V	A	0.324	2
HD 4628	K2V	A	0.314	1
HD 90839	F8V	A	0.313	1
HD 131977	K4V	A	0.307	1
HD 149661	K0V	A	0.297	1
HD 10360	K2V	A	0.281	1
HD 100623 A	K0V	A	0.256	1

Continued on next page

Table B.2 – continued from previous page

Star	SpT	Tier	CHZ_2 metric	Flag
HD 10361	K2V	A	0.243	1
HD 201091	K5V	A	0.231	2
HD 4813	F7V	A	0.188	1
HD 201092	K7V	A	0.171	2
HD 202560	M0V	A	0.155	2
HD 88230	K7V	A	0.140	2
HD 156026	K5V	A	0.132	1
HD 4614 A	F9V	A	0.129	1
HD 17206	F7V	A	0.106	1
HD 210302	F6V	A	0.099	1
HD 30652	F6V	A	0.002	1
HD 187691 A	F8V	B	0.788	1
HD 22484	F9IV-V	B	0.745	1
HD 69897	F6V	B	0.728	1
HD 160691	G3V	B	0.701	1
HD 58855	F6V	B	0.690	1
HD 143761	G0IV	B	0.674	1
HD 212330 A	G2IV-V	B	0.669	1
HD 86728 A	G4IV	B	0.665	1
HD 165499	G0V	B	0.665	1
HD 84737	G0V	B	0.642	1
HD 128620	G2V	B	0.626	1
HD 1581	F9.5V	B	0.604	1
HD 53705	G1.5V	B	0.574	1
HD 55575	F9V	B	0.568	1
HD 136352	G2.5V	B	0.547	1
HD 115617	G6.5V	B	0.546	1
HD 46588 A	F8V	B	0.538	1
HD 65907 A	F9.5V	B	0.523	1
HD 190360	G7V	B	0.502	1
HD 82885 A	G9IV-V	B	0.501	1
HD 165341 A	K0V	B	0.481	1
HD 39091	G0V	B	0.469	1
HD 10700	G8V	B	0.446	1
HD 50692	G0V	B	0.444	1
HD 131156 A	G8V	B	0.413	1
HD 156274 A	G9V	B	0.402	1

Continued on next page

Table B.2 – continued from previous page

Star	SpT	Tier	CHZ_2 metric	Flag
HD 7570	F9V	B	0.397	1
HD 33262 A	F9V	B	0.393	1
HD 155885	K1V	B	0.381	1
HD 155886	K1V	B	0.377	1
HD 3651 A	K0.5V	B	0.376	1
HD 20794	G6V	B	0.345	1
HD 32147	K3V	B	0.329	1
HD 30495	G1.5V	B	0.313	1
HD 38392	K2.5V	B	0.309	1
HD 140538 A	G5V	B	0.299	1
HD 4391	G5V	B	0.298	1
HD 17925	K1.5V	B	0.285	1
HD 128621	K1V	B	0.262	1
HD 37394	K1V	B	0.257	1
HD 166	G8V	B	0.218	1
HD 165341 B	K4V	B	0.209	2
HD 72905	G0.5V	B	0.203	1
HD 216803	K4V	B	0.140	1
HD 128167	F4V	B	0.090	1
HD 217987	M1V	B	0.087	2
HD 17051	F9V	B	0.064	1
HD 134083	F5V	B	0.051	1
HD 43386	F5V	B	0.017	1
HD 43042	F5.5IV-V	B	0.006	1
HD 95735	M2V	B	0.004	2
HD 102870	F9V	C	0.882	1
HD 126660 A	F7V	C	0.847	1
HD 78154 A	F7V	C	0.823	1
HD 9826 A	F8V	C	0.815	1
HD 168151	F5V	C	0.774	1
HD 5015	F8V	C	0.768	1
HD 160032	F4V	C	0.734	1
HD 114613	G4IV	C	0.729	1
HD 222368	F7V	C	0.699	1
HD 187013	F5.5IV-V	C	0.686	1
HD 182572	G7IV-V	C	0.679	1
HD 215648 A	F6V	C	0.673	1

Continued on next page

Table B.2 – continued from previous page

Star	SpT	Tier	CHZ_2 metric	Flag
HD 114837 A	F6V	C	0.667	1
HD 91324	F9V	C	0.664	1
HD 2151	G0V	C	0.663	1
HD 20010 A	F6V	C	0.659	1
HD 160915	F5V	C	0.651	1
HD 219623	F8V	C	0.641	1
HD 32923	G1V	C	0.611	1
HD 48682	F9V	C	0.582	1
HD 157214	G0V	C	0.554	1
HD 43834 A	G7V	C	0.529	1
HD 207129	G0V	C	0.509	1
HD 7788 A	F5V	C	0.485	1
HD 125276 A	F9V	C	0.473	1
HD 110897	F9V	C	0.457	1
HD 189567	G2V	C	0.402	1
HD 193664	G0V	C	0.400	1
HD 69830	G8V	C	0.397	1
HD 191408 A	K2.5V	C	0.372	2
HD 33564	F7V	C	0.372	1
HD 140901 A	G7IV-V	C	0.364	1
HD 76151	G2V	C	0.339	1
HD 75732 A	K0IV-V	C	0.334	1
HD 22049	K2V	C	0.303	1
HD 38858	G2V	C	0.292	1
HD 122064	K3V	C	0.279	1
HD 206860	G0IV-V	C	0.274	1
HD 166620	K2V	C	0.264	2
HD 14412	G8V	C	0.258	1
HD 158633	K0V	C	0.256	1
HD 115404 A	K2.5V	C	0.242	1
HD 72673	K1V	C	0.231	1
HD 103095	K1V	C	0.231	2
HD 74576	K2.5V	C	0.224	1
HD 89449	F6IV-V	C	0.210	1
HD 156897 A	F2V	C	0.193	1
HD 10647	F9V	C	0.183	1
HD 131156 B	K5V	C	0.176	1

Continued on next page

Table B.2 – continued from previous page

Star	SpT	Tier	CHZ_2 metric	Flag
HD 50281	K3.5V	C	0.165	1
HD 165185	G0V	C	0.147	1
HD 78366	G0IV-V	C	0.110	1
HD 105452 A	F1V	C	0.103	1
HD 199260	F6V	C	0.096	1
HD 25457	F7V	C	0.089	1
HD 739	F5V	C	0.067	1
HD 25998	F8V	C	0.050	1
HD 219482	F6V	C	0.038	1
HD 64379	F5V	C	0.014	1
HD 197692	F5V	C	0.005	1
HD 22001 A	F3V	C	0.004	1
HD 213845 A	F5V	C	0.001	1
HD 90589	F3V	C	0.000	1
HD 90089 A	F4V	C	0.000	1
HD 109085	F2V	C	0.000	1
HD 23754	F5IV-V	C	0.000	1

Note: Sorted according to EMSL tier and CHZ_2 metric. Flag = 1 indicates MCMC sampling was deemed reliable.